Elaboration and optimization of carbon nanotube-based polymer composites for electrical energy storage

Jinkai Yuan

ÉCOLE CENTRALE DES ARTS
ET MANUFACTURES
《ÉCOLE CENTRALE PARIS》

THÈSE

Présentée par

Jinkai YUAN

Pour l'obtention du

GRADE DE DOCTEUR

Spécialité : Science des matériaux

Laboratoire d'accueil : Laboratoire de Mécanique des Sols, Structures et Matériaux

Élaboration et optimisation des composites comportant des nanotubes de carbone pour le stockage de l'énergie électrique

Soutenue publiquement le 18 septembre 2012

Devant le jury composé de :

M.	Gilles REGNIER	Professeur, ENSAM	**Président**
M.	Alain SYLVESTRE	Professeur, UJF, G2Elab	**Rapporteur**
M.	Costantino CRETON	Directeur de Recherche, ESPCI	**Rapporteur**
Mme	Marie-Christine RECORD	Professeur, Université Aix-Marseille	**Examinateur**
M.	Laurent DIVAY	Ingénieur R&D, Thales R&T	**Examinateur**
M.	Arnaud MORIN	Ingénieur CEA, CEA Grenoble	**Examinateur**
M.	Jinbo BAI	Directeur de Recherche, ECP	**Directeur de thèse**

2012ECAP0034

Remerciments

Le travail de recherche présenté dans cette thèse a été réalisé au sein du laboratoire MSSMat (CNRS UMR 8579) de l'Ecole Centrale Paris en collaboration avec laboratoire G2Elab (CNRS UMR 5269) à Grenoble.

Le finacement de cette thèse a été assuré par le CSC (China Scholarship Council). Ce soutien a été précieux.

Je tiens à exprimer mes sincère reconnaissances envers mon directeur de thèse, M. Jinbo BAI, pour son soutien, son bons conseils, sa disponibilité et son encadrement instructif lors de ces années.

J'adresse mes respects et mes sinceres remerciments à M. Gilles REGNIER, Professeur à Ecole Nationale Supérieure d'Arts et Métiers, d'avoir accepté de présider le Jury désigné pour cette thèse.

Je remerci vivement M. Costantino CRETON, Directeur de Recherche à ESPCI, et M. Alain SYLVESTRE, Professeur à Université Joseph Fourier, d'avoir accepté d'être les rapporteur de cette thèse. Je leur exprime toute ma gratitude pour l'intérêt qu'ils ont exprimé à l'égard de ce travail et pour leurs évalutions.

Mme. Marie-Christine RECORD, M. Arnaud MORIN et M. Laurent DIVAY ont accepté d' examiner ce travail et d'être membre du jury, qu'il trouve ici l'expression de toute ma gratitude et de mon profond respect.

Je tiens également à remercier tous les thésards que j'ai eu l'occasion de connaître, et avec qui j'ai travaillé ensemble : Maxime Genestoux, Weilong Li, Michael Bozlar, Youqin Lin, Jing Zhang, Jing Shen, Delong He, Jérôme Helary, Anthony Dichiara, John Saba, Hassan Harris, Hande Yavuz, Weikang Li, Antinéa Einig, Pascale Gemeiner, Nicolas Guiblin, Gilles Boemare, Fançoise Garnier, Farida Djebbari, Sokona Konate, Sylviane Bourgeois. C'était avec grand plaisir de partager des expériences de la vie et de la recherche.

En fin, un grand merci pour ma famille, mes amis pour m'avoir soutenu moralement.

Table of Contents

Acronyms and Symbols

Acronyms

AFM	atomic force microscopy
AR	aspect ratio
BOPP	biaxially oriented polypropylene
CB	carbon black
CNT	carbon nanotube
CVD	chemical vapor deposition
DMF	dimethyl formamide
EC	electrochemical capacitor
EDLC	electrical double layer capacitor
LDPE	low density polyethylene
LIB	lithium-ion battery
MFI	melt flow index
MWNT	multiwalled carbon nanotube
MWS	Maxwell–Wagner–Sillars
PA	polyamide
PANI	polyaniline
PC	polycarbonate
PCB	printed circuit board
PE	polyethylene
PEKK	poly(etherketoneketone)
PET	polyethylene terephthalate
PHAE	polyhydroxyaminoether
PMMA	polymethyl methacrylate
PP	polypropylene
PPy	polypyrrole
PS	polystyrene
PSF	polysulfone
PVA	polyvinyl alcohol
PVDF	polyvinylidene fluoride
SEM	scanning electron microscopy
SSA	specific surface area
SWNT	single walled carbon nanotube
TEM	transmission electron microscopy
TFBB	3,4,5-trifluorobromobenzene

THF	tetrahydrofurane
TS	tensile strain
UHMWPE	ultrahigh molecular weight polyethylene

Symbols

f_c	percolation threshold
f_{CNT}	carbon nanotube concentration
wt %	weight fraction
σ	conductivity
τ	relaxation time
T	absolute temperature
C	capacitance
ε_0	dielectric permittivity of vacuum
ε_r	relative dielectric permittivity
E_b	dielectric breakdown strength
tanδ	loss tangent
ϕ_f	volume fraction of filler
U_e	energy density
E_a	activation energy
K_b	Boltzmann constant
ν	frequency
σ_{DC}	direct current electrical conductivity
ω	angular frequency

General Introduction

Ever-increasing energy requirement and exhaustion of fossil fuels demands improving efficiency of energy usage as well as seeking sustainable and renewable resources. Energy storage capacitors are devices that could take this responsibility, and have been the focus of increasing attention due to their advantages such as environment friendliness and very fast energy uptake and delivery. As the requirements grow for a low-cost and high-efficiency capacitive storage system, there is great need for the development of materials with high dielectric permittivity. Polymer composite dielectrics are arousing increasing attention due to their large tunability in dielectric performances. Polymer composites filled with ceramic particles have been used in some energy storage capacitors. Still, their applicability for practical devices is severely hindered by the low dielectric permittivity and deteriorated mechanical and processing properties due to the high content of rigid ceramic particles in the flexible polymer matrix. By replacing ceramic particles with conductive particles in the polymer composites, the percolative polymer composites can be made with the dielectric permittivity dramatically increased in the vicinity of the percolation threshold. Among the conductive fillers, carbon nanotubes (CNTs) have been most intensively studied, as their large aspect ratio coupled with high conductivity can lead to percolation levels in composites at much low loading. One of the greatest challenges for CNT usage in composites is to debundle pristine CNTs and realize uniform dispersion into polymers. This thesis focused on increasing the dielectric permittivity of CNT-based polymer composites by both carefully optimizing the dispersion of nanotubes as well as controlling the microstructure of the composites.

First, solution method was employed to prepare polymer composites. Pristine multiwalled CNT (MWNT) and polyvinylidene fluoride (PVDF) were selected as the conductive filler and polymer host respectively. The extremely large aspect ratio of MWNT gave rise to a percolation threshold as low as 1.91 vol%. By approaching the percolation threshold, microcapacitors with MWNT as electrode and PVDF as dielectric in between were formed so as to improve the dielectric permittivity. However, the enhancement in the

dielectric permittivity (27 times higher than PVDF) is limited due to the aggregated structure of MWNTs as well as the weak interfacial interaction between MWNTs and PVDF matrix, which also would make the microcapacitor structure rather fragile and easy to be destroyed by the external force field. A tensile test was conducted on the MWNT/PVDF composite near percolation threshold. Nanotubes were found to be aligned in response to the uniaxial mechanical stretching. The alignment of CNTs initially destroyed the readily formed microcapacitors yet subsequently induced more effective ones. The evolution of microcapacitors was well correlated with the complex variations in the dielectric permittivity and ac conductivity of the composites.

To enhance the interfacial interaction, and thus improve the stability of microcapacitor near the percolation threshold, we presented a robust and simple procedure to prepare composites with a remarkable molecular level interaction at interfaces through melt-mixing pristine MWNTs within PVDF matrix. A better dispersion of nanotubes by melt-mixing overcame the problems of nanotube sediment aggregation in polymer composites processed by the solution casting technique. In melt mixing, the high temperature and high shear forces would establish donor-acceptor complexes between the delocalized π-electron clouds of CNTs and strongly electrophilic F groups of PVDF chains. This interfacial interaction was confirmed by Raman spectroscopy as well as the formation of much thin PVDF layer on individual MWNT. The resultant composite with a huge interfacial area possessed a giant dielectric permittivity (3800) of three orders of magnitude higher than the PVDF matrix, while retaining a low conductivity level (6.3×10^{-5} $S.m^{-1}$) and an excellent thermal stability. These results could be explained by a reinforced Maxwell–Wagner–Sillars effect based on the remarkable molecular level interaction. Unfortunately, due to the inevitable breakage of CNT and the effective wrapping of PVDF on nanotube surfaces during the melt-mixing, the resultant MWNT/PVDF composites showed a relatively high percolation threshold (10.4 vol%).

Further study aimed on reducing the percolation threshold of the melt-processed polymer composite. We reported a percolative MWNT-filled low density polyethylene

(LDPE)/PVDF composite. As compared to the MWNT-filled single LDPE composites, this biphasic polymer composite displayed a significantly reduced percolation threshold (9.6 vol %→5.7 vol%) but still maintained the same permittivity to reach. This can be attributed to a double percolated structure observed on the basis of morphological evidence. MWNTs were selectively localized in LDPE phase during melt-mixing. This is contrary to the wetting coefficient evaluation yet still possible when the colossal difference in viscosity of two polymers was taken into account. The effect of double percolation on the dielectric properties was well illustrated by revealing the mechanism for the improved permittivity. A model based on the Lichtenecker rule and percolation theory was established and demonstrated to be effective to predict the dielectric permittivity in biphasic polymer composites.

The dielectric permittivity increment in the previous composite systems originated from the formation of microcapacitors. However, CNTs were always frizzy in the CNT/polymer composites, which was not beneficial in forming parallel pair electrodes of microcapacitors. To overcome this problem, we proposed a microarchitecture of hybrid SiC-CNT as conductive filler. Such micro/nano hybrids were produced by floating catalytic chemical vapor deposition method. The organization mode of CNTs on SiC particles could be effectively tuned by adjusting synthesis conditions. The results showed that asymmetric surface properties of 6H-SiC were prone to led to “single-direction” growth of CNTs on SiC particles, while the competition between the substrate nature and the experimental conditions could result in a “multi-directions” hybrid structure. Resultant SiC-CNT hybrids were further incorporated into PVDF to prepare percolative composites. It was found that the SiC-CNT hybrid can significantly improve the dielectric permittivity of PVDF composite with an extremely low CNT loading. CNTs on each SiC microplate are oriented along an axis and separated by a thin polymer matrix, giving rise to a network of microcapacitors. As a result, a large dielectric permittivity of more than 8700 and 2100 at 100 Hz could be obtained at a low CNT loading of 2.30 vol% and 1.48 vol% in the “multi-directions” and “single-direction” hybrid based composites respectively.

Key words: Polymer composites; Carbon nanotube; Dielectric properties; Energy storage

Résumé en français

L'augmentation croissante de la demande en énergie et l'épuisement des combustibles fossiles exigent l'amélioration de l'efficacité de l'utilisation de l'énergie ainsi que la recherche de ressources durables et renouvelables. Les condensateurs sont des systèmes de stockage de l'énergie qui se sont imposés comme une des solutions aux problèmes énergétiques en raison de leurs avantages, tels que le respect de l'environnement, et la charge et la décharge d'énergie très rapides. Des besoins se sont créés pour un système de stockage capacitif à faible coût et à haut rendement, il est donc nécessaire de développer des matériaux avec une forte permittivité diélectrique. A ce propos, les composites diélectriques à matrice polymère suscitent une attention croissante en raison de leurs bonnes performances diélectriques. Des composites à matrice polymère chargée de particules céramiques ont par exemple été utilisés dans certains condensateurs pour le stockage d'énergie. Pourtant, en pratique, l'applicabilité de tels dispositifs est sérieusement entravée par la faible permittivité diélectrique des matériaux d'une part, et par la détérioration des propriétés mécaniques en raison de la forte teneur en particules céramiques rigides dans la matrice polymère flexible d'autre part. En remplaçant ces particules céramiques par des particules conductrices dans la matrice polymère, des composites percolatifs peuvent être réalisés avec une permittivité diélectrique nettement accrue au voisinage du seuil de percolation. Parmi les charges conductrices, les nanotubes de carbone (NTC) ont été les plus étudiés. En effet, du fait de leur facteur d'aspect et de leur conductivité élevée, ces derniers peuvent conduire à des niveaux de percolation dans les composites pour une très faible quantité de charges. Un des plus grands défis pour l'utilisation des NTC dans les matériaux composites est de séparer les NTC les uns des autres afin de réaliser une dispersion uniforme dans les polymères. Les travaux présentés dans cette thèse ont porté sur l'augmentation de la permittivité diélectrique de matériaux composites à matrice polymère à base de NTC en optimisant à la fois la dispersion des nanotubes ainsi que le contrôle de la microstructure des matériaux composites finaux.

Tout d'abord, la méthode du coulage d'une solution qui a été utilisée pour préparer les

polymères composites consiste à introduire des nanotubes de carbone multifeuilles (MWNT) vierges utilisés comme charges conductrices dans une matrice de fluorure de polyvinylidène (PVDF). Le facteur d'aspect extrêmement haut des MWNT donne lieu à un seuil de percolation très bas de l'ordre de 1,91 % en volume. Lorsque le seuil de percolation est atteint, des microcondensateurs constituées de MWNT (électrode) entourés de PVDF (diélectrique) sont formés de manière à améliorer significativement la permittivité diélectrique du composite. Toutefois, l'augmentation de la permittivité diélectrique (27 fois plus élevée que le PVDF pur) reste limitée en raison de l'agrégation de MWNT ainsi que de la faible interaction interfaciale entre MWNT et PVDF, rendant la structure ainsi formée plutôt fragile et facilement destructible par l'application d'un champ de force externe. Un essai de traction a été menée sur un MWNT/PVDF composite jusqu'à atteindre le seuil de percolation. Les nanotubes se retrouvent alignés en réponse à l'étirement uniaxial mécanique appliqué. Cet alignement détruit donc les microcondensateurs initialement formées. L'évolution de ces microcondensateurs est alors bien corrélée avec les variations complexes de la conductivité et de la permittivité diélectrique du composite.

Afin d'améliorer l'interaction interfaciale et par conséquent augmenter la stabilité de ces microcondensateurs près du seuil de percolation, nous avons présenté une procédure simple et robuste visant à préparer des composites avec une interaction moléculaire remarquable au niveau des interfaces via la fusion-mélange des MWNTs vierges au sein de la matrice polymère. Une meilleure dispersion des MWNTs est alors obtenue par cette technique permettant de surmonter les problèmes d'agrégation des sédiments de NTC dans les composites polymères traitées par la technique de coulage d'une solution. En faisant fondre le mélange, la température et les forces de cisaillement élevées permettent d'établir un complexe de donneur-accepteur entre les électrons π délocalisés des nuages de NTC et les groupes F fortement électrophiles des chaînes du PVDF. Cette interaction interfaciale a été confirmée par spectroscopie Raman ainsi que par l'observation d'un grand nombre de MWNT individuels recouverts d'une couche mince de PVDF. Le composite ainsi préparé possède une vaste zone interfaciale lui conférant une permittivité diélectrique géante (3800) de trois

ordres de grandeur plus élevés que la matrice PVDF, tout en conservant une faible conductivité ($6,3 \times 10^{-5}$ $S.m^{-1}$) et une excellente stabilité thermique. Ces résultats peuvent s'expliquer par le modèle de renforcement de Maxwell-Wagner-Sillars basé sur l'interaction moléculaire forte entre charges et matrice. Néanmoins, en raison de la rupture inévitable de certains NTC et de l'enrobage efficace de la surface des nanotubes par le PVDF au cours de la fusion-mélange, les composites ainsi obtenus ont un seuil de percolation relativement élevé, de l'ordre de 10.4% en volume.

Une étude plus poussée a alors été réalisée visant à diminuer le seuil de percolation du matériau composite préparé par la méthode de mélange-fusion. Nous avons préparé un composite percolatif à matrice biphasique de polyéthylène basse densité (LDPE) et de PVDF rempli de MWNT. Par rapport aux composites de type MWNT/LDPE seul, le composite à matrice biphasique présente un seuil de percolation considérablement réduit (9,6 vol%→5,7 vol%) tout en conservant une même permittivité élevée. Les analyses morphologiques ont montré que cela peut être attribué à une structure à double percolation. En effet, les MWNT sont globalement localisés en phase LDPE au cours du procédé de mélange-fusion, ce qui paraît contraire à l'évaluation du coefficient de mouillage mais possible quand même au regard de la différence importante de viscosité des deux polymères. L'effet de double percolation sur les propriétés diélectriques est bien révélé en expliquant le mécanisme d'amélioration de la permittivité. Un modèle basé sur la règle Lichtenecker et la théorie de la percolation a été établi afin de prédire efficacement la permittivité diélectrique dans les matériaux composites de polymères biphasiques.

L'augmentation de la permittivité diélectrique dans les composites précédents provient de la formation de microcondensateurs au sein du matériau. Toutefois, les NTC ont toujours tendance à s'agglomérer dans le composite, ce qui n'est pas bénéfique à la formation de microcondensateurs. Pour surmonter ce problème, nous avons proposé une microarchitecture hybride SiC-NTC comme charge conductrice. Ces hybrides mulit-échelles ont été produits par dépôt chimique catalytique en phase vapeur assisté par aérosol. L'organisation des NTC sur les particules de SiC peut être efficacement contrôlée en ajustant les différents paramètres

de synthèse. Les résultats ont montré que les propriétés de surface asymétriques des micro-particules de SiC étaient plutôt favorables à la croissance des NTC sur SiC selon "une direction unique", alors que certaines conditions expérimentales particulières peuvent aboutir à une croissance "multi-directionnelle". Les particules hybrides de SiC-NTC ainsi obtenues ont également été incorporées dans le PVDF pour préparer des composites percolatifs. Il a été constaté que les hybrides SiC-NTC permettent d'améliorer considérablement la permittivité diélectrique du composite avec un chargement extrêmement faible en NTC. Les NTC sont orientés le long d'un axe sur chaque microplaque de SiC et séparés par une couche mince de polymère, donnant lieu à un réseau de microcondensateurs. Par conséquent, de grandes permittivités diélectriques de plus de 8700 et 2100 à 100 Hz peuvent être obtenues pour un faible taux de chargement de NTC de l'ordre de 2,30% et 1,48% en volume pour les composites à renforts "multi-directionnel" et "unidirectionnel" respectivement.

Mots clés: Composites polymères; Nanotubes de carbone; Propriétés diélectriques; Stockage de l'énergie

Chapter I
Carbon nanotubes for the energy storage

1.1 Carbon nanotubes

1.1.1 Structure and properties

Carbon nanotubes (CNTs) are allotropes of carbon, and can be envisioned as a rolled up graphene sheet into a seamless cylinder with fullerene caps for single-wall (SWNT) or multiple sheets as in the case of a multi-walled carbon nanotube (MWNT). Since their discovery in 1991 by Iijima,[1] the intriguing structure of CNTs with a combination of superlative electrical, mechanical, optical, chemical, and thermal properties has motivated worldwide efforts to understand their fundamental nature and explore their potential applications.

Characteristic of MWNTs are the concentric layers that are nested with an interlayer spacing of 0.34 nm, similar to the basal plane separation in graphite,[1] and clearly illustrated by the transmission electron micrograph (TEM) in Fig. 1-1a. In the case of SWNTs, the prominent van der Waals interactions between sidewalls generally lead to significantly close-packed bundles. The bundles are an important physical property and a corresponding TEM image from as-synthesized SWNTs is highlighted in Fig. 1-1b. As an ideal quasi-1D structure with an atomically monolayered surface and extended curved π-bonding configuration, an individual SWNT can exhibit semiconducting or metallic or semimetallic behavior, depending on the sheet direction about which the graphene sheet is rolled to form a nanotube cylinder. This direction in the graphene sheet plane along with the nanotube diameter determines SWNT chiralities that denote the nanotube type. Fig. 1-1c illustrates the basis for assigning chiralities with a roll-up vector (na_1+ma_2) from a point of origin on a graphene sheet. The chiral angle ($\theta \leq 30^{o}$) is the angle between the zigzag axis and the roll up vector.[2] Based on the appearance of a belt of carbon bonds around the nanotube

diameter, three chiralities of carbon nanotube can be realized, as shown in Fig. 1-1d. A 'zigzag' tube is formed when m=0 ($\theta = 0^{o}$), and an 'armchair' one when n=m ($\theta = 30^{o}$). The other types of tubes are 'chiral' ($0^{o} < \theta < 30^{o}$). All armchair SWNTs are metals. Those with *n*–*m*=3*k*, where *k* is a nonzero integer, are semi-metallic with a tiny band gap (~10 meV), and all others are semiconductors with a band gap that inversely depends on the nanotube diameter, [3] ranging from approximately 1.8 eV for very small diameter tubes to 0.18 eV for the widest possible stable SWNT. [4]

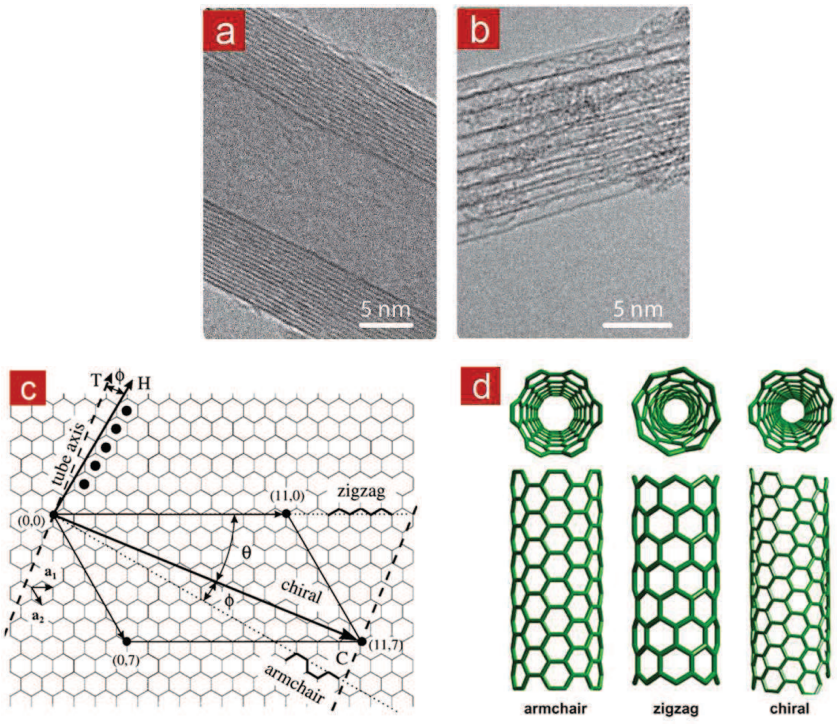

Fig. 1-1 *TEM images of an as-produced (a) MWNT and (b) SWNT bundle.[2] (c) Chirality chart illustrating the assignment of (n, m) SWNT structures using a roll-up vector from an origin point on a graphene sheet and the nanotube diameter.[5] (d) Three chiralities of carbon nanotube: 'armchair', 'zigzag' and 'chiral' (from left to right).*

Because of the weak coupling between the cylinders in MWNTs, the electronic properties of perfect MWNTs are rather similar to those of SWNTs. Due to the nearly one-dimensional electronic structure, charge carriers can travel without scattering in metallic

SWNTs and MWNTs over long nanotube length, allowing them to carry high currents with essentially no heating.[6] The resistivity of the crystalline ropes of metallic SWNTs has been measured to be in the order of 10^{-4} Ωcm at room temperature.[7] In addition, carrier mobility as high as 10^5 cm^2 V^{-1} s^{-1} have been observed in semi-conducting nanotubes, which is better than that of silicon.[8] Superconductivity has also been observed in SWNTs, albeit with transition temperature of 0.55 K [9] and 5 K [10] for SWNT with diameter of the order of 1.4 nm and 0.5 nm respectively. Phonons also propagate easily along the carbon nanotube. Theory predicted a room temperature thermal conductivity can reach up to 6000 W $m^{-1}K^{-1}$.[11] While this has not been fully attained, the highest value around 3000 W $m^{-1}K^{-1}$ has been measured for individual MWNT, which is still greater than that of natural diamond and the basal plane of graphite (both 2000 W $m^{-1}K^{-1}$). [12]

Besides the superlative electric and thermal properties, small-diameter CNTs are rather stiff and exceptionally strong, showing unprecedented mechanical property. Long before sufficient quantities of nanotubes were produced to allow mechanical measurements, a number of computer simulations were pursued to study CNT properties. Theoretical results predicted that CNTs have extremely high Young's modulus values, similar to that of graphite in-plane (1 TPa) and independent of the nanotube type and diameter. [13] The first direct mechanical measurement was not conducted until 1997 by Wong et al. [14] using atomic force microscopy (AFM). They demonstrated an average value of 1.28 TPa for Young's modulus of arc-MWNTs. However, the first ultimate measurement was carried by Yu et al in 2000 with applying a tensile load on nanotube inside an electron microscope, as demonstrated in Fig. 1-2. The Young's modulus is measured ranging from 320 to 1470 GPa for SWNT [15] and from 270 to 950 GPa for MWNT[16]. The tensile test showed that during the loading process only the outmost layer breaks and the tensile strength can range from 11 to 60 GPa. [16]

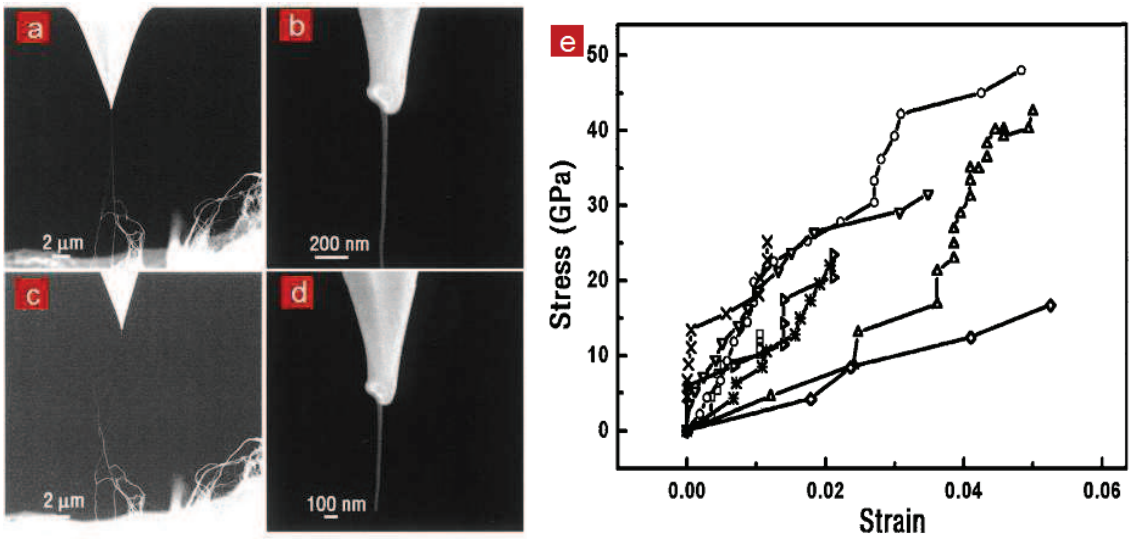

Fig. 1-2 *Scanning electron microscopy (SEM) images showing a SWNT rope tensile loading experiment, before and after the SWNT rope was broken. (a) A tensile loaded SWNT rope between an AFM tip and a SWNT "paper" sample. (b) Close-up view showing the attachment (carbonaceous deposit) of the end of the SWNT rope to the AFM tip. (c) The same SWNT rope after being loaded to the point where it broke. The image shows that one rope fragment was about 1 mm from the attachment region on the AFM tip. (d) Another close-up view of the attachment area after the rope was broken, showing the deposit was still robust. (e) Stress versus strain curves obtained from the tensile-loading experiments on individual SWNT ropes. [15]*

1.1.2 Carbon nanotube synthesis

To explore a variety of applications of CNT, [3, 17] there are tremendous ongoing efforts to develop control over individual CNT properties ranging from chirality, length, purity to electronic type ratio. This control can either be accomplished by optimizing synthesis condition or in conjunction with subsequent post-treatments (e.g., chemical modification of CNTs, and separation of SWNTs [18]). Synthesis of CNTs results from a wide variety of different methods that involve the catalytic decomposition of a carbon-containing gas or solid.[2] The most common synthesis techniques currently used are based on carbon-arc discharge,[19] laser ablation of carbon,[20] and chemical vapor

deposition (CVD, typically on catalytic particles) [21].

Both arc discharge and laser ablation are demonstrated to largely rely on the evaporation of carbon atoms from solid graphite targets at temperature as high as 3000 K, which greatly impedes CNTs' large scale applications. However, CVD produced MWNT are of increasing significance as they can be produced in very large quantities relatively cheaply at much lower temperatures (500-900 °C). Most importantly, CVD allows a selectively growth of nanotubes on a given substrate in controllable ways, resulting in desirable CNT-based architectures with controlled orientation and configurations for various potential applications.

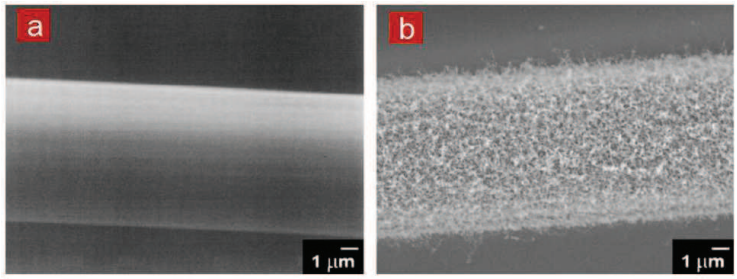

Fig. 1-3 *SEM micrographs of carbon fibers (a) before and (b) after surface modification with CNTs.[22]*

Thostenson et al. [22] modified the surface of pitch-based carbon fiber by growing CNTs directly on carbon fibers using a CVD process (Fig. 1-3). When embedded in a polymer matrix, the multiscale reinforcement can greatly improve interfacial load transfer through the local stiffening of polymer matrix near the fiber/matrix interface. Veedu et al. [23] have also used CVD process to grow well-aligned MWNT forest (about 60 µm long) perpendicular to 2D woven fabrics of SiC to produce 3D fabrics. The nanotube-grafted fabrics were stacked together and infiltrated with a high-temperature epoxy, as shown in Fig. 1-4. The presence of the CNT forests can significantly improve the interlaminar fracture toughness of the as-prepared 3D composites.

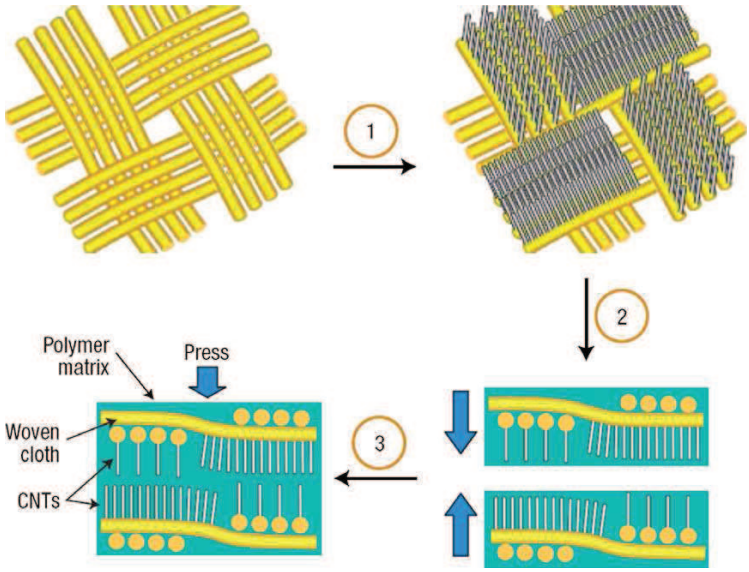

Fig. 1-4 *Schematic diagram of the steps involved in the hierarchical nanomanufacturing of a 3D composite. (1) Aligned nanotubes grown on the fiber cloth. (2) Stacking of matrix-infiltrated CNT-grown fiber cloth. (3) 3D composite fabrication by hand lay-up.[23]*

In our group, homogenously structured Al_2O_3-CNT micro/nano hybrids have been obtained via aerosol-assisted CVD synthesis (Fig. 1-5a). These multiscale fillers can provide efficient structures to disperse CNT network within the polymer matrix (Fig. 1-5b). Thermal conductivity results of the Al_2O_3-CNT hybrid based composites demonstrated a percolation due to the drastic decrease in the number of thermal contacts between the CNTs. As a result, an enhancement of 130% for thermal conductivity was observed at CNT mass fractions of only 0.15%, ten times lower than previous state-of-the-art research (Fig. 1-5c).

CVD process has exhibited unparallel advantages in mass production of CNTs as well as one-step direct construction of CNT assemblies, enabling nanotube of great importance in many potential applications of a wide range of fields. These applications include the use of CNTs in high conductivity or high strength composites, energy storage and conversion devices, hydrogen storage and drug delivery media, field emission devices, nanometer-sized electronic devices, sensors and probes.[3] As energy and environment becomes one of the most important issues in 21st century, we will focus on the energy storage application of CNTs in this thesis.

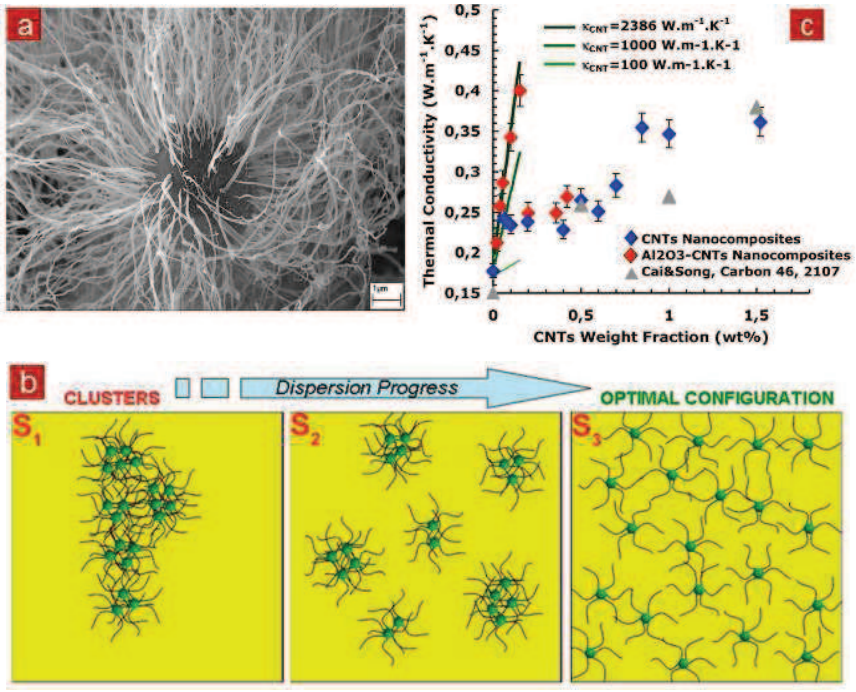

Fig. 1-5 *(a) SEM images of Al_2O_3-CNT hybrids. Thermogravimetric analyses indicate that the average wt% of CNTs on one alumina particle is 20 %. (b) The schematic represents the spatial arrangements of Al_2O_3-CNT fillers within a polymer. Fillers dispersion is represented from the state S_1 (beginning of the dispersion process) to S_3 (end). (c) The measured thermal conductivity of the hybrid Al_2O_3-CNT fillers (red diamonds) and of the CNTs (blue diamonds) based composites described in this work are reported as well as the recent data from the literature (grey triangles).[24]*

1.2 Carbon nanotubes for the energy storage

The increasing energy consumption and decreasing availability of fossil fuels require society to move towards sustainable and renewable resources. As a result, there is an increase in the development of the renewable energy production from solar and wind technologies. Due to the intermittency of such production and consumption requirements, the energy storage systems are starting to play a larger part in our lives. At the forefront of these are electrical energy storage systems, such as batteries,[2] electrochemical capacitors (ECs)[25] and dielectric-based capacitors.[26] However, we need to improve their performance substantially to meet the higher requirements of future systems, ranging from portable

electronics to hybrid electric vehicles and large industrial equipment, by developing new materials and advancing our understanding of charge storage mechanisms. Fig. 1-6 shows the plot of power against energy density for the most important energy storage systems. The general goal for energy storage development is to increase energy density and power density, while minimizing volumetric and mass constraints. Herein, in the following sections we will first briefly introduce CNTs' effect on the performances of electrochemical capacitor and lithium ion battery, and then thoroughly review the state-of-the-art research on energy storage in CNT-based composite used for capacitors.

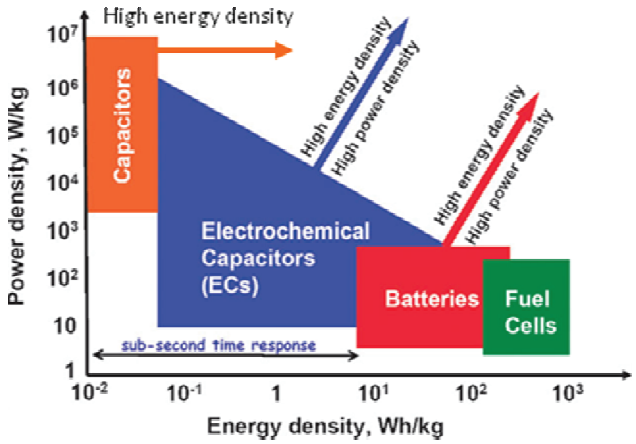

Fig. 1-6 *Comparison of the operational characteristics of energy storage and conversion devices indicating the desire to improve both energy density and power density.[27]*

1.2.1 Supercapacitors

Electrochemical capacitors, also called supercapacitors, store energy using either ion adsorption (electrical double layer capacitors (EDLC)) or fast surface redox reactions (pseudo-capacitors), depending on the electrode materials used. In detail, the former arises from pure electrostatic attraction between ions of the electrolyte and carbon materials[28] that are electrochemically stable and have high accessible specific surface area (SSA). While the latter is associated with Faradaic charge transfer reactions or reversible oxidation/reduction of the electro-active species on the surface of electrode, such as transition metal oxides[29] and conducting polymers.[30, 31] Fig. 1-7 represents a scheme of a typical

EDLC in its charged state. The positive electrode attracts the anions of electrolytes, whereas cations are accumulated near the surface of the negative electrode. Charge separation occurs on polarization at the electrode-electrolyte interface, leading to a double layer capacitance C described as:

$$C = \frac{\varepsilon_r \varepsilon_0 A}{d} \qquad (1\text{-}1)$$

where, ε_r is the electrolyte dielectric permittivity, ε_0 is the dielectric permittivity of vacuum, d is the effective charge separation distance (the Debye length), and A is the electrode surface area accessible to electrolyte ions. This storage mechanism allows for very high charging/discharging rate capability along with near-infinite long life cyclability.

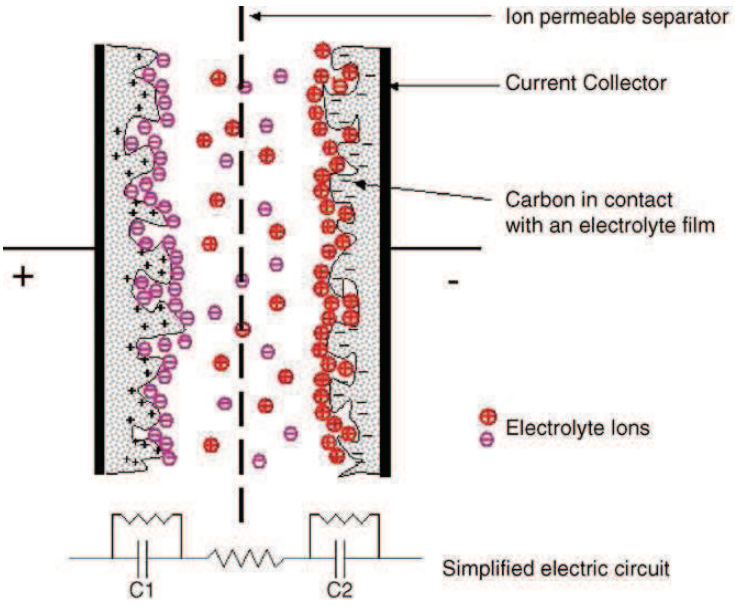

Fig.1-7 Scheme of an electrochemical double layer capacitor (in its charged state).

In contrast to EDLCs, charges stored in the pseudo-capacitors are much related to the electrode potential, as

$$C = dQ / dV \qquad (1\text{-}2)$$

where C is the capacitance of the pseudo-capacitor, Q is the charge quantity, and V is the potential. Pseudo-capacitors typically show much higher capacitance than that of EDLCs, yet often suffer from low power density and lack of stability due to poor electrical conductivity and framework swelling during charge/discharge cycles. Therefore, to realize the goal of

increasing power and energy density aforementioned, the key is to enhance the kinetics of ions as well as optimize pore structure, surface properties and conductivity of the electrode materials. Hence, electrode with proper porous structure and superior electrical conductivity are highly desirable.

CNTs exhibit high electrochemically accessible SSA, along with superior electrical properties, fast ion and electron transportation.[3] These properties are extremely amenable to the capacitive energy storage. The use of carbon nanotubes as electrode in EDLC has been expected to further advance micro-electrochemical capacitors, enabling flexible and adaptable devices to be made.

In 1997, Niu and his coworker [32] first utilized free-standing mats of entangled MWNTs as electrode to produce EDLC cells. Maximum capacitance values close to 113 F/g have been reported for frequencies below 1 Hz, on a single cell device with 38 wt % H_2SO_4 as the electrolyte. The cell can also show a power density of 8 kW/kg. These performances were achieved due mainly to the desirable electrochemical properties of MWNTs used, such as narrow distribution of pore sizes, highly accessible surface area, low resistivity, and high stability. Years later, An et al. [33] showed that SWNT composites with poly(vinyledene chloride) could reach a specific capacitance of 180 F/g at a power density of 20 kW/kg. In this case, the polymer binder yielded carbon residue with a pore diameter below 5 nm, further increasing the final composites SSA and electrical conductivity while lowering the series resistance of the cell.

Another possible strategy to improve both energy and power density for electrochemical capacitors is depositing nano-sized pseudo-capacitive materials (transition metal oxides or conducting polymers) onto the CNTs to form a hybrid system, as shown in Fig. 1-8. The appropriate combination of an EDLC electrode with a pseudo-capacitive electrode can increase the cell voltage, further contributing to improvement in energy and power densities. CNT/polypyrrole (PPy) nanocomposites can be a good example.[34] The MWNT with uniform 5 nm thick PPy coatings showed a capacity of nearly 130 F/g, which is much higher than that (5 F/g) of pristine MWNTs. The reason can be the increase of both internal and

external surfaces of the MWNTs coated during the electrochemical polymerization of pyrroles. PPy also provided additional contributions from pseudo faradaic processes to the final capacitance of the nanocomposites, making CNT/PPy promising materials for electrochemical capacitors. [34]

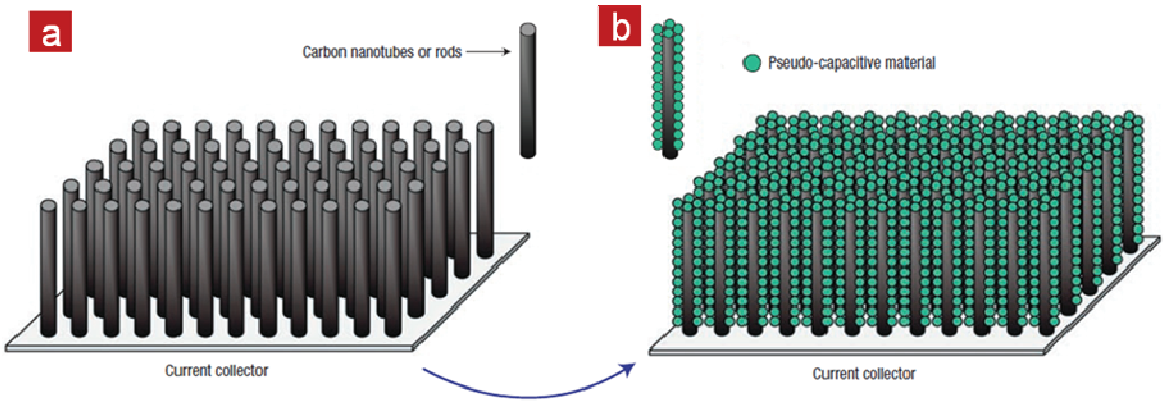

Fig.1-8 *A possible strategy to improve both energy and power densities for electrochemical capacitors by achieving conformal deposit of pseudo-capacitive materials (b) onto highly ordered high-surface-area CNTs (a).[25]*

It has been predicted that the performance of electrochemical capacitor can likely be improved further with replacing SWNT bundles and MWNTs with unbundled SWNTs.[3] However, the higher synthesis cost of SWNTs largely hampered their mass usages when compared to other types of porous carbon materials. Most synthetic procedures for CNTs require high energy input and purification procedures with a low yield, especially in the case of SWNTs where precise control over electronic properties makes them cost prohibitive. Therefore, further lowering the price of CNTs will definitely make a big step towards the large-scale application of CNTs in commercial electrochemical capacitors.

1.2.2 Lithium ion batteries

A lithium-ion battery (LIB) is mainly composed of a lithium-ion intercalation anode (generally graphite), a cathode (typically the lithium metal oxide, $LiCoO_2$), an electrolyte (ionic conductor and electronic insulator) and a separator.[35] The LIBs operates through

movement of lithium ions from the cathode to the anode upon charge and its reversible process during discharging, as demonstrated by the schematic in Fig. 1-9.

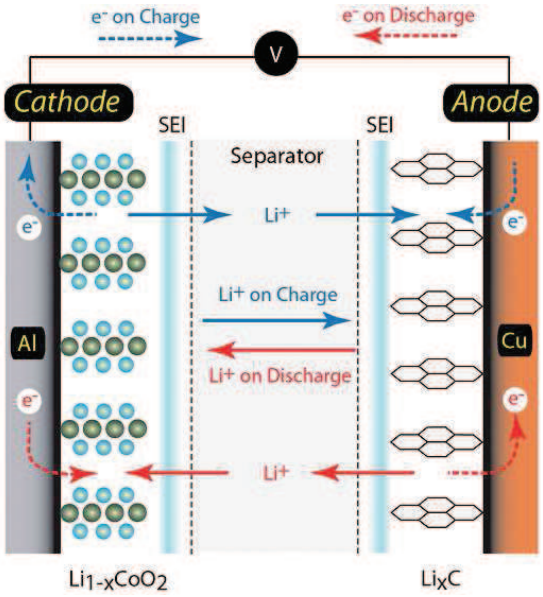

Fig.1-9 *Schematic image for illustrating the mechanism of operation for a LIB including the movement of ions between electrodes (solid lines) and the electron transport through the complete electrical circuit (dashed lines) during charge (blue) and discharge (red) states.[2]*

LIBs can benefit from an increase in energy density, cycle life and rate capabilities by a desirable modification of cell design and selection of novel active materials.[36] CNTs are a good candidate material for use in LIBs because of the high reversible component of storage capacity at high discharge rates. CNTs have the capability to be assembled into free-standing electrodes (without any binder or current collector) as an active lithium ion storage material. The lithium ion capacity in CNTs results from effective diffusion of lithium ions into stable sites located on the nanotube surface and/or inside individual nanotubes through topological defects on the side walls and open ends.[2] The maximum reported reversible capacity is 1000 mAh g^{-1} for SWNTs mechanically milled,[3] as compared to 372 mAh g^{-1} [37] for graphite and 708 mAh g^{-1} [38] for ball-milled graphite. Due to the absence of rigid metal

current collector, the free-standing electrode holds promise for flexible lithium rechargeable battery, which is much desirable for various types of soft portable electronic equipment, such as roll-up displays.[39]

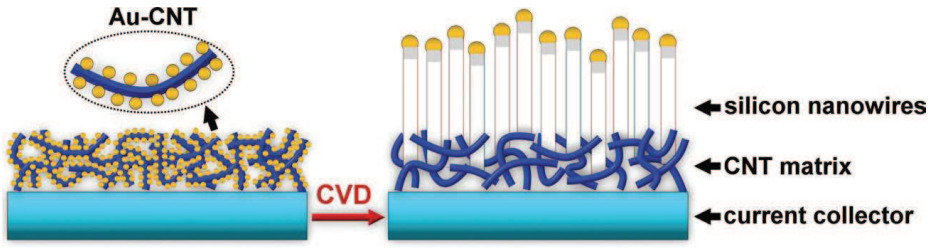

Fig. 1-10 *Schematic diagram showing the fabrication of the silicon nanowire arrays on carbon nanotube (Si nanowire-CNT) arrays on a current collector (stainless steel substrate).[40]*

In addition to the free-standing electrode application of CNTs, there are further benefits to LIBs using CNTs as additives in composite electrodes (anode or cathode) and as a physical support for ultra high capacity nanostrucured anode material, like Germanium nanoparticles (1600 mAh g^{-1}),[41] Si nanowires (4200 mAh g^{-1}) [40] and SnO_2 nanofilms (781 mAh g^{-1})[42]. Typically, the challenging issues for both conventional cathode (e.g. $LiMn_2O_4$) and anode materials (e.g. Si) in LIBs are the low intrinsic electronic conductivity and severe volume swing (>300%) during Li insertion/extraction processes, leading to severe pulverization and electrical disconnection from the current collector, and thus a poor cyclability and fading capacity.[40] The introduction of CNTs into composite electrodes as conductive additive or physical support can effectively solve such problems. The high accessible surface area not only can enable good contact between electrode particles, but also can effectively prevent the volume expansion/contraction during Li charge/discharge process as a soft matrix which absorbs the internal stress.[42, 43] Very recently, Li and his coworker [40] reported the utilization of CNT-metal nanoparticle hybrids to grow one-dimensional Si nanowires and thus synthesized well-aligned Si nanowire-CNT arrays on stainless steel substrates (Fig. 1-10). The CNTs provided a robust electrical contact between Si nanowires and current collectors. As compared to the Si nanowires grown directly on substrates, the

electrodes composed of Si nanowires arrays on CNT matrix show a significantly improvement (2300→3050 mAh g^{-1}) in areal capacity at high charge/discharge current rates because of improved utilization of the CVD Si deposition.

Despite of great improvement in reversible capacity and rate capability achieved by introducing CNT into LIBs, the first cycle charge loss and discharge voltage profile currently limit energy storage density and energy efficiency, [2, 3] as compared with those of other competing materials. Opening nanotube ends and separating chiral fractions are expected to offer significantly improvements in CNT electrode over state-of-the-art.

1.2.3 Dielectric-based capacitors

A dielectric capacitor is a passive component used to store energy in an electric field. One common construction consists of two electrodes separated by a dielectric. If a potential difference (voltage) is connected across the electrodes, a static electric field develops across the dielectric, causing accumulation of charges on plates and polarizations inside the dielectric (Fig. 1-11). This storage mechanism allows for very fast energy uptake and delivery (milliseconds to nanoseconds, Fig. 1-6) due to the absence of limitation of electrochemical kinetics, as is the case of electrochemical capacitors and/or LIBs.[2, 25]

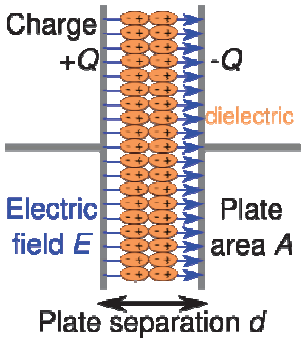

Fig. 1-11 *Simple schematic of a standard capacitor with a dielectric.*

The dielectric capacitors have had an important role in complementing or replacing batteries in the energy storage field, such as pulsed power systems, which converse prime electric energy into short pulses that are used to energize loads for directed kinetic energy

weapons and high power microwaves, and electromagnetic armor.[44, 45] However, these potential applications are severely hindered by the low energy density of capacitors with currently commercial dielectrics.

Generally, the energy density (U_e) of a dielectric material is the shaded area as illustrated schematically in Fig. 1-12, which is equal to the integral

$$U_e = \int EdD \tag{1-3}$$

where E is the electric field and D is the electric displacement (charge density). For a linear dielectric material, such as polymers and their composites,

$$U_e = \frac{1}{2} DE \tag{1-4}$$

$$D = \varepsilon_r \varepsilon_0 E \tag{1-5}$$

$$U_e = \frac{1}{2} \varepsilon_r \varepsilon_0 E^2 \tag{1-6}$$

where ε_r is the effective dielectric permittivity, ε_0 is the permittivity of free space ($=8.85\times10^{-12}$ F/m).

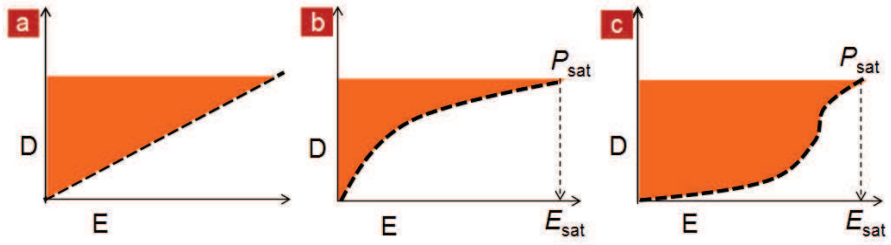

Fig. 1-12 *Electric energy density of (a) linear, (b) ferroelectric, and (c) antiferroelectric dielectrics. The shaded area is related to the stored energy density.*

In the linear dielectric, the dielectric constant does not change with applied electric field, Energy storage is dominated by the field that can be applied on a capacitor, which is limited by the film's dielectric breakdown strength (E_b). Therefore, to increase the energy density of capacitors, it is essential to develop dielectric materials with high permittivity (ε_r) and high

strength E_b.

Conventional high-ε_r ceramic material such as barium titanate ($BaTiO_3$) can be fabricated into thin films by using chemical solution deposition yielding a high dielectric permittivity of about 2500 and relatively low loss tangent (tanδ). [46] However, they require a sintering process at high temperature, which is not compatible with most of substrate materials. Furthermore, the ceramic is easy to be fractured under a stress and a poor flexibility so that they are not suitable to fabricate a large area thin film. Also high cost for production and large density are disadvantages for the use of high-ε_r ceramic materials. Polymer dielectric materials have good processability with high electric breakdown field, which is suitable for high-U_E capacitors, but the low dielectric permittivity (usually ε_r<3) may cause the high energy density in the dielectric polymers to strongly rely on the high electric breakdown field (E_b >500 MV/m). [47] For example, biaxially oriented polypropylene (BOPP) has high dielectric strength (E_b=640 MV/m), but the maximum of energy density is only 1.2 J/cm^3, which is limited by the low dielectric permittivity of BOPP (ca. 2.2).[45]

Recently, a few strategies, including modification of polymers, [47-49] polymeric foamed structure[50] as well as random composite[26], have been developed to increase the energy density of polymers. Chu et al. [47] obtained a very high energy density with fast discharge speed and low loss in defect modified polyvinylidene fluoride (PVDF) polymers. The resultant ferroelectric terpolymer poly(vinylidene fluoride-trifluoroethylene -chlorofluoroethylene) [P(VDF-TrFE-CFE)] has a dielectric permittivity as high as 50, the highest in known unfilled polymers. An electric energy density can thus be measured at 9 J/cm^3 under 400 MV/m, which is higher than known polymers and other film capacitors.[48] However, the use of toxic chemicals is not favorable from the environmental and health point of view. Thakur et al.[51], for the first time, successfully realized an environmentally friendly aqueous functionalized PVDF through the refluxing method. The detailed functionalization

procedures and possible mechanism are presented in Fig. 1-13. The dielectric permittivity and loss tangent for the dopamine functionalized PVDF have been found to be of 32 (higher than 10 for pristine PVDF) and 0.04 respectively. An energy density of 2.7 J/cm^3 was achieved at 140 MV/m well below the breakdown strength of the polymer film.

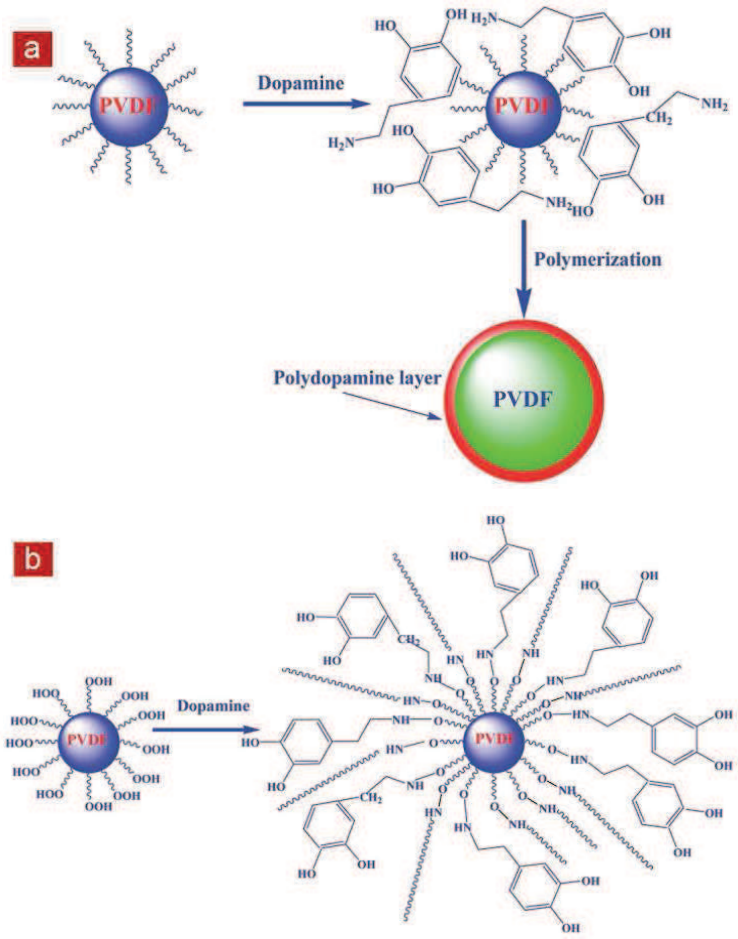

Fig. 1-13 *(a) Schematic illustration of the procedure for functionalization of PVDF with dopamine and (b) the possible mechanism for bonding of dopamine with PVDF. [51]*

Rahimabady et al. also [52] prepared a dense α-phase blend films of VDF oligomer and PVDF of various compositions from chemical solution deposition. The microstructure of the blend was schematically illustrated in Fig. 1-14. Despite the dielectric permittivity of the films was unexpectedly lower than either of the two components, the dielectric breakdown strength is much high (>850 MV/m vs. 300-500 MV/m for typical PVDF films), leading to a

maximum polarization of 162 mC/m^2 and a large electric energy density up to 27.3 J/cm^3. The properties were attributed to the unique blend structure with high crystallinity and densely packed rigid amorphous phase incorporating long and short chains (Fig. 1-14).

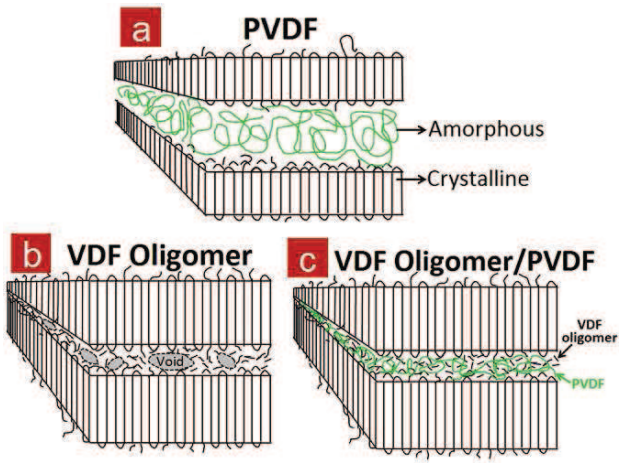

Fig. 1-14 *Schematic illustrations of the microstructure of (a) PVDF, (b) VDF oligomer, and (c) VDF oligomer/PVDF blend. The green (or light) and black lines represent PVDF and VDF oligomer molecular chains, respectively.[52]*

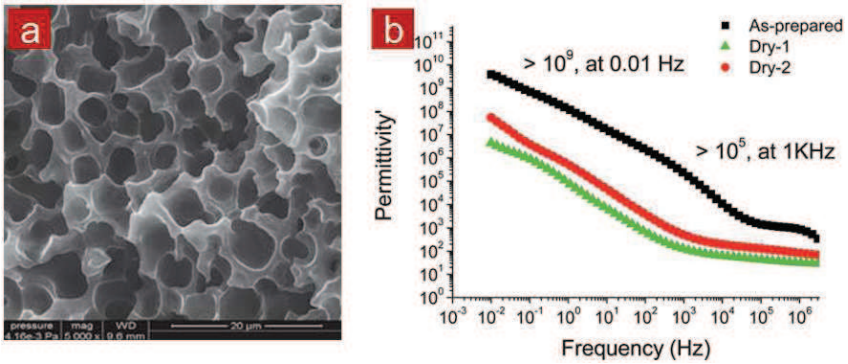

Fig. 1-15 *(a) SEM images of porous structures of PEKK foam and (b) its relative permittivity as a function of frequency. [50]*

Li et al. [50] fabricated a homogeneous sulfonated poly(etherketoneketone) (PEKK) foam through a facile and energy efficient hydration reaction induced self-foaming approach with water serving as the blowing agent. The resulting microcellular PEKK foam possessed a dramatically high permittivity (10^9 at 0.01 Hz and ca. 10^6 at 1000 Hz) (Fig. 1-15).

Unfortunately, the dielectric loss, between 2 and 10 over the whole frequency range, is a little high for usage in energy storage devices.

Among all the approaches to increase the permittivity of polymers, the composite technology is most intensively studied due to its processing ease and a large tunability of dielectric properties by selection of fillers with various properties (e.g., size, shape and conductivity etc.) as well as control of the microstructures of composites (e.g., filler dispersion and distribution). The introduction of ceramic nanoparticles into polymer matrices to form 0-3 dielectric nanocomposites represents one of most promising and exciting avenues in this field. [53, 54] The created composites combine the advantages of ceramics and polymers, and represent a novel type of material that is flexible and easy to process, and is of relatively high dielectric permittivity and high breakdown strength. To realize a high enough value of dielectric permittivity, very high filler loading is in general necessary, usually over 50 vol% to reach. Such high loading of ceramic powders significantly deteriorates the mechanical performance of final composites. The porosity caused by high loading can dramatically decrease the dielectric properties of the composites.

An alternative strategy is to develop high-ε_r percolative composites filled with conductive or semiconductive fillers, such as metal particles,[55-57] carbon fiber,[58] CNTs,[59-61] and graphite nanoplates.[62] As described by the power law, the ε_r of polymer can be dramatically increased by the introduction of conductive fillers near the percolation threshold (f_c). In light of the microcapacitor model,[56-59, 62] fillers distributed in the insulated polymer matrix can form into a large number of microcapacitors so as to improve the ε_r of the polymer composites greatly. Among these fillers, CNTs have been most intensively studied, as their large aspect ratio can lead to percolation levels in nanocomposites at much low loading.[60] To clarify the emerging problems and to provide a comprehensive understanding to this topic, we will review the recent progress in the fundamentals, processes and properties of CNT-based polymer composites in the following sections. Some long-standing problems and topics that warrant further investigations in the

near future will be addressed.

1.3 CNT-based dielectrics for energy storage

As a milestone, superior electrical properties of nanotubes offer exciting opportunities for new high-ε_r polymer composites. Apart from electrical properties, nanotubes also impart better mechanical properties to composites at relatively low filler content.[63, 64] Higher surface area and larger aspect ratios are responsible for superior dielectric properties of nanotube composites. [26, 59, 65, 66]

1.3.1 Fundamental aspect of high-permittivity composites

1.3.1.1 Polarization and relaxation of dielectric materials

In general, the permittivity of an insulating material depends on the frequency (ν) in Hertz (Hz) of the applied electric field and can be described as a complex physical quantity, where the imaginary part is related to dielectric loss. The frequency dependence reflects the possible existence of dispersive behaviors somewhere in the electromagnetic spectrum. The relative dielectric permittivity is a frequency dependent complex quantity.

$$\varepsilon^*(\omega) = \varepsilon'(\omega) - \mathrm{j}\varepsilon''(\omega) \tag{1-7}$$

where ω is angular frequency and $\omega = 2\pi\nu$, $\varepsilon'(\omega)$ denotes the real part of dielectric permittivity and $\varepsilon''(\omega)$, the imaginary part. Usually the dielectric permittivities of materials listed in databases are measured at a frequency of 1 MHz unless otherwise specified. The real part ε' is always above 1 and represents the contribution to the polarization responsible for the energy storage in the material. In order to address its substantial independence on the electric field, it is often referred to as the relative dielectric permittivity of a material. The imaginary part ε'', usually called dielectric loss, shows possible dissipative effects and its frequency spectrum differs from zero only in dispersive regions. Sometimes, the dissipative behavior is characterized by means of the so-called loss tangent, which is defined as:

$$\tan\delta(\omega) = \varepsilon''(\omega)/\varepsilon'(\omega) \tag{1-8}$$

In a homogeneous material, the polarization and thus $\varepsilon''(\omega)$ result from various contributions. The latter add up to give an effective relative complex dielectric permittivity ($\varepsilon^*_{\text{eff}}$), which may be defined in a very general form as follows:

$$\begin{aligned}\varepsilon^*_{\text{eff}} &= \varepsilon^*(\omega) + \sum_i \varepsilon^*_{\text{MW,i}}(\omega) + j\left(\frac{\sigma_{\text{DC}}}{\omega\varepsilon_0}\right) \\ &= \left(\varepsilon'(\omega) + \sum_i \varepsilon'_{\text{MW,i}}(\omega)\right) + \text{j}\left(\varepsilon''(\omega) + \sum_i \varepsilon''_{\text{MW,i}}(\omega) + \frac{\sigma_{\text{DC}}}{\omega\varepsilon_0}\right)\end{aligned} \tag{1-9}$$

where $\varepsilon'_{\text{MW,i}}$ accounts for the i^{th} interfacial contribution and σ_{DC} is direct current (DC) electrical conductivity. It is worth noting that all the dispersive phenomena associated with the intrinsic polarization are accounted for $\varepsilon^*(\omega)$ in Eq. 1-9. In the presence of multiple intrinsic relaxations, $\varepsilon^*(\omega)$ can be expressed as a superposition of individual contributions. Indeed, each relaxation process, either orientational or interfacial, can be analytically described by means of a proper relaxation function. In the simplest case of a material consisting of identical and non-interacting dipoles and whose relaxation is characterized by a unique time constant τ, Debye derived a relaxation function for the complex permittivity in the associated dispersion region.[37] In the frequency domain, the Dyebe model gives the well-known formula:

$$\varepsilon^*(\omega) = \varepsilon_\infty + \frac{\varepsilon_s - \varepsilon_\infty}{1 + j\omega\tau} \tag{1-10}$$

where ε_s and ε_∞ represent, respectively, the static (relaxed) and the high frequency (unrelaxed) values of the permittivity with respect to the considered process. For a material showing a unique dipolar relaxation in its whole spectrum, ε_∞ in turn coincides with the aforementioned relaxed value of the deformational permittivity. Eq. 1-10 can be spitted in its real and imaginary parts and then equivalently expressed by the following pair of equations:

$$\varepsilon'(\omega) = \varepsilon_\infty + \frac{\varepsilon_s - \varepsilon_\infty}{1 + \omega^2\tau} \tag{1-11a}$$

$$\varepsilon''(\omega) = \frac{(\varepsilon_s - \varepsilon_\infty)\omega\tau}{1 + \omega^2\tau} \tag{1-11b}$$

Due to the very simplistic assumptions above, the Debye model fails in describing

relaxation phenomena in complex systems. Thus, Havriliak et al. proposed a more general formula using a phenomenological approach. [37] It has the merit of including the possibility of a distribution of different time constants through the introduction in Eq. 1-11a of two shape parameters α and β:

$$\varepsilon^*(\omega) = \varepsilon_\infty + \frac{\varepsilon_s - \varepsilon_\infty}{[1+(j\omega\tau)^{1-\alpha}]^\beta} \quad \text{(For polymer, } 0<\alpha<1,\ 0<\beta<1\text{)} \tag{1-12}$$

Actually, the occurrence of a dispersive process of any nature in the frequency region of interest represents a drawback. In order to advantageously exploit the application of a dielectric material, the effective loss factor should be kept as low as possible. In fact, losses not only waste part of the input energy, but also worsen the insulation properties of the materials. In particular, for any dielectric material it is possible to identify a threshold electric field, which generates irreversible modifications in the medium accompanied by the onset of an intense and disruptive flow of charges. Such a sudden loss of insulation due to a very high electric field is called dielectric breakdown of the material. The minimum field responsible for such an effect is named breakdown field or breakdown strength (E_b). For most polymers, E_b is in the range 10^6-10^8 V/m. Up to now, it is still difficult to make a reliable prediction of E_b according to the present physical models. In fact, there are several possible causes and processes related to dielectric breakdown. However, it is generally accepted that mechanisms responsible for dielectric discharges have both thermal and intrinsic (bulk) origins. In the first case, both dielectric polarization and conduction losses determine a temperature increase of the material. Indeed, the power density dissipated into the dielectric medium, at the expense of the electric field, is proportional to $\varepsilon''_{\text{eff}}(\omega)$:

$$W \propto \omega \left|\vec{E}\right|^2 \varepsilon''_{\text{eff}}(\omega) \tag{1-13}$$

Such a heating in turn enhances the conductivity in a self-amplified process with catastrophic consequences. In fact, the amount of heat that the material is not able to dissipate drives it to the breakdown. As a second possibility, breakdown may be related to an avalanche discharge process that begins with the promotion of few valence electrons to the

conduction band. These electrons, being accelerated by the applied electric field, strike against other valence electrons, driving them to the conduction band by a kinetic energy transfer; as this process of charge carrier multiplication goes on, the current flow grows rapidly in the dielectric and the material can locally melt.

1.3.1.2 Theoretical models for dielectric properties

In a high-ε_r composite, fillers impart mainly dielectric properties while the matrix phase imparts mechanical properties. Properties of composite generally show different trends in electrical properties compared to pure constituent phases. Several mixing rules have been proposed to account for the effective permittivity improvement of a system consisting of two immiscible phases or multiphase.

Maxwell-Garnett equation

A number of models have been proposed and used for predicting the effects of second phases on the dielectric properties of the composites. Among these models, those pertaining to continuous media filled with spherical particles are considered as a starting point for discussion. To start with mixing rules, consider an isotropic medium (matrix) of dielectric permittivity ε_m filled with spheroids of permittivity ε_f. The volume fraction of filler particles is designated as ϕ_f and the resulting volume faction of the matrix $\phi_{\mathrm{m}} = 1 - \phi_f$. It is assumed that both the filler and matrix components have no dielectric loss in frequency regions of interest.

For any two-phase composite one can write the lower permittivity, which denotes a series model as shown in Fig. 1-16a,

$$\varepsilon_{\mathrm{c,min}} = \frac{\varepsilon_m \varepsilon_f}{\varepsilon_m \phi_f + \varepsilon_f \phi_m} \tag{1-14}$$

and the upper dielectric permittivity, which corresponds to a parallel model as shown in Fig. 1-16b.

$$\varepsilon_{c,max} = \varepsilon_m \phi_m + \varepsilon_f \phi_f \quad (1\text{-}15)$$

This means that for a given physical system, the dielectric function ε_c must lie between these bounds. Namely, the permittivity of a two-phase composite is between the $\varepsilon_{c,min}$ and $\varepsilon_{c,max}$ ($\varepsilon_{c,min} \le \varepsilon_c \le \varepsilon_{c,max}$), which can be described by mixing models with series and parallel in consistent with practical composites as shown in Fig. 1-16c.

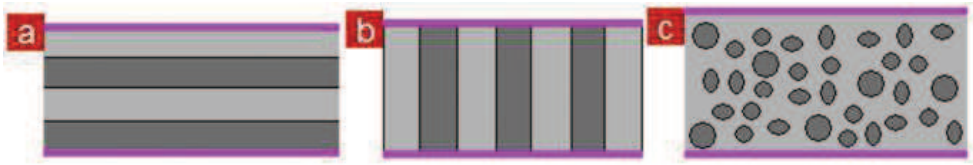

Fig. 1-16 *Ideal connection ways of two-phase composites, (a) series model, (b) parallel model, and (c) a mixing model, pink lines stand for electrodes.[26]*

Beyond such rough limits, further steps in modeling the dielectric properties of binary mixtures have been accomplished in the framework of the so-called Wagner theoretical schemes.[26] By equating these two alternative expressions, the so-called Sillars [67] or Landzu-Lifshitz [68] rules can be obtained as follows:

$$\varepsilon_c = \varepsilon_m [1 + \frac{3\phi_f (\varepsilon_f - \varepsilon_m)}{2\varepsilon_m + \varepsilon_f}] \quad (1\text{-}16)$$

However, these rules hold only for low volume fractions of filler and are restricted by electrical conductivity values of filler and matrix. More accurate equation for predicting dielectric properties can be achieved by the following equation known as Maxwell-Garnett equation.[69-71]

$$\varepsilon_c = \varepsilon_m [1 + \frac{3\phi_f (\varepsilon_f - \varepsilon_m)}{(1-\phi_f)(\varepsilon_f - \varepsilon_m) + 3\varepsilon_m}] \quad (1\text{-}17)$$

This equation considers the dielectric permittivity arising from spherical fillers dispersed in a medium. It should be noted that Maxwell-Garnett rule does not consider the resistivity of medium or filler particles and hence gives advantage over Landu-Lifshitz mixing rule, which

is limited only to composites where fillers should have higher electrical resistivity than matrix. In the literature, Maxwell-Garnett equation is expressed in many forms and is also referred to several other names such as Maxwell-Wagner[72] or Rayleigh [73]or Kernner-Bottcher [74] equation. One of such Maxwell-Garnett equation forms is given below,

$$\frac{\varepsilon_c - \varepsilon_m}{\varepsilon_c + 2\varepsilon_m} = \phi_f \frac{\varepsilon_f - \varepsilon_m}{\varepsilon_f + 2\varepsilon_m} \tag{1-18}$$

This equation is applicable only to spherical particles. However, when dispersed particles are not spherical in shape, it needs to be modified in order to take into account the geometry of dispersed particles. A common way to include the information about the geometry of dispersed particles is to introduce a depolarization factor, which is related to their deviation from sphericity. Thus, Maxwell-Garnett could be changed into this form to make it more general.[75]

$$\varepsilon_c = \varepsilon_m[1 + \frac{\varepsilon_f(\varepsilon_f - \varepsilon_m)}{A(1-\phi_f)(\varepsilon_f - \varepsilon_m) + \varepsilon_m}] \quad \text{for} \quad \phi_f < 0.1 \tag{1-19}$$

where the parameter A is the depolarization. When A = 1/3 equation turns back to Eq. (1-18). The value of A can be calculated or can be found in the literature. [37]

Lichtenecker rule

Lichtenecker's idea was based on the Wiener theory for bounds of effective dielectric function or effective conductivity of a composite.[76] According to Weiner's theory, the lower and upper bounds are represented in Eqs. 1-14 and 1-15. The upper bound for this effective dielectric function is reached in a system consisting of plane-parallel layers disposed along the electric field. The lower bound is reached in a similar system, but with the layers perpendicular to the field. Similar results were obtained using the method of cross-sections. Starting from Eqs. 1-14 and 1-15, Lichtenecker assumed that the effective dielectric function of the considered composite satisfies the equation:

$$\varepsilon_c^{\alpha} = \phi_m \varepsilon_m^{\alpha} + \phi_f \varepsilon_f^{\alpha} \tag{1-20}$$

where the parameter α varies from -1 to 1. Thus, the extreme values of this α index correspond to the Wiener boundary values. The parameter α may be considered as describing a transition from anisotropy at α = -1 to isotropy at α =1. Each α value describes a specific microgeometrical topology of a composite. One can therefore expect that the applicability of Eq. 1-20 is wider than that of the well-known Maxwell-Garnett and Bruggeman equations that, in general, have no free parameters related to the topology. Several examples of applications of Lichtenecker's equation can be found, especially in Ref. [76]. At the same time, it is not very clear for what systems this Eq. 1-20 is valid, and what is the range of its universality.

Percolation model

The use of conducting fillers is motivated by the fact that they not only increase conductivity but also induce Maxwell-Wagner polarization. As a result, the polarization leads to a high dielectric permittivity in filler-polymer composites. In general, the electrical conductivity of conductive filler-polymer composites exhibits a non-linear increase when the concentration of fillers approaches a percolation threshold. This phenomenon cannot be explained by classical mixing rules but by percolation theories. At low concentration of filler, conductive particles are separated from each other (see Fig. 1-17a and b) and the electrical properties of the composites are dominated by the matrix. With increasing filler concentration, local clusters of particles are formed, which is shown in Fig. 1-17c. At the percolation threshold, these clusters form a connected three-dimensional network through the component (see Fig. 1-17d), resulting in a jump in the electrical conductivity.

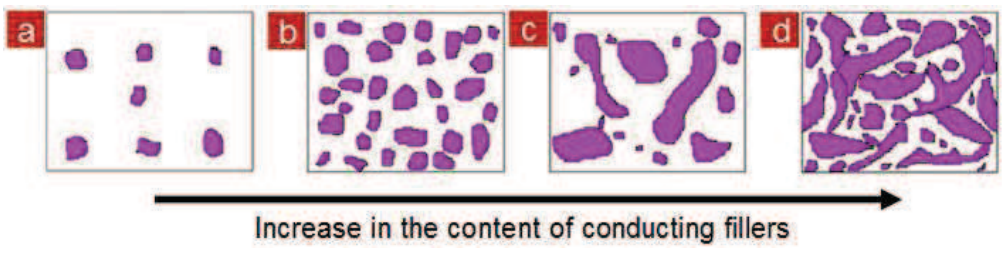

Fig. 1-17 *Schemes showing the formation of a percolation-like clusters structure with an increase in the concentration of conducting fillers in a composite. (a) randomly dispersed grain structure; (b) uniformly dispersed grain structure; (c) aggregated grain structure; (d) percolation-like clusters structure.[37]*

The microstructures shown in Fig. 1-17 are isotropic, which are formed by spheres or spheroids with random orientation. When the spheroid grains of the minor phase are oriented, the microstructures become anisotropic, as shown in Fig. 1-18. Furthermore, if conducting fillers have a high aspect (length/diameter) ratio, the anisotropic microstructure of composites can more easily be formed. In this case, the percolation threshold in the oriented direction can be very low and the composite can exhibit excellent flexibility.

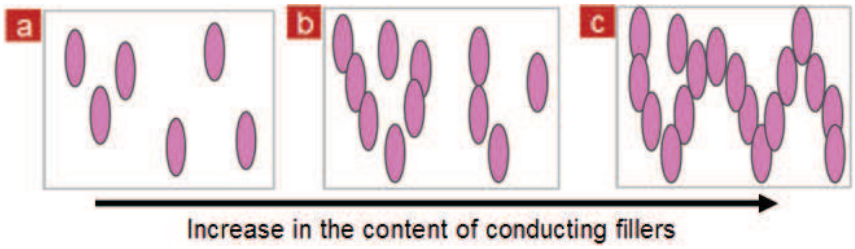

Fig. 1-18 *Schematic microstructure of a two-phase composite with oriented minor-phase spheroids. [37]*

In fact, when the concentration of conducting fillers is close to the percolation threshold, the composites often display a metal-insulator transition in electrical property. Namely, the percolation threshold represents the filler concentration at which conducting paths come into contact with each other throughout the medium. The percolation theory allows estimating f_c with power laws describing the conductivity of the composite near the metal-insulator transition by fitting the experimental σ data for $f_{filler} > f_c$ and $f_{filler} < f_c$. They often abide the following relations:[26, 37]

$$\sigma_c \propto \sigma_m (f_{filler} - f_c)^t \qquad \text{for} \quad f_{filler} > f_c \tag{1-21a}$$

$$\sigma_c \propto \sigma_{filler} (f_c - f_{filler})^{-s} \qquad \text{for} \quad f_{filler} < f_c \tag{1-21b}$$

$$\sigma_c \propto \sigma_{filler}^{u} \sigma_m^{1-u} \qquad \text{for } |f_{filler} - f_c| \to 0 \qquad (1\text{-}21c)$$

where σ_c, σ_{filler}, σ_m are the conductivity of composites, filler and matrix, respectively, f_c is the percolation threshold, t the critical exponent in the conducting region, s the critical exponent in the insulating region, and $u = t/(t+s)$. Two-phase random media normally have a value of about 0.16 for the percolation threshold. The universal values of both critical exponents t and s are commonly 1.1-1.3 for two dimensional fillers, while t=1.6-2.0 and s=0.7-1.0 for three-dimensional ones.

Besides the conducting network established through the intimate connection between adjacent conducting fillers (Fig. 1-17d and Fig. 1-18c), there is another mechanism for the percolation, namely the Coulomb blockage and tunneling. In this case, the conductive particles are connected not geometrically but electrically via tunneling. Such a tunneling mechanism would lead to the nonuniversality of the critical exponents. Actually, a nonunversal critical exponent t as large as 5-10 has been observed in percolative composites. [37, 77-79]

When the percolation threshold is approached from below, the dielectric permittivity ε'_c of the composites diverges as follows:[26, 37]

$$\varepsilon'_c \propto \varepsilon'_m (f_c - f_{filler})^{-q} \qquad \text{for } f_{filler} < f_c \qquad (1\text{-}22)$$

where ε'_m is the permittivity of the matrix, and q dielectric critical exponent of approximately 1. The critical behavior of the dielectric permittivity near percolation can be explained by employing the microcapacitor model. Namely, each two neighboring conductive particles are treated as a local capacitor with the fillers as two electrodes and a very thin layer of dielectric in between, and a network of local capacitors expands between two virtual electrodes with increasing the filler content. Each microcapacitor contributes an abnormally large capacitance. The large capacitance contributed by each of these microcapacitors can then be correlated with a significant increase in the intensity of local electric field when the conductive filler are very close to each other near f_c. The significant increase in the intensity

of the local electric field promotes the migration and accumulation of the charge carriers at the filler/matrix interfaces. These charges are generated either by surface plasma resonance or by charge injection from the external electrodes, depending on the relaxation times of the two phases. This interfacial polarization, also known as the Maxwell-Wagner effect, is responsible for the significant increase in permittivity at low frequency.[78] Whereas, the comparatively frequency-independent dielectric permittivity comes from the frequency response of the matrix.

Additionally, the percolation threshold also depends upon the size and shape of conducting fillers. Common conductive fillers are metallic or graphitic and are in different shapes (spherical, platelet-like or fibrous) and sizes. However, the incorporation of CNT, because of their large aspect ratio, allows for a low percolation threshold,[80] as illustrated in Fig. 1-18. In addition, the dielectric values in these percolative systems are very sensitive to the concentration of fillers. A slight change in concentration near the percolation threshold can bring about a drastic change in dielectric properties. Parallel increases of dielectric permittivity and loss are frequently observed and needed to be largely suppressed.

1.3.2 Processing for CNT-based dielectric composites

Homogeneous dispersion of CNTs into polymer matrices is crucial to the properties of high-ε_r composites, especially in the field of functional applications. All the processes used normally aim at distributing and dispersing the CNTs in the polymer matrices in a desired manner. There are mainly two types of dispersion processes: solid phase processes and liquid ones. The former often call up mechanical approaches. Usually they are very simple and straightforward and rely directly on mixing the nanotube with the aid of mechanical force and can be used widely in practical production due to their convenience, low cost and mass production. Mechanical mixing processes can be divided into categories: direct mixing and melt mixing. A big challenging issue for mechanical mixing processes lies in relatively poor dispersion and weak interfacial interaction between fillers and polymer matrices in comparison to chemical ones (also named as liquid phase processes), which often ensure

better dispersion of fillers and stronger interfacial interaction.

1.3.2.1 Direct compounding

Direct mixing involves the mixture of CNTs and polymer without any pre-treatment. Such a process has been attempted by Haggenmueller et al. [81] They cut into small pieces a MWNT/PMMA composite sample in which the MWNT were visibly not well dispersed. They mixed those pieces and hot pressed the mixture to create a new sample. They repeated this cutting and mixing procedure 20 times and found that the MWNT dispersion quality was improved. Their comment about the quality was based on sections of the sample observed under an optical microscope. By employing a direct mixing process, Dang et al. fabricated PVDF composites based on MWNT,[64] and (MWNT-$BaTiO_3$)[82]. Those composites showed different dielectric properties, depending on the type of the filler. A big disadvantage of the direct mixing process lies in that it is not efficient at dispersing fillers at the nanoscale if fillers tend to agglomerate. A pre-treatment for fillers is usually necessary to achieve reasonable dispersion.

1.3.2.2 Melt mixing

To mix CNT with highly viscous fluids, especially thermoplastic melts such as polyethylene (PE) and polystyrene (PS), one could rely on high shear forces to break down CNT aggregates and to improve CNT dispersion. Twin screw extruders are the most popular equipment for dispersing and processing CNT-based composites owing to their good dispersive and distributive mixing capability[83]. For example, McNally et al. [84] incorporated MWNTs into PE matrix by melt mixing using a mini-twin screw extruder. The electrical conductivity of PE was increased significantly, by 16 orders of magnitude, from 10^{-18} to 10^{-2} $S.m^{-1}$. However the percolation threshold (f_c =7.5 wt %) was relatively high due to the decrease of MWNT aspect ratio as a consequence of inevitable breakage during melt-mixing. In our group, we also fabricated a nanocomposite by melt-blending the pristine MWNTs within PVDF.[65] A giant dielectric permittivity (ca. 3800) was observed over a

critical content of MWNT. Unfortunately, the composites possessed a high value of f_c (10.4 vol %) mainly due to a significant polymer wrapping on the nanotubes. Moniruzzaman et al.[85] mixed SWNTs in epoxy at 100 rpm for 1 h in a twin-screw batch mixer and claimed that a uniform dispersion was achieved. However, Sandler et al.[86] used a stir to mix MWNT in epoxy at 2000 rpm for 5 min and still found MWNT aggregates dispersed in the resin. The discrepancy shows the fact that the high speed mechanical stir or magnetic stir can not generate sufficiently high shear stress to break down nanotube aggregates as an extruder does. Safadi et al.[87] found that ultrasonic agitation improved the CNT dispersion by decreasing the CNT aggregates in size and in some cases even separated the CNT. However, the usefulness of ultrasonic agitation is limited to low viscosity media. It should also be emphasized that extrusion and ultrasonic agitation, the two most frequently used processes for dispersion, may cause damage to CNT surface and may also lead to attrition in CNT length which may be partially responsible for deterioration of mechanical and dielectric properties of CNT-based polymer composites. However, the viscosity of polymer melts usually increases after addition of fillers, especially at high concentrations of fillers. In such cases, processing of polymer melts becomes more difficult.

1.3.2.3 Solution route

At high filler concentration, melt mixing is not necessarily the best choice for composite processing because of higher viscosity of the mixture. By contrast, high concentrations of fillers can be incorporated into polymer matrices by using solution processing. This process involves dispersion of both polymer and filler in a solvent. However, most systems require the use of large volumes of solvents to fully dissolve the polymer and disperse the filler. Since common solvents such as toluene, chloroform, tetrahydrofurane (THF), or dimethyl formamide (DMF) are of high toxicity, a number of aqueous systems have been explored. Solution casting has been used to manufacture MWNT-based PS, [87-89] polyhydroxyaminoether (PHAE), [90] polyvinyl alcohol (PVA), [91] and ultrahigh molecular weight polyethylene (UHMWPE) [92] composite films with homogeneous nanotube

dispersions. Similarly, SWNT-based polypropylene (PP),[93] PVA,[94] composite films have been prepared. For example, Zhang et al.[95] prepared a CNT/polymer nanocomposite by using a coagulation method. The permittivity enhancement ($\varepsilon_r/\varepsilon_m$ at 10^2 Hz) was 2 for the nanocomposite with 2 wt % CNT. Besides, untreated MWNTs have been ultrasonically dispersed into PVDF solution. A $\varepsilon_r/\varepsilon_m$ (at 10^2 Hz) of 6 was observed in the resultant composite at f_c =1.6 vol %.[64] Ultrasonication processes are evidenced to effectively aid nanotube dispersion in liquid media. Nevertheless, prolonged high-energy sonication has the potential to introduce defects to nanotubes.[96] Ultrasonic treatment may also stabilize the dispersion by grafting polymers onto the CNT surface through trapping of radicals generated as a result of chain scission.[97] In addition, surfactants,[98] polymer-functionalized nanotubes,[94] and other chemical treatments of the constituents[99] are often employed.

DMF dissolves PVDF well. As a result, it is often used to prepare CNT/PVDF composites with high dielectric permittivity. After the PVDF is dissolved in DMF, MWNT are mixed with PVDF solution, respectively [7, 26, 60, 63, 64, 100, 101]. In short, solution processes can be very efficient to disperse fillers into PVDF polymer matrix.

1.3.2.4 In situ polymerization process

In situ polymerization processes for fabricating polymer composites are usually associated with better filler to matrix interactions leading to improved electrical and mechanical properties. A number of works have used such processes to prepare nanotube/polymer composites.[102, 103] Cochet et al. [103] prepared polyaniline (PANI)/MWNT composites by an in situ polymerization process in the presence of MWNT. Their results revealed site-selective interaction between the quinoid ring of the PANI and MWNT, thus paving the way to charge transfer processes, and improving the electrical properties of the final composites. Clayton et al. [104] prepared polymethyl methacrylate (PMMA)/SWNT composites via in situ polymerization induced either by heat, ultraviolet light, or ionizing radiation. The composites exhibited an enhanced transparency and improved dielectric permittivity. Xie et al. [105] reported the synthesis of

poly(2,5-benzoxazole)/MWNT composites by in-situ polycondensation and found the dielectric permittivity of the composites was significantly enhanced from 4 of the polymer matrix to 65 with the incorporation of 5 wt% MWNTs. In situ polymerization processes allow for homogenous dispersion of functional fillers and therefore ensure strong interfacial interaction between the fillers and the polymer. As a result, the composites display excellent electrical properties. However, the narrow monomer selection window impedes its wide application in various composites.

In summary, the preparation process is very important for polymer composites because it has a crucial effect on their dielectric properties. The type of process and its operation conditions should be defined based on the physical, chemical, rheological and thermal characteristics of the system.

1.3.3 Dielectric properties of CNT-based composites

To date, CNT based composites are the most intensively studied percolative system with high permittivity. [59, 60, 63, 64, 106] Enhanced permittivity values have been observed from hundreds [59, 64] to more than 4000 [60]. The large deviations of the dielectric permittivity observed by different researchers can be largely attributed to differences in the properties of the matrices and CNTs employed, as well as the dispersion state and spatial distribution of CNTs in the polymer matrix. In this section, we will discuss in detail the parameters that largely influence the dielectric properties, and strategies proposed accordingly to increase permittivity of the CNT-based composites.

1.3.3.1 Effect of polymer matrix

As seen from Eq. 1-22, polymers with higher intrinsic dielectric permittivity are desirable for pursuing the high-permittivity polymer composites. However, most polymers exhibit an intrinsic dielectric permittivity of less than 5. Ferroelectric polymers, such as PVDF ($\varepsilon_r \approx 10$),[107] or relaxor ferroelectric polymers, such as P(VDF–TrFE–CFE) ($\varepsilon_r \approx 50$),[48] possess higher dielectric permittivities than normal polymers. Numerous

works have demonstrated successful applications of these polymers in percolative polymer composites with high permittivity.[26, 59, 60, 64, 82, 95, 108-111] However, the dielectric performance of the final composites with these ferroelectric polymer matrices was largely compromised by their high dielectric loss, which is usually caused by the dipole-dipole interaction within the polymer chains, especially near the resonance frequency.

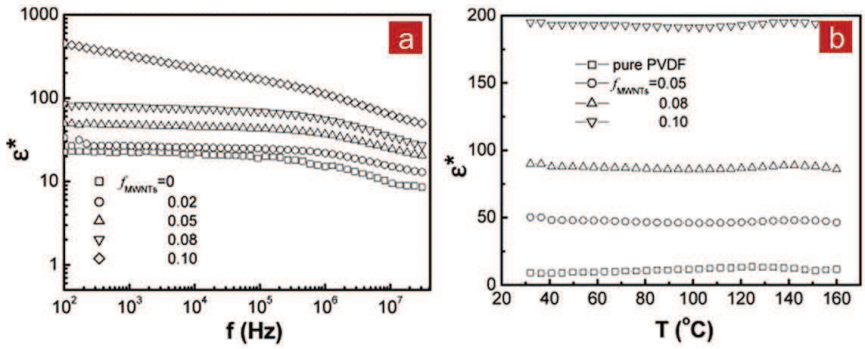

Fig. 1-19 *The dielectric permittivity of the (MWNTs-$BaTiO_3$)/PVDF composites as a function of frequency and temperature. [82]*

Due to the little choice of pure polymer with high permittivity, other strategies have been proposed to obtain percolative composites. Among them, Dang et al. [82] demonstrated a mixture-matrix approach, where 20 vol% of $BaTiO_3$ particles was compounded with PVDF to form a mixture matrix with an improved permittivity (10→40), and following the incorporation of MWNTs. The MWNT particles formed a percolating network in a three-phase composite, resulting in a high permittivity of 450 (Fig.1-19a). Additionally, the dielectric permittivity had a good thermal stability in the temperature range of 30-160 ℃ (Fig.1-19b). Unfortunately, the percolation threshold observed was a little higher (9 vol%) than that reported for most other CNT/polymer two-phase composites.[60, 64, 95, 112] The higher f_c may be as a consequence of the fact that MWNTs in the three-phase composites were not straight tubes but twisting ones and prone to aggregate into clusters.

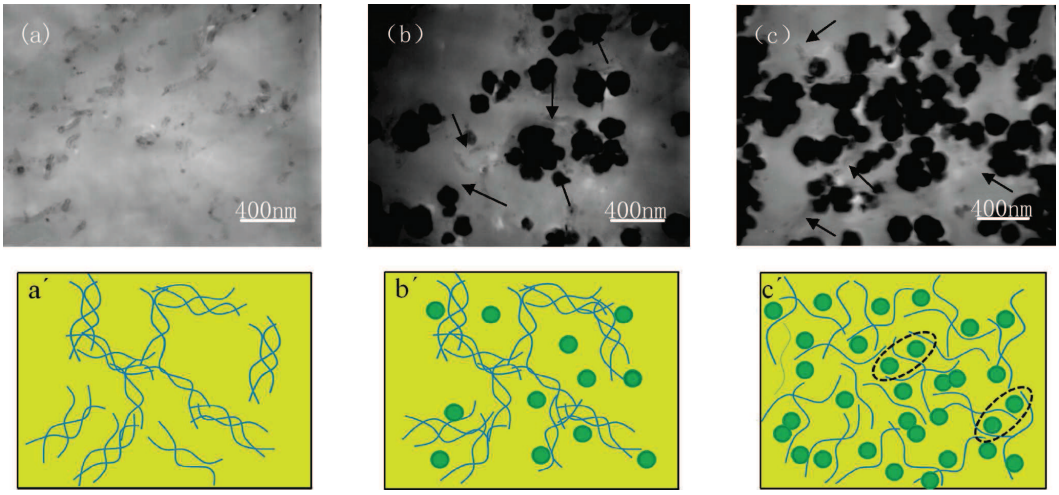

Fig. 1-20 *TEM images of the freeze-fractured (MWNT-$BaTiO_3$)/PVDF composites with $BaTiO_3$ loading at (a) 0, (b) 5 vol%, (c) 20 vol%, and the corresponding schematic illustration of the microstructure of the (MWNT-$BaTiO_3$) /PVDF composites at (a') 0, (b') 5 vol%, (c') 20 vol%, in which the blue lines stand for the MWNTs and the green balls are $BaTiO_3$, and the region in dash circles shows the interfaces and microcapacitor structure.[113]*

Yao et al.[63, 108, 113] then further studied the effect of $BaTiO_3$ particle content on the dielectric behavior in a (MWNT-$BaTiO_3$)/PVDF system. The results showed that when the content of MWNTs was 1 vol% and 2 vol% respectively, the increase in dielectric permittivity of the three-phase (MWNT-$BaTiO_3$)/PVDF composites was different, largely depending on the $BaTiO_3$ loading. This difference can be attributed to the detailed microstructure of the three-phase (MWNT-BaTiO3)/PVDF composites due to the loading variation of MWNT and $BaTiO_3$. Fig. 1-20 shows TEM images of the fractured two-phase and three-phase composites with a fixed MWNT content of 2 vol%. With the absence of nanosized $BaTiO_3$, MWNTs trend to be poorly dispersed and a network of aggregated MWNT bundles is observed (Fig. 1-20 a and a'). Moreover, a more effective three-dimensional conductive network has been formed because of the additional connection of the isolated MWNT bundles (Fig. 1-20 b and b'), when the volume fraction of $BaTiO_3$ is increased to 5vol%. In contrast, the image of composites with the 20 vol% of $BaTiO_3$ shows

significant improvement in MWNT dispersion. MWNT particles are well separated by $BaTiO_3$ particles rich areas. The aggregated MWNT bundles mentioned above cannot be seen any more (Fig. 1-20 c and c'). Based on the microstructure evolution processes, an adjustable dielectric property can be obtained and presented in Fig. 1-21. A significantly enhanced dielectric permittivity (643 at 10^3 Hz) and a gradually decreased loss are found in the three-phase (MWNT-$BaTiO_3$)/PVDF composite.

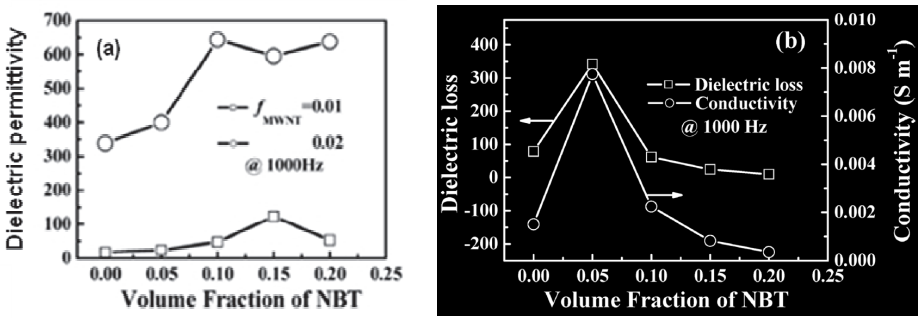

Fig. 1-21 *(a) Dielectric permittivity, (b) dielectric loss (left) and AC conductivity (right) as a function of the volume fraction of $BaTiO_3$ measured at room temperature and 10^3 Hz. [113]*

The major drawback of such a three-phase approach is that the additional inorganic particles, such as ceramic [63, 108, 113], increase the total loading of rigid particles in the polymer matrix and thus decrease the flexibility of the polymer composites.

1.3.3.2 Effect of CNT morphology

CNT aspect ratio

When spherical conducting fillers are used to improve the dielectric permittivity of the composites, the percolation threshold is often very high. This is a big disadvantage for flexibility of polymer composites. Therefore, conducting fillers with high aspect ratio (AR) are often used in order to have a lower percolation threshold. [59, 60, 63, 64, 106] The morphology of CNT has a remarkable effect on the dielectric properties of composites.

Higher aspect ratio of nanotube is an obvious advantage for their use in high-permittivity composite. However, in some cases extremely large AR would tend to give rise to the entanglement of nanotubes and destroy their effectiveness.

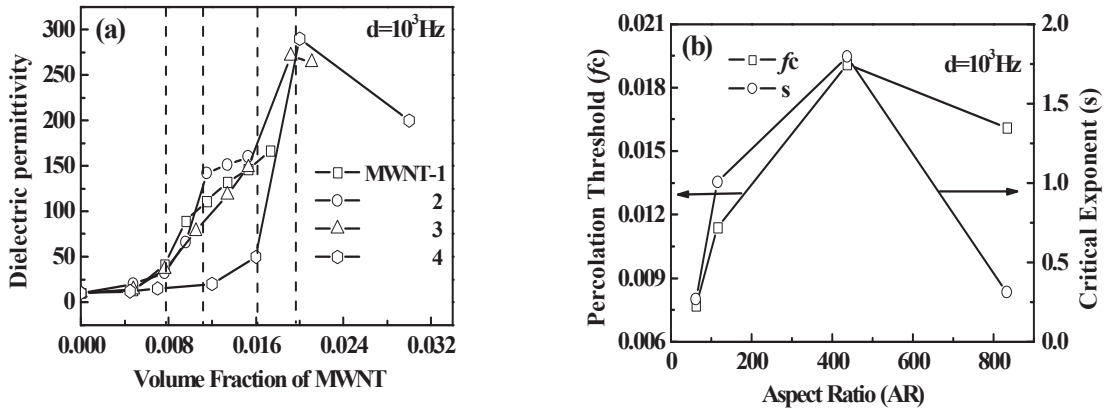

Fig. 1-22 *(a) Dependence of dielectric permittivity of MWNT/PVDF composites on the MWNT volume fraction measured at room temperature and 10^3 Hz. (b) Dependence of percolation threshold and critical exponent on the average AR value of MWNT. [59]*

Yao et al. [59] studied the effect of aspect ratio of MWNT on the percolation threshold, as shown in Fig. 1-22. An increase in dielectric permittivity with increasing AR of MWNT was observed in the composites. Meanwhile, the change in percolation threshold was complex and at the first glance surprising. The percolation threshold first increased with increasing AR, reached a maximum at a certain AR and then decreased with further increasing AR. Entanglement of the nanotubes would explain the results. An increase in the entanglement of nanotubes results in an increase in the percolation threshold. It is likely that the entanglement reduced the effective aspect ratio of the nanotubes. As MWNT become more flexible with increasing AR, they may have strong tendency to form interlocked inherent structures, like group of threads, and would not exhibit rod like rigidity anymore. In spite of nanotube entanglement at highest AR, MWNT provide enough conductive paths to eclipse the effect of entanglement and would result in lower percolation threshold in practice.

CNT surface modification

Previous studies have demonstrated that large slenderness ratio of CNT can always result in a very low f_c. However, a critical obstacle in using CNT filler is that it is difficult to disperse them well in most polymer matrices because of the presence of strong interaction among nanotubes. This interaction originates from physical attraction via van der walls forces, hydrogen bonding and chemical bonding. A great effort has been put to find suitable processes to disperse nanotubes into polymer matrices. One of the most effective ways is to create interfacial bonding between nanotubes and polymer matrices. For this purpose, surfaces of nanotubes are modified with certain organic groups such as carboxylic, fluoro, amino.[26] In fact, this method is not only limited to nanotubes but can also be used for other types of fillers. The increase in interfacial bonding promotes the dispersion of nanotubes, which in turn improves the dielectric properties. Several studies have shown improved dielectric properties of composite after surface treatment of fillers like CNTs.

Dang et al.[60] reported very high dielectric permittivity for functionalized TFP-MWNT/PVDF nanocomposites using MWNT that was chemically modified with 3,4,5-trifluorobromobenzene (TFBB). The dielectric permittivity can reach 4000 when the volume fraction of TFP-MWNT is 0.15 (Fig. 1-23). The very high dielectric permittivity originated from the Maxwell-Wagner-Sillars (MWS) effect at percolation threshold, and was attributed to a thin insulating layer of PVDF that was part of the TFP-MWNT. The nomadic charge carriers were blocked at the internal interfaces between the TFP-MWNT and the PVDF, and the large π-orbital of the MWNT provided the nomadic electrons with large domains. Strongly electrophilic F groups on the TFP-MWNTs further reinforced the MWS effect.

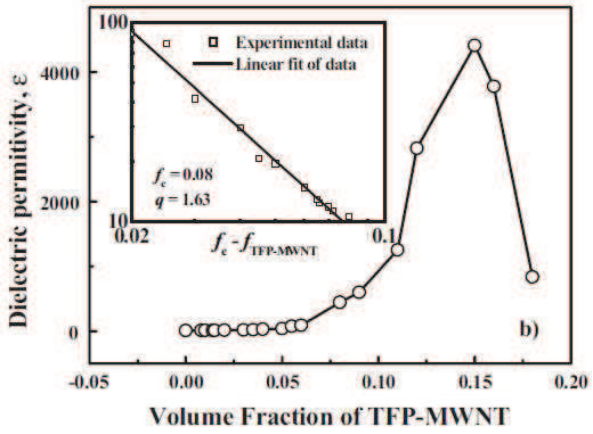

Fig. 1-23 *Dependence of the dielectric permittivity of the TFP-MWNT/PVDF nanocomposites on the TFP-MWNT volume fraction, measured at room temperature and* 10^3 *Hz. The inset shows the best fit of the dielectric permittivity to Eq. 1-22. [60]*

It is very difficult to gauge the interfacial bonding. Researchers have used atomic force microscopy to measure the force required to separate an embedded nanotube from a polymer matrix, which can be used to estimate the interfacial bonding.

Core-shell structures of CNTs

With approaching the percolation threshold, the remarkable improvement in the permittivity is always accompanied by an unacceptable dielectric loss due to the tunneling or ohmic conduction between the neighboring particles. To overcome this issue, one straightforward approach is to introduce additional interlayers or insulating shells on the conductive fillers to prevent them from connecting with each other directly. The rationales are as follows: i the tunneling current between the neighboring fillers can be suppressed and hence lead to lower dielectric loss; ii the interlayers make control of the detailed and sensitive microcapacitor structures near f_c more easier, which generally gives rise to a considerably expanded compositional window for percolative composites.

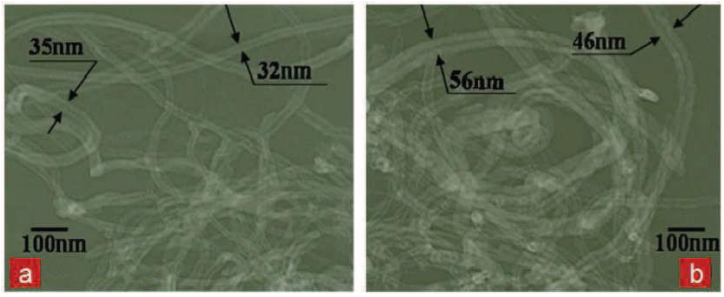

Fig. 1-24 *TEM micrographs of (a) uncoated MWNTs and (b) MWNTs@PPy.*

A number of researchers have actively investigated the effect of shell on filler surfaces on the dielectric behavior of percolative composites. Yang et al. [114] successfully coated the MWNTs with organic shells PPy by an inverse microemulsion polymerization. TEM images of MWNT gave the thickness of the PPy layer was in the order of 10 nm (Fig. 1-24). Such PPy-coated MWNT/polystyrene composites presented a high dielectric permittivity (~44), low loss (< 0.07), and thus a high energy density (4.95 Jcm^{-3}). The significantly enhanced dielectric performance originated from the organic shell PPy, which not only enable good dispersion of MWNTs in the polymer matrix but also screen charge movement to shut off leakage current as a barrier.

Very recently, Liu et al. [115] modified MWNTs with jeffamines T403 and established a strong interaction between T403-functionalized MWNTs (MWNT-T403) and polysulfone (PSF) polymer matrix due to the ester and ether groups on the surface of MWNT-T403. Afterwards, they used a simple electrospinning method (Fig. 1-25a) rather than directly adding the MWNT-T403 into PSF to prepare MWNT-T403/PSF composite nanofibers with MWNT-T403 coated by PSF (Fig. 1-25b). These electrospun composite nanofibers were then collected in the form of a sheet on a rotating drum, and several plies of the sheets were stacked along the same fiber direction. These sheets with nanofibers lying down in the plane were finally molded by the hot-pressing near the softening temperature of PSF perpendicular to the fiber direction to form the MWNTs array (Fig. 1-25a). The organic PSF dielectric coating on MWNT not only acts as a barrier to prevent MWNTs from direct connection, but also as a polymer matrix after fusion by hot-pressing at 175 °C. The resultant

MWNT-T403/PSF composites showed a high permittivity (ca. 58) when the content of MWNT-T403 reached 25 vol%, while there is only a slight change in loss (0.02→0.05 at 1 MHz) (Fig. 1-25d). And also, a maximum energy density of 4.98 kJ L^{-1} was observed when MWNT-T403 was up to 15 vol%, as shown in Fig. 1-25e.

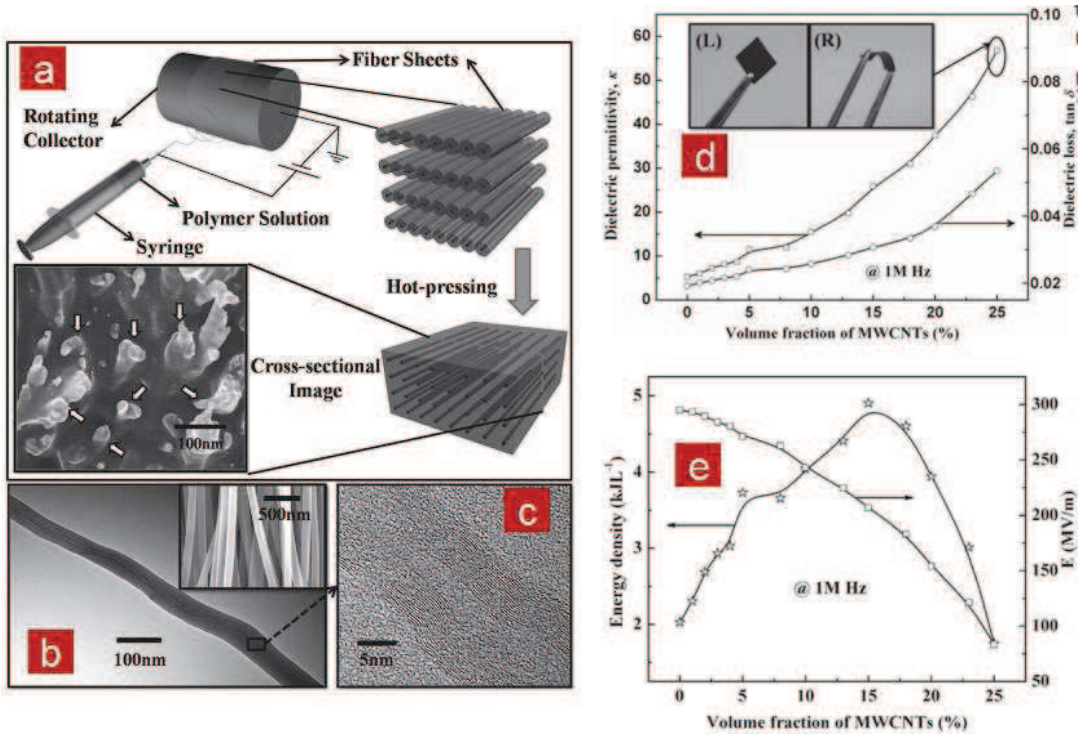

Fig. 1-25 *(a) Schematic for preparation of MWNT-T403/PSF composites. The inset shows the cross-sectional SEM image of the composites perpendicular to the fiber direction, MWNTs are indicated by arrows. (b) TEM images for MWNT-T403/PSF core/shell nanostructure. The SEM image in the inset shows the MWNT-T403/PSF nanofiberous sheet prepared by electrospinning. (c) High-resolution TEM image of a MWNT. (d) Dependence of the dielectric permittivity and loss of the composites on the MWNT-T403 loading, measured at room temperature and 1 MHz. The flexibility of the composite is demonstrated in the photograph in the inset. (e) Energy density and breakdown strength of the composites with different MWNT-T403 loading. [115]*

Shells on the conductive fillers with good integrity are desirable in the pursuit of high dielectric permittivity in that they provide a better insulating barrier for quantum tunneling and suppress the leak current resulting from quantum tunneling. However, the existed preparation methods for the organic shells on CNTs are time and energy consuming. Future efforts should be directed more toward the cost-effective methods which also show good compatibility with the current electronic industry.

1.3.3.3 Spatial distribution of CNTs

To improve the performance of CNT-based dielectric composites, continuous effort has been devoted to raise the dielectric permittivity of composites at low f_c in order to maintain the inherent polymer matrix flexibility and low cost. The recent theoretical and experimental investigations indicate that the percolation threshold of CNT/polymer composites depends strongly on not only the physical properties of CNTs[59] (e.g., conductivity and aspect ratio) but also their dispersion state[116] and distribution status[117] in polymer matrices. Therefore, tremendous research and development efforts are devoted to design an optimized state of aggregation and distribution of CNTs in host polymers to reduce the percolation threshold. An efficient strategy is to confine CNTs in any one of the phases of a co-continuous biphasic polymer blend or at the interface, by which the percolation threshold can be substantially reduced due to the double percolation. The concept of double percolation was initially described by Sumita et al.[118] in 1991 for carbon black (CB) filled immiscible blends. Since then, it has been implemented for several blend systems and can be applied to a variety of carbonaceous fillers, such as CB,[118-120] carbon fibers,[121] CNTs,[83, 117, 122-124] and graphite nanosheets.[125] In the case of CNT-filled polymer blends, preliminary studies have explicitly studied the heterogeneous morphologies (sea-island or co-continuous phase structure) of various blend systems characterized by the preferential location of CNTs in one of the phases. It has been substantially demonstrated that the electrical and/or mechanical properties of CNT-filled polymer blends can be significantly improved, once the double percolation occurs, i.e., the CNT-filled blend phase percolates

(first percolation) and the CNTs forms a network within the percolated blend phase (second percolation).

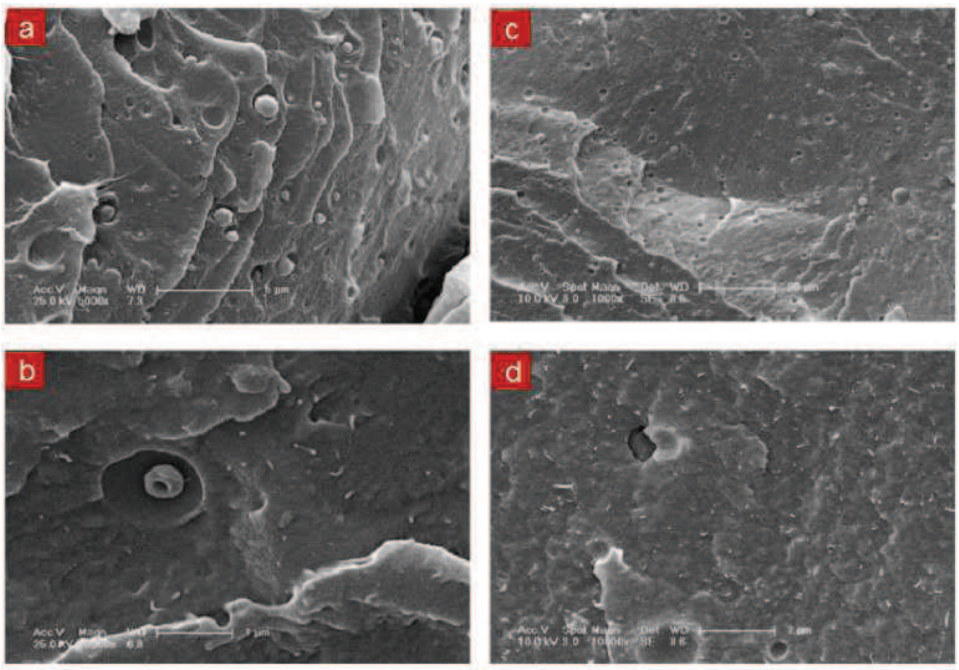

Fig. 1-26 *SEM images of cryofractured surfaces of blend composites. (a,b) based on PC containing 0.25 wt% MWNT, prepared from a PE concentrate with (a) 24 wt% MWNT and (b) 44 wt% MWNT; (c,d) based on PA containing 1 wt% MWNT prepared from a PE concentrate with 24 % MWNT illustrating the blend structure (c) and the homogeneous dispersion of nanotubes in the PA matrix (d). [117]*

Pötschke et al.[117] have introduced MWNTs into thermoplastic matrices, polycarbonate (PC) and polyamide (PA), by melt blending using PE based concentrates with high MWNT loading (24-44 wt%). The MWNTs migrated from PE concentrates to PC or PA phase and remained in their excellent dispersion state (Fig. 1-26). Thus, electrical percolation is achieved at significantly lower MWNT contents as compared to direct incorporation. For PC, it is shifted from 0.75 to 0.25 wt%.

Wu et al.[124] have prepared CNT-filled polyethylene terephthalate (PET)/PVDF blend composites. It was observed a 2500 % improvement in electrical conductivity, 36 % augment

in tensile strength and 320 % increase in elongation over the CNT-filled PET with the same filler content. The author ascribed the improved properties to the formation of a double percolated structure resulting from the selective location of CNTs in the PET phase.

Based on the progress toward understanding the effect of the double percolated structure on the electrical and mechanical properties,[83, 122-124] it is reasonable to expect that such double percolated structure allows for using few amount of CNTs to raise the permittivity to a same level with CNT-filled single phase polymer composites. However, to the best of our knowledge, dielectric blends with CNTs have rarely been investigated in the literature. The effect of double percolation on the dielectric permittivity is still elusive and requires a thorough investigation, especially when the interactions between the two continuous polymer phases would be involved.

1.3.3.4 External field effect

Despite tremendous progress towards understanding the CNT's effect on dielectric behaviors of polymer composites, most of the reported studies either challenged the uniform dispersion of CNTs in polymer matrices, or revealed the mechanisms of the high dielectric permittivity. However, little was found on the dependence of the dielectric properties on the extensive external fields such as force (tensile strain), electric and magnetic field. It has been demonstrated that these external fields played a crucial role in defining the internal microstructure of composites, such as molecular arrangement of polymers and the spatial distribution of CNT fillers, which in turn highly affected the macroscopic physical properties of composites.[63, 126-130]

Choi et al.[127] prepared an aligned CNT/epoxy composite by using a 25 T magnetic field processing. The thermal and electrical conductivity along magnetic field alignment direction were increased by 10% and 35% respectively, relative to those of randomly-oriented CNT composites.

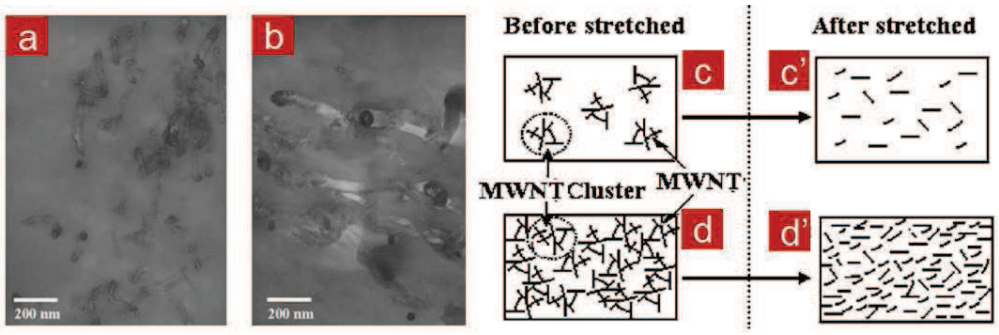

Fig. 1-27 *Morphologies of samples (a) perpendicular and (b) parallel to the tensile-strain direction in the MWNT/PVDF composite with 2.0 wt% MWNT. Schematic images of MWNT distribution in polymer composites at low (c) and (c') and high (d) and (d') concentrations of MWNT before (c) and (d) and after (c') and (d') stretching, respectively. [131]*

Dang et al. [131] studied the effect of tensile strain on the dielectric properties of MWNT/PVDF composites by comparing dielectric permittivity and conductivity of composites before and after stretching. After stretching, CNTs were prone to align in the direction parallel to the tensile-strain direction, as shown in Fig. 1-27a and b. The dielectric permittivity and conductivity after stretching were always lower than those before stretching. In the composites with high concentration of MWNT, the decreases in dielectric permittivity and conductivity were very significant. This variation in dielectric properties was derived from the disentanglement of MWNT clusters and the rearrangement of individual MWNT along the tensile-strain direction as a preferential orientation (Fig. 1-27c and d). This suggested that the detailed microcapacitor structure of CNTs responsible for the high permittivity is very sensitive to the external tensile stretching.

1.4 Concluding remarks

This chapter provides a thorough review on the structure and properties of CNTs and their applications in the energy storage systems, especially the use in percolative dielectric composites. Despite significant progress has been made in the development of high-energy-density composites based on CNTs, there still exist some challenging issues that hamper the further improvement of dielectric performances.

Firstly, CNT/polymer composites can display high dielectric permittivity near the percolation threshold as a result of the formation of microcapacitors with CNTs as electrode and polymer matrix layer as dielectric in between. However, such microcapacitor structure near percolation threshold is much sensitive to the external extensive fields such as force (tensile strain), electric and magnetic field. These external fields can significantly influence the macroscopic dielectric properties of composites through redefining the microstructure of composites, such as molecular rearrangement of polymers and the change of CNT spatial distributions. Therefore clarifying such effect is of utmost importance and necessity for the real-world applications of such high permittivity CNT/polymer composites.

Secondly, interfaces between CNTs and polymer matrices are crucial for the dielectric performance of the percolative composites. Appropriate surface modification of CNTs can improve their compatibility with polymers and thus result a homogenous dispersion of nanotubes. Better CNT-polymer compatibility can improve the stability of the microcapacitor structure formed near percolation threshold in the composites. It can also minimize defects or voids in the composites that may deteriorate the breakdown strength and thus the overall energy density. Two modification methods have been developed to enhance the interfacial interaction between CNT and polymer matrices. i.e. covalent and non-covalent methods. However, the covalent modification may disrupt the conducting network in the carbon nanotube, thus resulting in a drastic decrease in the electronic properties of CNTs. Hence, non-covalent modification of CNTs seems a promising approach to improve the dielectric performance due to avoidance of scarifying inherent properties of CNTs.

Thirdly, percolation curve is an important characteristic of CNT/polymer composites.

This curve determines the enhancement in permittivity and also the cost of the final composite. Lowering the percolation threshold is always the focus of the whole scientific society. Among all the approaches, the multiphase matrix method is the most simple and effective one, which can be highly compatible with the industry mass production. The percolation threshold can be definitely decreased by a proper selection of biphasic polymer blend as matrix. However, the effect of the double percolation on the permittivity enhancement is still elusive and needs a thorough investigation.

Fourthly, according to the microcapacitor model, CNTs distributed in the insulated polymer matrix can form into a large number of microcapacitors so as to improve the permittivity of the polymer composites greatly. However, CNTs are always frizzy in the CNT/polymer composites, which is not beneficial in forming parallel pair electrodes of microcapacitors. Additionally, the traditional approach to form the microcapacitors is to increase the CNT content and thus decrease the inter-nanotube distance. However, when this distance between neighboring CNTs is reduced down to a certain value, there is a risk of tunneling that would relax the charges generated at CNT/polymer interfaces. To overcome these two issues, aligned CNT arrays can be used as filler to form local microcapacitors in series to store the charges, meanwhile good dispersion of CNT arrays ensures a large separation distance between each other, thus avoids the tunneling conduction between CNT arrays and thus leakage current between two sample surface electrodes. Therefore, the synthesis of CNT array and their isolate distribution into polymer matrix is the key to realize this end.

In this thesis, we will definitely challenge these issues one by one, aiming to elaborate and optimize the CNT-based polymer composites in the view of the electrical energy storage.

Chapter II
Solution-casted MWNT/PVDF composites

2.1 Introduction

CNTs are currently of intense interest as highly promising building block for manufacturing nanostuctured low-cost and high-performance polymer composites. This increasing interest stems from their nanometer-scale dimension, along with their large shape anisotropy and a unique combination of exotic mechanical, thermal and electrical properties.[11, 132-135] As compared to the polymer matrices, CNT composites show significant improvement in tensile modulus,[136] thermal conductivity,[137] electrical conductivity[138, 139] and dielectric properties.[64, 66, 115, 140] Preliminary studies have demonstrated that an ultrahigh dielectric permittivity can be predicted by the implementation of percolation theory just below the threshold, [60, 64-66, 95]. Additionally, the high thermal conductivity of CNTs can improve the heat dissipation and quickly release the undesired heat generated by loss tangent, thus preventing materials from dielectric breakdown. [3, 95] More importantly, these improvements are achieved at a very low loading due to the extremely high aspect ratio of CNT.

Despite tremendous progress towards understanding the CNT's effect on dielectric behaviors of polymer composites, most of the reported studies either challenged the uniform dispersion of CNTs in polymer matrixes, or revealed the mechanisms of the high dielectric permittivity. However, little was found on the dependence of the dielectric properties on the extensive external fields such as force (tensile strain), electric and magnetic field. It has been demonstrated that these external fields played a crucial role in defining the internal microstructure of composites, such as molecular arrangement of polymers and the spatial distribution of CNT fillers, which in turn highly affected the macroscopic physical properties of composites.[63, 126-130] For example, Chio et al.[127] prepared an aligned CNT/epoxy

composite by using a 25 T magnetic field processing. The thermal and electrical conductivity along magnetic field alignment direction were increased by 10% and 35% respectively, relative to those of randomly-oriented CNT composites. Although several studies reported that a unidirectional stretching would also induce the alignment of CNTs in polymer matrices,[63, 126] establishing a correlation of the degree of tube alignment with dielectric properties still remains challenging due to the lack of an effective characterization of the CNT orientation states at different tensile strains.

In this chapter, we prepared a MWNT/PVDF nanocomposite via solution casting, followed by hot-pressing technology. The dielectric permittivity of the composite could be increased to 270 (27 times higher than that of pure PVDF) when approaching the percolation threshold as low as 1.91 vol%. The increase in dielectric permittivity could be derived from the formation of microcapacitor with CNTs as electrode and polymer matrix layer as dielectric in between. To investigate the sensitivity of such microcapacitor structure to the external tensile stress, a composite with MWNT at 2.0 vol% (near the percolation threshold) was chosen to conduct the tensile test and align the CNTs inside the polymer matrix by uniaxial mechanical stretching. The alignment degree of tube was varied by controlling the tensile strain (TS) applied on the composite. The orientation states of MWNTs at different TS were fully quantified by employing an orientation tensor description and further graphically presented with elongated ellipses. The alignment degree of the tube was well correlated with the evolution of dielectric properties of composites.

2.2 Experimental

2.2.1 Materials and sample preparation

The MWNTs were synthesized by CVD method, provided by Shenzhen Nanotech Port Company (China). Their diameter was of the order of 20–40 nm and the length was in the range of 5–15 μm. Semicrystalline polymer PVDF was used as host polymer due to its superior ferroelectric nature. The MWNT/PVDF nanocomposites were prepared via solution casting, followed by hot-pressing technology. Without further purification, MWNTs at an

appropriate amount were mixed with a solvent DMF and pulsated in ultrasonic water bath for 2 h. Meanwhile, PVDF powder was dissolved in the DMF solvent at 50 °C. Then, the MWNT suspension was added into PVDF solution and ultrasonically treated for another 10 min. Afterwards the solution was heated at 60 °C for 8 h to completely remove the solvent. The resultant composite films were then folded and molded by hot-pressing technique at 200 °C and 15 MPa to prepare 1.0 mm-thick plates. Ultimately, the composite plates were cut into dumbbell-shape samples with 50.0 mm in length, 1.0 mm in thickness, and 8.5 and 4.0 mm in maximal and minimal widths, respectively.

2.2.2 Sample characterizations

Tensile tests of the as-prepared dumbbell-shaped composite with 2.0 vol% of MWNT were conducted on CMT4104 electric tensile tester (SANS, China) according to GB/T 528-1998 (ISO 37, 1994) by employing a tensile rate of 10 mm/min. The MWNT/PVDF nanocomposite was mechanically stretched up to the TS of 6.3%, 12.5%, 18.8%, 25.0%, 31.3%, and 37.5% respectively and then the load released. The microstructure of the samples parallel to the tensile-strain direction was examined by TEM (Hitachi H-800), and the ultrathin sections were sliced by microtome under liquid nitrogen cooling. The dielectric properties of all the MWNT/PVDF nanocomposites were measured using an impedance analyzer (Agilent 4294A) in the frequency range from 10^2 to 10^6 Hz at room temperature. The impedance magnitude and the impedance phase were measured using an impedance analyzer (Solartron 1260) in a broader frequency range (10^{-3}-10^7 Hz) at room temperature. For a good electrical contact, sample surfaces were painted with silver paste.

2.3 Results and discussion

2.3.1 Enhanced dielectric permittivity

As expected, the dielectric permittivity increases greatly below percolation threshold. Fig. 2-1a presents that the attained maximum value of the permittivity of the percolative MWNT/PVDF composite is 271, which is 27 times higher than that of pure PVDF (ca.10). The dielectric permittivity shows a divergence at both sides near to the percolation threshold. Such variation of the dielectric permittivity in the neighborhood of the percolation threshold can be well described by the power law (Eq. 1-22).

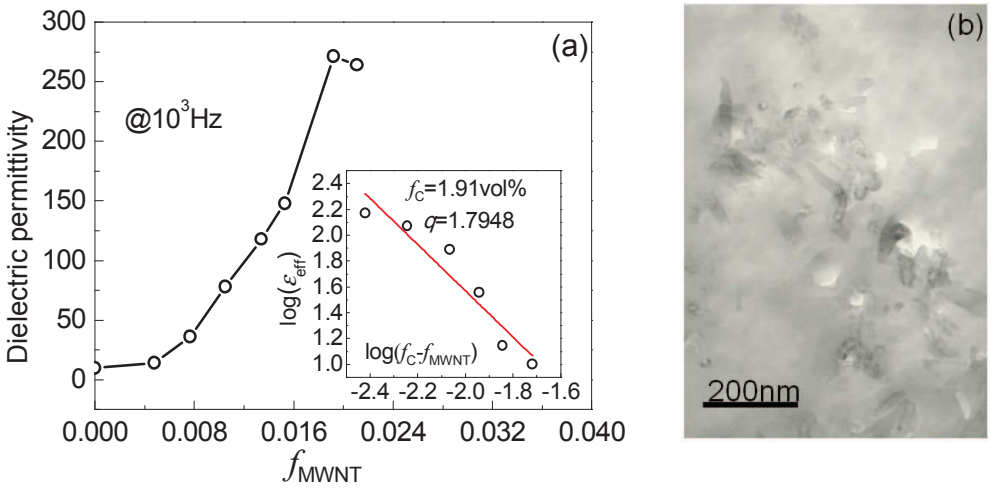

Fig. 2-1 *(a) Dependence of the dielectric permittivity of the MWNT/PVDF composites on the MWNT volumetric fraction, f_{MWNT}, measured at room temperature and 10^3 Hz and the inset in (a) shows the best linear fit of the permittivity to Eq. 1-22. (b) TEM micrographs of the fractured MWNT/PVDF composites with MWNT volume fraction near percolation threshold.*

The best linear fit of the data to the log-log plot of the power law gives f_c=1.91 vol% and q=1.7948. The value of f_c in this case is ten times smaller than that of common two-phase random composites with spherical particles.[37] This is attributed to the extremely large aspect ratio of MWNTs used (~437). However, the dielectric critical exponent is large than the universal one (q_{un}=1) but nearly the same with the 3D lattice value (q_{3D}=2).[64] This

suggests that it is MWNT cluster (3D) rather than individual MWNT (quasi 1D) that forms the percolating path in the composite near percolation threshold. In our case, the nanotubes with extremely large aspect ratio could become flexible and exhibit a strong tendency to form interlocked coherent structures, like a group of threads. Fig. 2-1b shows the TEM image of the MWNT/PVDF composites near percolation threshold. It can be clearly observed the loose aggregations of MWNT, in which it is of large difficulty to distinguish each MWNT.

The increase of the dielectric permittivity can be generally understood from gradually assessing the formation of microcapacitor with MWNTs as electrode and polymer matrix layer as dielectric in between, when the concentration of MWNT increases. The permittivity enhancement ($\varepsilon_r/\varepsilon_m$ at 10^3 Hz) was 27 for the composite with 1.92 vol % MWNT (near f_c), which is much lower than that reported for the chemically modified-MWNT/PVDF composites ($\varepsilon_r/\varepsilon_m$=60 at 10^3 Hz).[60] This limited permittivity enhancement derives from the inefficiency of a part of microcapacitors as a result of the aggregated structure of MWNT as well as the weak interfacial interaction between the pristine MWNTs and PVDF matrix.

2.3.2 Frequency dependence of the dielectric properties

Fig. 2-2 shows the frequency dependence of the dielectric properties of the MWNT/PVDF composites at room temperature. Towards low frequency, the dielectric permittivity of a composite with only 2.0 vol% of MWNT is more than 30 times higher than that of the PVDF matrix (10), reaching up to about 300 (Fig. 2-2a). Of particular interest is that the dielectric permittivity of the MWNT/PVDF composites with low MWNT loadings (e.g., <1.0 vol%) shows a slight correlation to the frequency, while the dielectric permittivity of the MWNT/PVDF composite near the percolation threshold decreases dramatically when the measured frequency is as high as 10^4 Hz. This remarkable relaxation in dielectric permittivity can be attributed to a strong interfacial polarization, which generally occurs at interfaces between electrodes (MWNTs) and dielectrics (PVDF) of the microcapacitors.

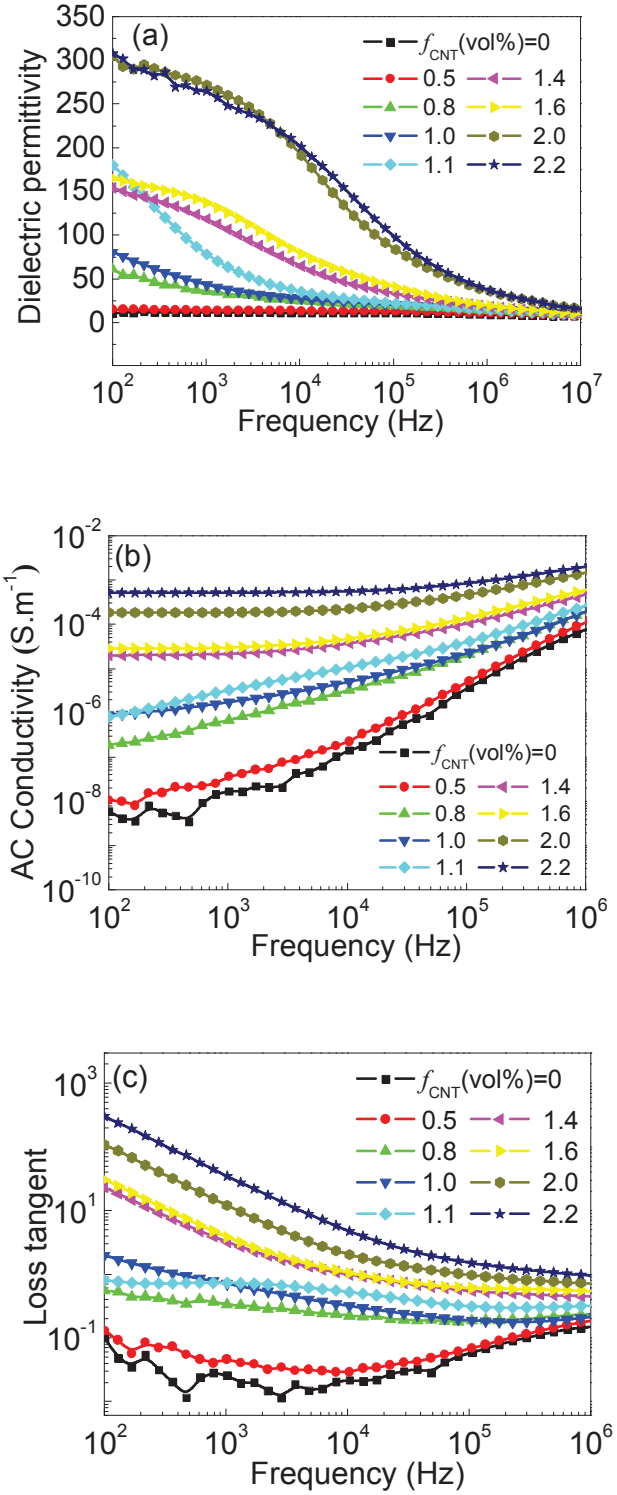

Fig. 2-2 *Dependence of the (a) dielectric permittivity, (b) AC conductivity and (c) loss tangent of the MWNT/PVDF composites on frequency at room temperature.*

According to Fig. 2-2b, at low loadings (<1.0 vol%), the conductivity increases with frequency, showing a nearly linear dependence. The exhibited typical dielectric behavior indicates the absence of conductive path in the composites, which may largely ascribe to the formation of MWNT clusters. In this case, the conductivity is mainly determined by the polarization effects and electron motion in the polymer matrix, which is highly dependent on the frequency.[141] While with the concentration of MWNT approaching f_c, the conductivity values are greatly enhanced and almost independent of the change of frequency in the low frequency range (10^2-10^4 Hz, Fig. 2-2b). The corresponding composites exhibit a DC conductivity behavior, since their conductivity does not change with the frequency. Such DC characteristic in the low frequency range is induced by few percolating paths formed through the polymer matrix. As shown in Fig. 2-2c, the loss tangent maintains at low values (0.04) and displays a similar dielectric relaxation with PVDF matrix only at very low MWNT concentrations (≤0.5 vol%). In this case, MWNT cluster dispersed in PVDF are isolated to each other and the loss tangent originates from the Debye-relaxation.[78] However, once the MWNT loading exceeds 0.8 vol%, a significant increase in loss tangent can be observed, especially at low frequency range, which is not favorable for the energy storage devices. This increase in loss tangent is due to the leakage current induced by the direct contact of inter-and intra-MWNT clusters.

To improve the dielectric performance further, ones have to realize individual nanotube dispersion to create fully efficient microcapacitors. Meanwhile, strong interfacial interaction can bring forth a desirable insulating barrier for the electron transportation between neighboring CNTs and thus reduce the loss tangent of the composites.

2.3.3 Sensitivity of microcapacitor to tensile strain

2.3.3.1 Mechanical behavior

Before investigating the effect of tensile strains on the alignment of MWNTs, it would be of large importance to gain insight into the mechanical behavior of the composites in response to the uniaxial stretching. Fig. 2-3 presents the tensile stress-strain curve of the

MWNT/PVDF nanocomposites. (We are not discussing here the improvement of mechanical property imparted from CNT reinforcement in comparison with the neat polymer.) It can be clearly seen that the tensile stress initially increases linearly with the strain until the proportional limit (TS=6.0%) is reached, which is reconciled with the well-known Hooke's Law. It indicates that in this range (TS<6.0%) the composite behaves elastically and the deformation can be reversible. On the contrary, from TS=6.0% on, the stress-strain curve deviates from the straight-line relationship and the Law no longer applies as the strain increases faster than the stress. When the stress reaches the ultimate tensile strength, the necking begins in the sample. Hence, in the range of TS>6.0%, the material could not return to its initial undeformed state after unloading and ultimately generate permanent deformation in the composite. Therefore, in this study, the tensile strains uniaxially applied on the samples are controlled to start from 6.3% to 37.5% with an interval of ~6.2%, ensuring all the strains are in the plastic region. That means after the release of the load, the stretch-induced tubes alignment can be partially retained inside the composites.

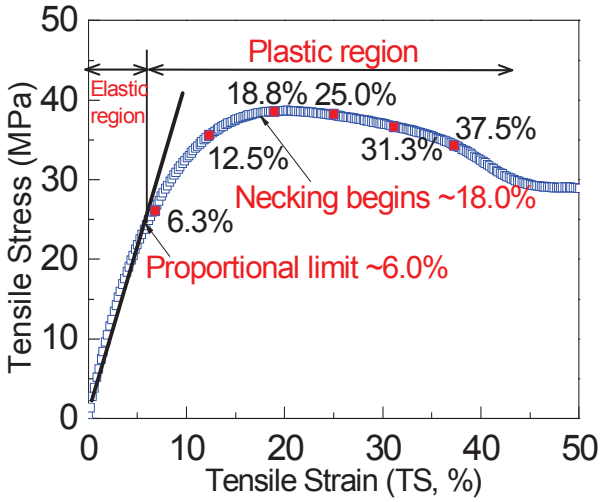

Fig. 2-3 *Tensile stress-strain curve of the MWNT/PVDF nanocomposites with* f_{MWNT}*=2 wt %.*

2.3.3.2 Characterization of the CNT orientation

To elucidate a picture of strains' effect on the tube alignment, it is essential to represent the orientation state of MWNTs at different TS. Development of the orientation tensor description provides an effective way to embody all MWNT directions in the selected region, which has been successfully used to describe the orientation states of short fibers.[142, 143] The second moments of the probability distribution function would be adopted in our study, which are called orientation tensors and are defined as following:[144]

$$\langle a \rangle = \langle p_i p_j \rangle = \oint p_i p_j \varphi(P) dP \tag{3-1}$$

where **P** is the unit vector placed in the average direction of the tube length, as shown in Fig. 2-4a. p_i and p_j are components of this vector along the coordinate directions. In our study, we apply the orientation tensor description in 2D plane (Fig. 2-4b). Thus in two dimensions,

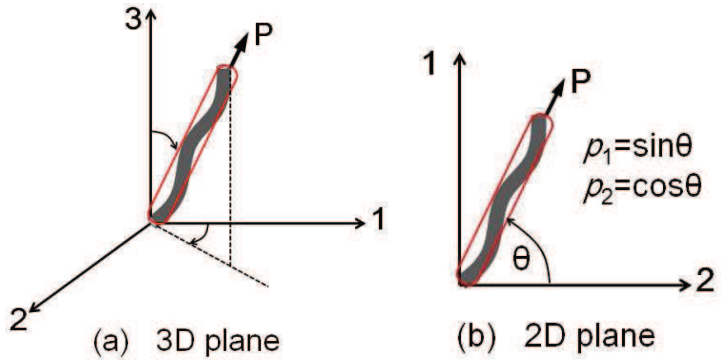

Fig. 2-4 *Definition of the direction of single MWNT by a unit vector* ***P*** *in the (a) 3D plane and (b) 2D plane, respectively.* θ *is the orientation angle of single MWNT in the 2D plane.*

$$p_1 = \sin\theta\,,\ p_2 = \cos\theta \tag{3-2}$$

where θ is the orientation angle of a single MWNT. Remarkably, to calculate the components of the orientation tensor $\langle a \rangle$ in the given region, one has to experimentally measure the direction of each MWNT. Being different from the indirect measurement of the CNT directions, such as X-ray,[126] Raman spectroscopy,[145] and polarized light

diffraction,[146] the approach used in our study is to digitize MWNT orientation angles directly by microtoming composites as well as detecting all the MWNTs present inside the sections. Vectors are placed in the TEM images and associated with the length direction of each tube, as shown in Fig. 2-5a. The orientation angle of each MWNT is measured by using software Image J. Components a_{ij} in any section where N carbon nanotubes present is calculated by the following equation.[144]

$$a_{ij} = \frac{1}{N}\sum_{k=1}^{N} p_i^k p_j^k \tag{3-3}$$

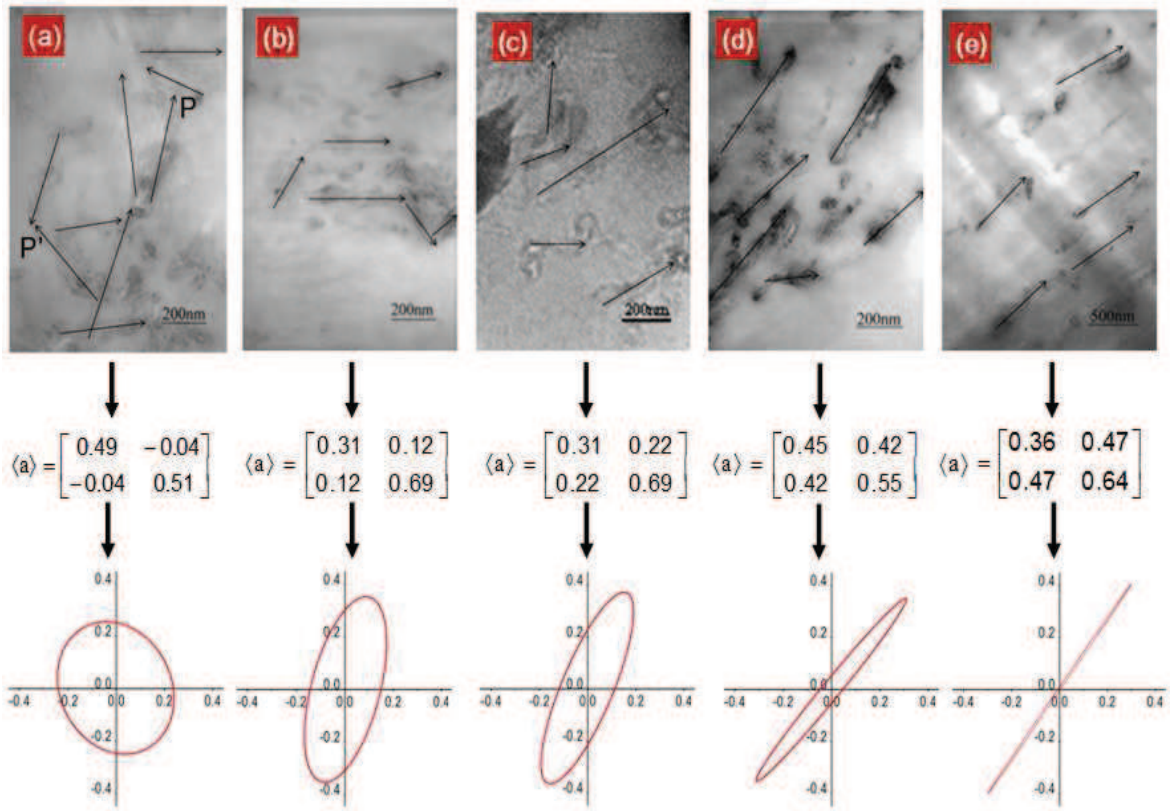

Fig. 2-5 *TEM images, second order orientation tensor and ellipses of samples parallel to the tensile-strain direction in the MWNT/PVDF nanocomposites with 2.0 wt % MWNT, respectively. (a) TS=0; (b)=6.3%; (c)=12.5%; (d)=25%; (e)=37.5%.*

The orientation tensor results at different TS are shown in Fig. 2-5. To vividly represent the MWNT alignment, we draw ellipses to graphically describe the orientation state. The

parameters of ellipses are automatically obtained by diagonalization from $\langle a \rangle$ to the second order orientation tensor $\langle a \rangle^*$ using the following Equation.[144]

$$Q\langle a \rangle Q^T = \begin{bmatrix} \cos\varphi & \sin\varphi \\ -\sin\varphi & \cos\varphi \end{bmatrix} \begin{bmatrix} a_{11} & a_{12} \\ a_{21} & a_{22} \end{bmatrix} \begin{bmatrix} \cos\varphi & \sin\varphi \\ -\sin\varphi & \cos\varphi \end{bmatrix}^T = \begin{bmatrix} a_{11}^* & 0 \\ 0 & a_{22}^* \end{bmatrix} = \langle a \rangle^* \qquad (3\text{-}4)$$

Where a_{11}^* and a_{22}^* are the length of mayor and minor axes of the ellipse, respectively. φ in the rotation matrix $\langle Q \rangle$ is the angle of major axis rotated anticlockwise from horizon axis X. The principle values for $\langle a \rangle^*$ at different TS are listed in Table 3-1. The ellipses are drawn accordingly as illustrated in Fig. 2-5.

Table 3-1. Principle values of the second order orientation tensor $\langle a \rangle^*$ and PAD values at different TS.

TS (%)	Mayor axes length (a_{11}^*)	Minor axes length (a_{22}^*)	φ in $\langle Q \rangle$	PAD
0	0.53	0.45	-52.0	0.08
6.3	0.72	0.28	73.9	0.44
12.5	0.79	0.21	65.4	0.58
25.0	0.92	0.07	48.4	0.85
37.5	0.99	0.01	53.29	0.98

The ellipses are drawn accordingly as illustrated in Fig. 2-5. In these ellipses, the values of the major and minor axes describe the degree of orientation in that direction.[142, 144] Hence, the major axes represent the direction of preferential alignment of MWNTs and the preferential alignment degree (PAD) can be quantificationally defined as:

$$\text{PAD} = \frac{a_{11}^* - a_{22}^*}{a_{11}^* + a_{22}^*} \qquad (3\text{-}5)$$

PADs are also listed in Table 3-1. The subcircular geometry of the ellipse at TS=0 (Fig. 2-5a) gives a much low PAD value (0.08), thus signifies a randomly-oriented MWNT structure, namely no particular preference of orientation before stretching. Whereas after loading (6.3% $\leqslant$ TS $\leqslant$ 37.5%), the ellipses become more elongated in shape (Fig. 2-5b-e), and the

corresponding PADs increase with tensile strain, namely the MWNT orientation degree can be modulated by controlling the external tensile strains applied on the composite. Of particular interest is that when TS increases from 0 to 6.3% and from 12.5 to 25.0%, the PAD increases drastically from 0.08 to 0.44 and from 0.58 to 0.85, respectively. The MWNT orientation state reacts much sensitively to the composite deformation in these two ranges. Therefore, two conclusions can be drawn. i) The tensile strain can strongly affect the MWNT redistribution once it goes into the plastic region, even exceeds the proportional limit slightly ($\Delta TS = 0.3\%$). ii) A much high PAD (>0.80) can be achieved only when the necking begins in the composite (at TS=18.0%, Fig. 2-3 and Table 3-1). From that point on, apart from the in-plane elongation, a significant out-of-plane geometric reduction also starts to contribute to the tube alignment until the composite is fractured.

2.3.3.3 Influence of tensile strain on the dielectric properties

In order to examine the strain's impact on the dielectric properties, we choose composites with f_{MWNT}=2.0 vol% to study, because it is in the vicinity of the threshold (f_c=1.8 wt %) that the dielectric behaviors would be much sensitive to the microstructure shift and affected greatly by the external tensile strains. Fig. 2-6 shows the dependence of dielectric properties on the frequency and tensile strain at room temperature. We first focus on the composite before stretching (TS=0). As compared to the pure PVDF (Fig. 2-6a), the percolation-type enhancement (10→300) in dielectric permittivity is visible (Fig. 2-6b) and results from an insulation-conduction transition based on the network formation of MWNT clusters near f_c.[59, 63, 64, 95] Additionally, the effect of interfacial polarization can be invoked as being responsible for the remarkable permittivity relaxation at low frequencies (10^2-10^4).[64, 65] Nevertheless, after stretching, the dielectric properties exhibit a complicate changing law with TS ranging from 0 to 37.5%.

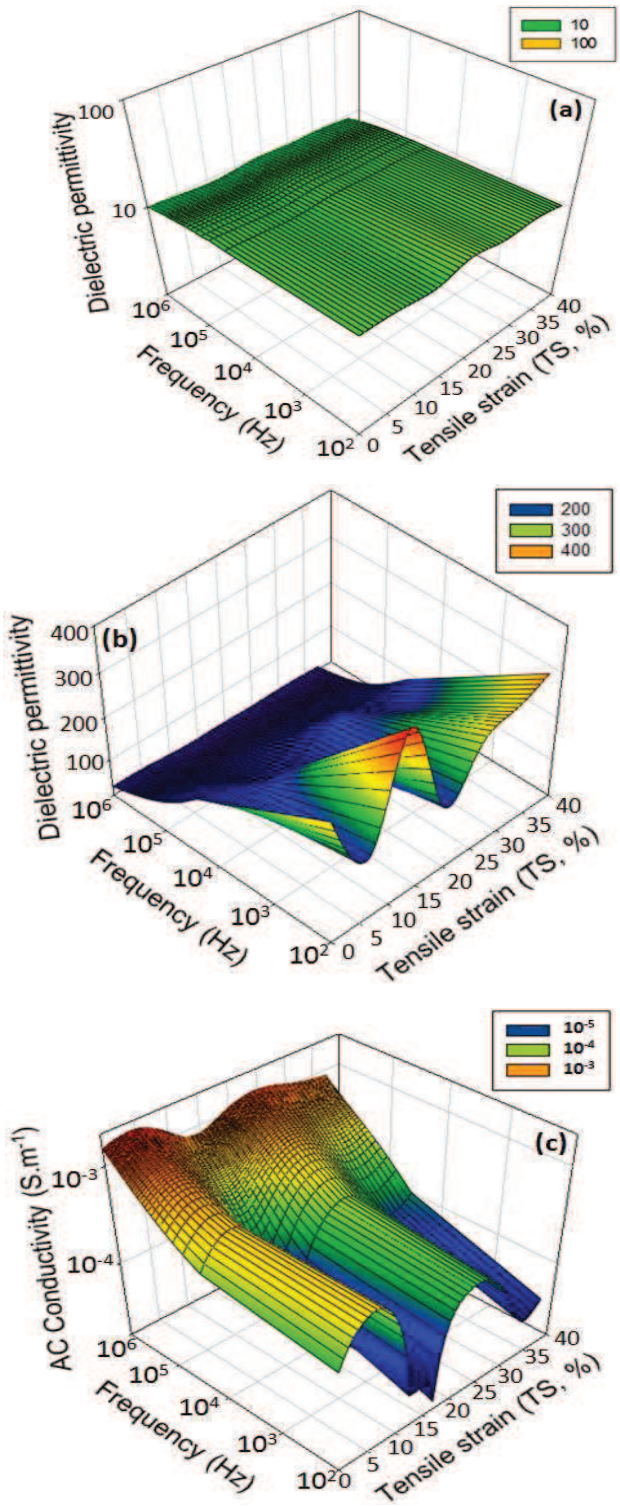

Fig. 2-6 *(a) Plots of the dielectric permittivity of pure PVDF against the frequency and tensile strain. Dependence of (b) the dielectric permittivity and (c) ac conductivity of the MWNT/PVDF nanocomposites with f_{MWNT}=2 wt% on the frequency and tensile strain at room temperature.*

As indicated in Fig. 2-6b, the dielectric permittivity at low frequencies (10^2-10^4 Hz) would be affected more by strain than those at higher frequencies. In detail, although all the dielectric permittivity decreases with increasing frequency in the whole TS range, the significant low-frequency permittivity relaxation only appears at certain strain levels (TS=0, 12.5, 37.5%). Similar influence of the strain on the ac conductivity can be observed in Fig. 2-6c, namely low-frequency conductivity would be more sensitive to the TS variations than others at higher frequencies, showing a large variation of the flat plateau level of the curves (corresponding to the dc conductivity). However, the relaxation of ac conductivity is almost the same at different TS.

To give a detailed description of the changing law, dependences of the dielectric permittivity and ac conductivity on TS at 10^2 Hz are plotted in Fig. 2-7a. It is noticeable that with TS increasing from 0 to 37.5%, the dielectric permittivity initially begins to decrease dramatically at TS=6.3%, following a remarkable increase to maximum value at TS=12.5%, a significant decrease again at TS=18.8% and finally increases gradually while TS is up to 37.5%. Nearly opposite rule happens to the variation of ac conductivity for the composites. The results indicate that by employing the stretching method, in comparison with TS=0, the increment in the dielectric permittivity of the f_{MWNT}=2 wt% composite can reach 30% at 10^2 Hz, and the corresponding ac conductivity decreases by 92%.

2.3.3.4 Correlation of MWNT alignment with dielectric property evolution

The following possible mechanisms can be suggested to explain the observed evolution of dielectric properties. A first possibility is associated with the PVDF matrix, i.e., the phase transition from α- to β-PVDF owing to the mechanical stretching.[147] Compared to the most common α-phase, β-phase characterized by all-trans planar zig-zag conformation with all the fluorine atoms located on the same side of the polymer chains can give PVDF a much higher polarity due to the net dipole moment.[107, 147] Thus a remarkable α- to β-phase transition would certainly change the dielectric properties of the composite. However, according to the literature,[147-150] such phase transformation was basically achieved when PVDF were

stretched at a high temperature (70-100 °C) with a colossal tensile strain (200-400%). In our case, the tensile strain values are far below this transition-required level, even for the largest TS (37.5%). Therefore, the phase structure of PVDF matrix remains stable during stretching, which can be further confirmed by the dependence of dielectric permittivity of pure PVDF on the frequency and strain (Fig. 2-6a, at each frequency the dielectric permittivity remains nearly stable, regardless of the increase of TS). Hence, the strain effect on the dielectric properties of PVDF matrix can be neglected.

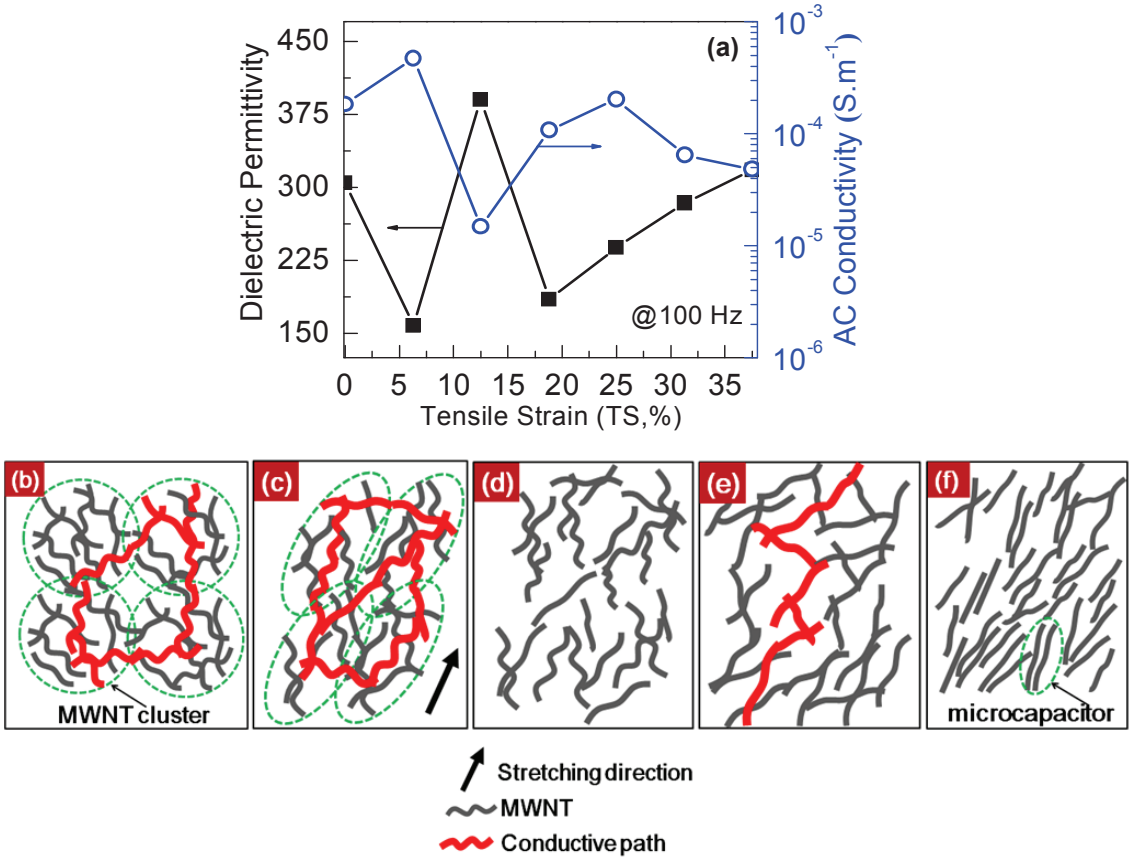

Fig. 2-7 *(a) Plots of the dielectric permittivity and ac conductivity at 10^2 Hz against the tensile strain, TS, for the f_{MWNT}=2 wt % composites. (b-f) Schematic change of the MWNT distribution in the composite with (b) TS=0, (c) TS=6.3%, (d) TS=12.5%, (e) TS=18.8% and (f) 18.8%<TS≤37.5% , respectively.*

Recall that MWNT clusters and interfacial polarization play an important role in determining the dielectric properties of composites. Thereby, other mechanisms based on these two factors should be put forward. The evolution of conductive path and the formation of microcapacitor network made from the aligned MWNTs in the direction of tensile strain would take charge for the complex changes of dielectric properties in Fig. 2-7a. When the composites are subject to a uniaxially stretching at a low strain level (TS=6.3%), the original MWNT clusters can retain but be elongated, which has been evidenced by the sharp variation of the PAD of MWNTs (Table 3-1). This induces additional conductive paths between clusters (as illustrated in Fig. 2-7c) and subsequently increases the conductivity (Fig. 2-7, TS=6.3%). (There already exist conductive paths between original MWNT clusters (dashed circle area in Fig. 2-7b) before stretching, because of the MWNT content higher than f_c [59, 63] as illustrated in Fig. 2-7b) The enhanced conductivity is nevertheless not desirable for preserving charges blocked at the MWNT-PVDF interfaces. Hence the permittivity relaxation becomes less significant and leads to a sharp decrease in permittivity (Fig. 2-6b and Fig. 2-7a, TS=6.3%). With TS increasing further, the elongated MWNT cluster would be largely destroyed and numerous fresh MWNT-PVDF interfaces form (MWNT-MWNT contacts change partially into MWNT-PVDF contacts) because of the continuous displacement of MWNT along the stretching direction (Fig. 2-7d, TS=12.5%). The damage of conductive paths between neighboring clusters would result in a dramatic decrease in conductivity. However, the enhanced interfacial polarization is prone to induce a much more remarkable relaxation at low frequency, leading to an increase in the dielectric permittivity (Fig. 2-6b, TS =12.5%). From TS of 18.0% on, a high degree of MWNT alignment could be expected because of the occurrence of necking in the composites (Fig. 2-3). The straightening of tube flexure enables heads of one MWNT meet ends of others, thus reconstructs conductive paths among individual MWNT (Fig. 2-7e). This would increase conductivity and decrease permittivity again (Fig. 2-7a, TS=18.8%). The high PAD level (>0.8) in this range (18.8-37.5%) signifies that MWNTs are highly oriented along the stretching direction, giving rise to a network of microcapacitor with the MWNTs as electrodes and a very thin PVDF

layer in between (Fig. 2-7f). For each microcapacitor, the capacitance, *C*, can be calculated by

$$C = \frac{\varepsilon_0 \varepsilon_r S}{d} \tag{3-6}$$

Where ε_0 is the dielectric permittivity of the free space ($\varepsilon_0 \approx 8.854\times10^{-12}$ F m^{-1}), ε_r is the dielectric permittivity of PVDF, *S* is the area of overlap of the two MWNT electrodes, and *d* is the separation between the two electrodes. With TS increasing from 18.8 to 37.5%, the thickness of PVDF layers, *d*, would decrease gradually and improve the effective capacitance of both the microcapacitors and the whole composite, then the composites' dielectric permittivity due to the proportional relationship between the permittivity and the capacitance as shown in Eq. 3-6.[101] However, the conductivity in this range (18.8-37.5%) does not vary with TS monotonously, possibly because of the local fluctuations in the distance between the neighboring MWNTs during stretching.

2.3.3.5 Impedance analysis

Dielectric properties of the CNT composite can also be explored by its equivalent circuit model composed of three elements: resistor (*R*), capacitor (*C*) and inductor (*L*) elements.[101, 113] The polarization and ac conduction mechanisms can be revealed according to the basic composition elements of the composites. [113, 151] To verify the above mechanisms for the dielectric evolution, we establish an equivalent circuit model of two parallel *RC* circuits in series for our MWNT/PVDF nanocomposites, as illustrated in Fig. 2-8a. The constant phase elements (CPEs) are used to simulate the impedance data instead of the ideal capacitor. Fig. 2-8b presents the Nyquist plots of the composites at different TS with frequency increasing from right (10^{-3} Hz) to left (10^{7} Hz). They are shown as half circles indicating the existence of interparticle current flow and the polarization resistance at interfaces.[113]

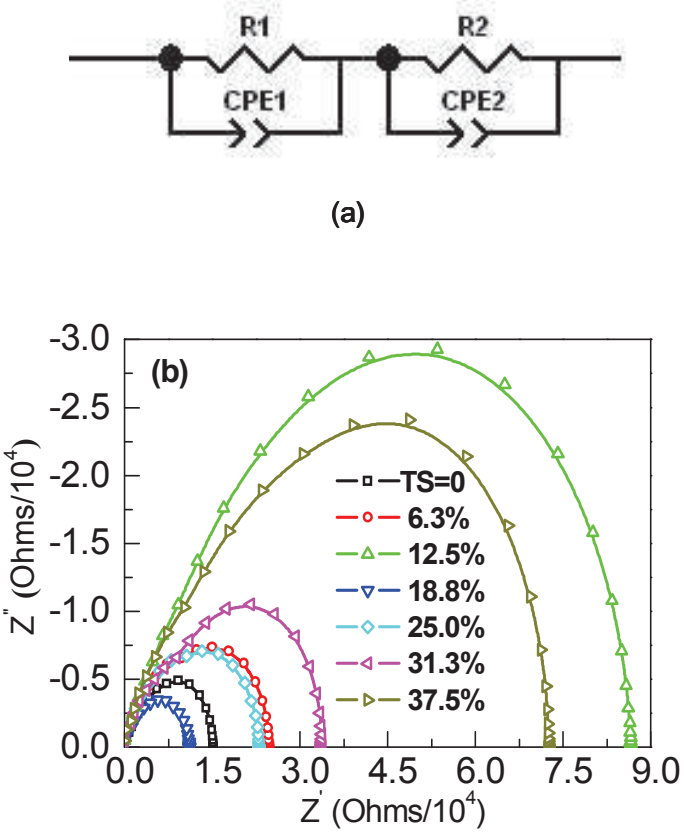

Fig. 2-8 *(a) Equivalent circuit of the MWNT/PVDF nanocomposites with f_{MWNT}=2 wt %, and (b) Nyquist plots of the composites at different TS.*

The diameters of these semicircles correspond to the bulk resistivity of the composites at different TS levels. With the increase in TS, the variation of this resistivity is nearly identical to that in Fig. 2-7a. For example, the Nyquist plot at TS of 12.5% has the largest diameter, meaning that the composite at this strain level possess lowest conductivity, similar to Fig. 2-7a. By using the Zview2 software, the impedance data of sample can be analyzed and the parameters of equivalent circuits are calculated according to the following equation.

$$Z^* = \frac{R}{1 + j\omega CR} = \frac{R}{1 + j\omega\tau} \tag{3-7}$$

Where $\tau = RC$ is the time constant of circuits. The simulated values of each element by fitting the impedance data to the equivalent circuit are shown in Table 3-2.

Table 3-2 Simulated values of each element according to the impedance data and equivalent circuit in Fig. 3-8a.

TS (%)	R1($\Omega/10^5$)	CPE1($F/10^{-10}$)	R2($\Omega/10^5$)	CPE2($F/10^{-10}$)
0	0.53	4.83	0.51	21.63
6.3	0.29	2.67	0.25	11.81
12.5	16.85	3.66	3.23	19.27
18.8	1.93	1.92	0.37	21.95
25	0.70	3.51	0.59	23.68
31.3	2.46	5.06	1.86	14.73
37.5	3.50	3.11	0.99	35.47

It should be emphasized that no semicircle has been experimentally observed for the Nyquist plot of PVDF matrix, suggesting that the electrical polarization in composites is much concerned with MWNT additives.[108] Considering the great effect of interfacial polarization on the dielectric properties, it is reasonable to conclude that the adscription of CPE1 and CPE2 is to the MWNT polarization and MWNT-PVDF interface polarizations, respectively, as the value of CPE2 is an order magnitude larger than that of CPE1. It should be also noted that the highest R values are obtained at TS =12.5%, which is nearly consistent with the variation of conductivity in Fig. 2-7a. Moreover, when the high PAD value is reached (e.g., TS=37.5%), we obtain the high CPE2 values (Table 3-2), indicating the great contribution of the interfacial polarization to the macroscopic dielectric properties. Overall, the analysis of impedance spectra and the established equivalent circuit well verify the mechanisms proposed for the evolution of dielectric properties.

2.4 Conclusions

We prepared a percolative MWNT/PVDF composite via solution casting, followed by hot-pressing technology. Without any treatment of MWNT, the nanotubes with extremely large aspect ratio exhibited a strong tendency to form interlocked cluster structures, which yet could give rise to a percolation threshold as low as 1.91 vol%. Near the percolation threshold, the MWNT/PVDF composites displayed a permittivity enhancement of 27 ($\varepsilon_r/\varepsilon_m$ at 10^3 Hz). This medium dielectric performance could largely derive from the limited number of microcapacitors as a result of the aggregated structure of MWNT as well as the weak interfacial interaction between the pristine MWNTs and PVDF matrix.

To investigate the sensitivity of the microcapacitor to the tensile strain, the MWNT/PVDF composite near percolation threshold has been chosen to conduct tensile test. The orientation of the MWNTs inside the composites can be changed by uniaxial mechanical stretching. The nanotube orientation state was quantitatively characterized by using TEM as well as the second order orientation tensor at a selected location. A high alignment degree happened when the necking began in composites. The change of nanotube distribution state highly affected the dielectric properties. A correlation of the tube orientation state with the evolution of dielectric properties was established. With increasing the alignment degree of nanotubes, the dielectric permittivity and ac conductivity exhibited complex but nearly opposite changing tendency. This could be attributed to the conductive pathways shift and microcapactor evolution during the tensile deformation. This was further confirmed by using an equivalent circuit model of two parallel RC circuits in series to analyze the impedance data. We hope that our study would form a helpful reference to predict the strain-induced change of dielectric properties of electroactive composites in practical applications.

Chapter III
Melt-processed MWNT/PVDF composites

3.1 Introduction

Among various passive components in the electronic system, capacitors have drawn intensive interest due to its variety of functions such as decoupling, bypassing, filtering, and timing capacitor.[152] Higher function and further miniaturization of electronics demand embedding capacitors into the inner layers of organic printed circuit boards (PCB).[153-155] To meet this requirement, polymer-based materials with high ε_r were developed as dielectrics for embedded capacitors because of their flexibility and good compatibility with PCB. However, for such applications, the dielectric permittivity of common polymers is too low ($\varepsilon_r \leqslant 3$). Thus, a key issue is to substantially raise the dielectric permittivity of polymers while retaining the polymer matrix flexibility.[156]

It is known that CNTs have high aspect ratio and large specific surface area, exhibit exotic mechanical and nonlinear optical properties, also present high electrical and thermal conductivities.[1, 3] Employing CNT as nanofiber to pursue high-ε_r polymer composites has recently aroused considerable interest. As the CNT content (f_{CNT}) increases to the vicinity of the f_c, the dielectric permittivity of the composites can be enhanced significantly according to the Eq. 1-22.[37, 60]

To achieve flexibility and thus desired adaptability between the composites and the PCB, it is important for the polymer-based composites to exhibit a low f_c. Previous studies have demonstrated that large slenderness ratio of CNT can always result in a very low f_c, but permittivity enhancement $\varepsilon_r/\varepsilon_m$ differs depending on the experimental conditions. Zhang et al.[95] prepared a CNT/polymer nanocomposite by using a coagulation method. The permittivity enhancement ($\varepsilon_r/\varepsilon_m$ at 10^2 Hz) was 2 for the nanocomposite with 2 wt % CNT ($>f_c$). Besides, untreated MWNT have been ultrasonically dispersed into PVDF solution. A ε_r

/ε_m (at 10^2 Hz) of 6 was observed in the resultant composite at f_c =1.6 vol %.[64] The limited enhancement (low $\varepsilon_r/\varepsilon_m$) has not only been attributed to the finite CNT-polymer interfaces caused by the poor dispersion of CNTs in the composites, but it also reflects the weak interactions between CNTs and the polymer matrix. To overcome these problems, organic modification or in situ polymerization of CNTs with specific organic molecules is often adopted to realize the uniform dispersion of CNTs in composites.[60, 157-160] For instance, Dang et al.[60] have modified the MWNT with TFBB by wet-chemistry procedure and created a novel functionalized MWNT/PVDF nanocomposite, which displayed a large permittivity enhancement ($\varepsilon_r/\varepsilon_m$ =60 at 10^3 Hz) at percolation threshold (ca.8.0 vol %). The high dielectric permittivity was mainly attributed to the interfacial polarization because of the rich interfaces between the modified MWNTs and PVDF.

Despite the dielectric permittivity could be notably enhanced by improving CNT dispersion, the chemical modification may disrupt the conducting network in the carbon nanotube, thus resulting in a drastic decrease in the electronic properties.[161, 162] It has been evidenced that the bulk permittivity of composites with modified CNTs was considerably lower than those with only raw CNTs at the same f_{CNT}.[162] Therefore, homogenously distributing pristine CNTs into host polymer while increasing their interactions seems to be more efficient way to attain high dielectric permittivity.

Melt mixing can be a promising route for this purpose. Because in melt mixing, the high temperature and high shear forces often cause chemical and/or physical interactions between CNTs and macromolecules, such as CH-π interaction and π-π stacking, thus may improve the overall CNT dispersion in polymer matrix.[112, 163-165] Additionally, it combines speed with simplicity, and is also free of excessive toxic and/or volatile solvents, [163, 166] which make it possible for bulk production of composites in industry. However, the dielectric properties of melt-processed CNT/polymer nanocomposites have been seldom addressed. The effect of melt mixing on dielectric permittivity is still obscured and requires a thorough investigation, especially when the chemical and/or physical interactions between CNTs and host polymer would be involved.

In this chapter, MWNT/PVDF nanocomposites are prepared by blending pristine MWNT within PVDF in molten state using a small scale-conical twin screw compounder. During the melt mixing, a remarkable interaction at molecular level is achieved by establishing donor-acceptor complexes between the delocalized 'π-electron' clouds of MWNTs and strongly electrophilic F groups of PVDF chains. This enhanced interaction creates an advanced nanocomposite with an individual MWNT dispersion, which possesses a giant dielectric permittivity of 3800 ($\varepsilon_r/\varepsilon_m$ =380) over a critical content of MWNT, while retaining the flexibility of the polymer matrix used. The giant dielectric permittivity originates from the reinforced MWS effect [60, 167] based on the donor-acceptor complexes. The delocalized 'π-electron' clouds of MWNTs provide large domains for nomadic electrons, and the electrophilic F groups strongly attract these electrons. As a result of such combination, the MWS effect at interfaces is reinforced significantly. Furthermore, the donor-acceptor complexes induce a much thin insulating layer of PVDF on individual MWNT surface. This nanoscale structure can fully realize the advantage of MWNT (i.e., large specific surface area) and result in a huge interfacial area in the nanocomposite, which in turn provides numerous sites for the reinforced MWS effect. These results clearly indicate that melt mixing can result in advanced high-ε_r nanocomposites, which can be potentially applied to the electronic field such as embedded capacitors with high dielectric performances.

3.2 Experimental

3.2.1 Materials and sample preparation

Semicrystalline polymer PVDF (Kynar 721, Arkema Group, France), was used as polymer host due to its superior ferroelectric nature. The MWNTs were synthesized by CVD method, provided by Shenzhen Nanotech Port Company (China). Their diameter and length were about 20~40 nm and 5~15μm, respectively. The MWNT/PVDF nanocomposites were prepared by melt mixing the nanotubes within PVDF host polymer in the molten sate. (Procedures are illustrated in Fig. 3-1).The mixing was done in a co-rotating, conical, twin-screw micro-extruder/compounder (Micro 5cc Twin Screw Compounder, DSM) at

200 °C, for over 30 min and at a mixing speed of 60 rpm in Ar atmosphere. Slabs with a thickness of 1.5 mm were prepared by injection molding of the mixed composites (Micro 5cc Injection Molder, DSM) using a press at 1.6 MPa for 1 min, while the temperature was kept at 60 °C. Then, the temperature would be decreased from 60 °C to room temperature at a sufficiently low rate. The final obtained concentration of MWNT in the prepared nanocomposites varied from 0 to 14 vol %.

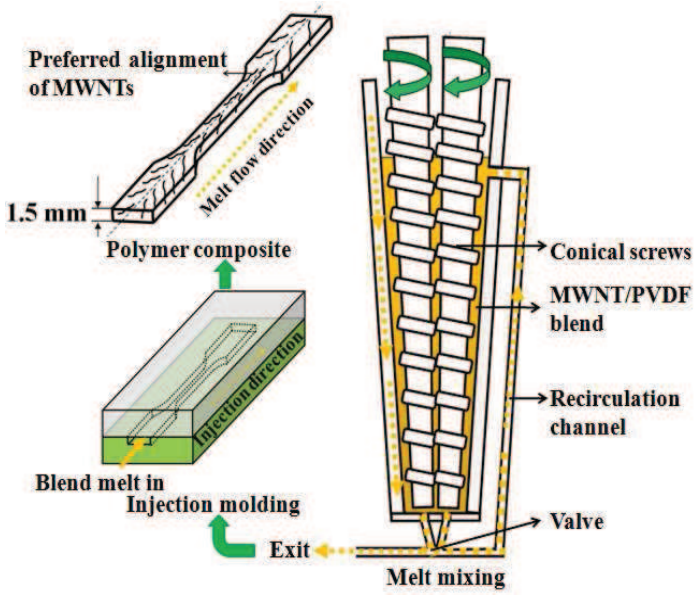

Fig. 3-1 *The MWNT/PVDF nanocomposites are prepared by melt mixing using a co-rotating, conical, twin-screw microcompounder, followed by injection molding.*

3.2.2 MWNT/PVDF composite characterizaitons

The dielectric properties were measured in the frequency range of 1~10^6 Hz using a broadband dielectric spectrometer (Novocontrol BDS 20). Before the dielectric characterization, electrodes were painted on the sample using silver paste. Raman spectroscopy was performed using a microspectrometer (Horiba Jobin-Yvon LabRam) with a resolution of 1 cm^{-1}. The morphology of the MWNT/PVDF nanocomposites was observed using a SEM (LEO Gemini 1530). The MWNT morphology was observed using a TEM (Jeol 1200EX).

3.3 Results and discussion

3.3.1 Raman spectra

It is known that the CNTs are electron-rich molecules and any electron-deficient molecules can interact with them and form donor-acceptor complexes,[168] much the same way as the electron-rich molecules form π-π complexes.[169, 170] This molecular level interaction between MWNTs and PVDF matrix is confirmed with Raman spectroscopy, as shown in Fig. 3-2a.

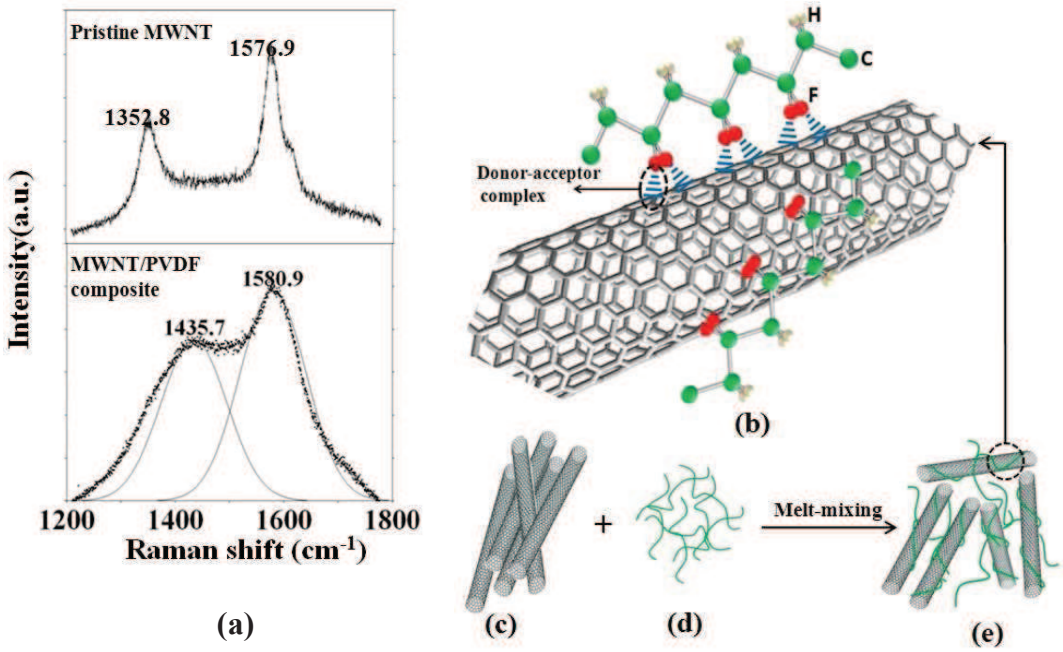

Fig. 3-2 *(a) Raman spectra of pristine MWNT and the MWNT/PVDF nanocomposite with* f_{MWNT}*=0.10, (b-e) Illustration of the polymer wrapping over MWNTs via the remarkable donor-acceptor complexes: (b) schematic image of donor-acceptor complexes between PVDF chains and individual MWNT (c) MWNTs bundles (d) PVDF chains (e) PVDF-wrapped MWNTs.*

The first-order spectrum of pristine MWNTs shows two characteristic peaks. The first centers at 1352.8 cm^{-1} assigned to the disorder-induced D band and derives from the multiple phonon scattering of defects or amorphous carbon. The second locates at 1576.9 cm^{-1} assigned to the G band and is attributed to the stretching of conjugated double bonds corresponding to sp^2 hybridization during the formation of the arylnanotube bond.[114, 171] Upon addition of MWNTs in the polymer matrix, the D band shifts to higher frequency substantially so that it is overlapped by the G band. Band component analysis clearly gives the location of two broaden peaks at 1435.7 cm^{-1} and 1580.9 cm^{-1} corresponding to the D and G band respectively. The up-shift and width change of D and G band peaks undoubtedly provide a strong evidence for the interaction between PVDF chain and individual MWNT, [172-174] presumably as a consequence of the formation of donor-acceptor complexes. In detail, the shifting (4 cm^{-1}) of the G band peak to higher frequency indicates that the interaction likely arises from the sp^2 graphic carbons of MWNT sidewalls. It has been also demonstrated that when CNTs were functionalized with potassium (electron-donor) and bromine (electron-acceptor), the G band would shift substantially to lower and higher frequencies, respectively.[175] In this case, the strongly electrophilic F groups of PVDF chain could sufficiently interact with MWNT as an electron acceptor and it is reasonable to result in a up-shift of G band. Therefore we can conclude that it is between the delocalized 'π-electron' clouds of MWNTs and the fluorine of PVDF chains that the donor-acceptor complexes are achieved (illustrated in Fig. 3-2b).

Furthermore, a larger up-shift of D band (83 cm^{-1}) is found and can attribute to the strong compressive forces associated with polymer chains on MWNTs,[176] indicating the disentanglement of the MWNTs and subsequent dispersion in the PVDF matrix as a consequence of polymer penetration into the MWNT bundles during melt mixing (schematically shown in Fig. 3-2c-e). Similarity, an up-shifting of the D band (40 cm^{-1}) has been also reported for MWNTs after they were coated with a thin PPy layer.[114] Additionally, the intensity ratio of D-band to G-band (I_D/I_G) is often taken to characterize the number of defects and impurities in CNTs.[176] After melt-blending MWNTs with PVDF

matrix, a slight increase in I_D/I_G from 0.61 to 0.75 is observed, implying that the high shear force may shorten carbon nanotubes and induce some additional defects in MWNTs.

3.3.2 SEM and TEM morphologies

Based on the remarkable donor-acceptor complexes achieved during the melt-mixing, PVDF chains can effectively wrap over individual MWNT and form a much thin polymer layer on the nanotube surface. This effect can significantly disentangle MWNT bundles and sufficiently avoid the MWNT reaggregation, thus ensure an individual MWNT dispersion in nanocomposites.

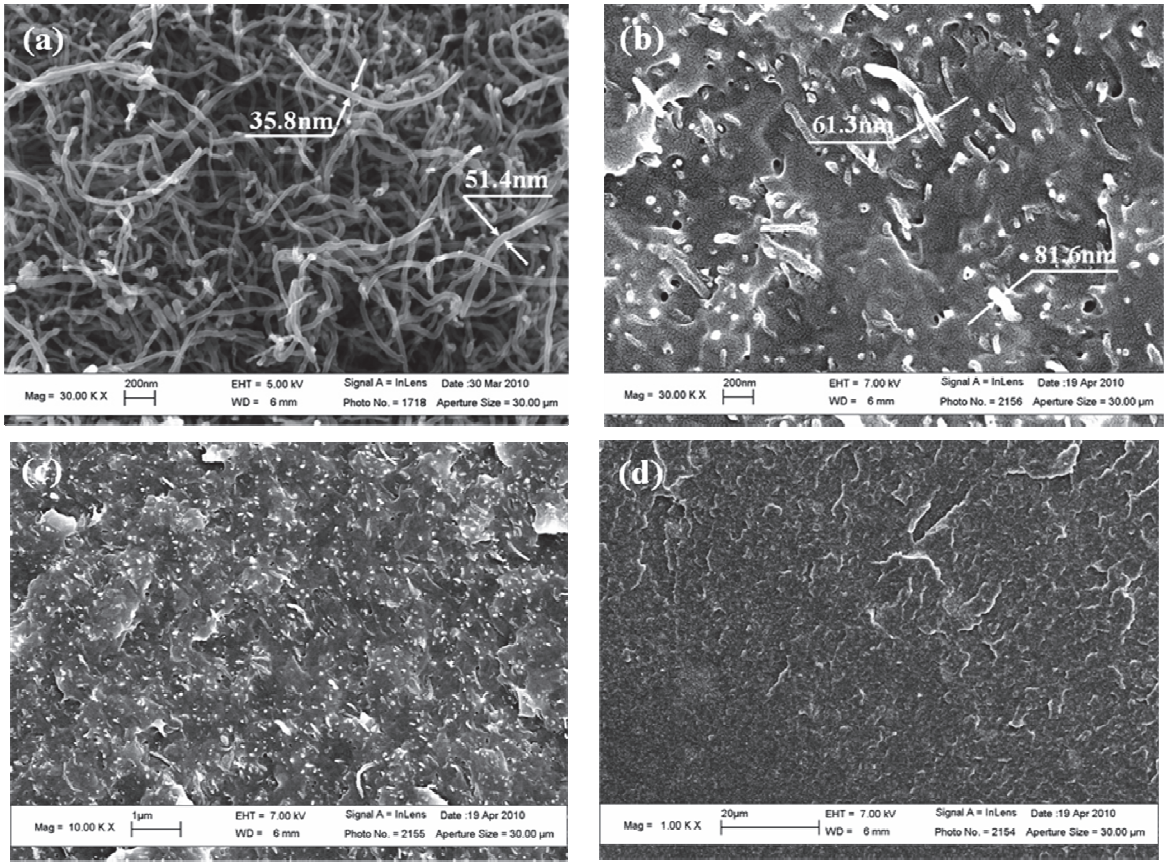

Fig. 3-3 *SEM images of (a) pristine MWNTs, and fractured surface of MWNT/PVDF nanocomposite with f_{MWNT}=0.10 observed under different magnifications ((b) 30 k, (c)10 k , (d) 1k).*

SEM images in Fig. 3-3 can give evidence for the existence of the PVDF layer as well as the individual dispersion of MWNTs. As shown in Fig. 3-3a, the pristine MWNTs have diameters ranging from 35.8 to 51.4 nm. However, after melt-blended with PVDF, the morphology of the MWNTs obviously changes, and the diameter of the MWNTs in composite becomes large, i.e., about 61.3-81.6nm (Fig. 3-3b), indicating that the MWNTs are wrapped with host polymer chains and the thickness of the PVDF layer is ranging from about 10 to 30 nm. Similar change of the apparent CNT diameter was also found in MWNT/polycarbonate system by the SEM observation for its fractured surface, which has been taken as evidence to verify the polymer adhesion on the nanotube surface.[164]

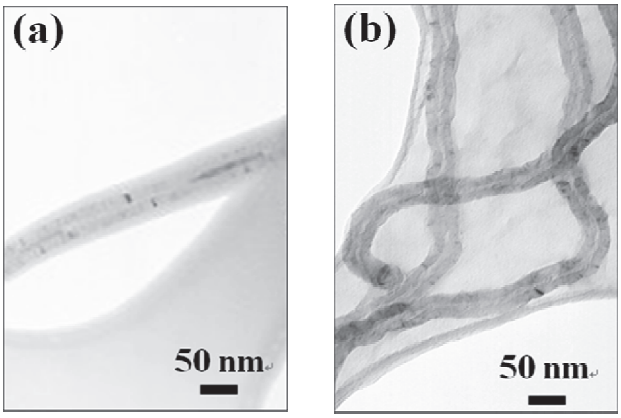

Fig. 3-4 *TEM images of (a) MWNT with a PVDF thin layer and (b) pristine MWNT.*

To further confirm the existence of PVDF layers on MWNTs, we dissolved a small piece of prepared MWNT/PVDF composite in the solvent of DMF completely. The MWNTs were then filtered from the solution using a copper grid, and followed by a TEM characterization. Meanwhile, pristine MWNT powders were treated with the same procedures. The resultant TEM images are shown in Fig. 3-4. We can clearly see a PVDF layer of 10-30 nm thick coated on MWNT. This layer could not be dissolved and retained due to the strong interaction with MWNT. Moreover, it is widely accepted that the dispersion state of CNTs in polymer matrix can be totally different depending on the magnification or scale.[116] Therefore it is important to clearly define the dispersion based on the different scales. Here, SEM images of the fractured surface of the MWNT/PVDF nanocomposite are observed

under different magnification levels, as shown in Fig. 3-3b-d. It is clearly found that MWNT agglomerates are completely disentangled, showing a good 'nanoscopic dispersion' (Fig. 3-3b-c). Moreover, uniform distribution of individual CNTs throughout the nanocomposites can be confirmed by SEM at lower magnification level (Fig. 3-3d), which is excellent 'micro- and macroscopic dispersion'.[116] Additionally, a certain degree of alignment of MWNTs is also found in the MWNT/PVDF nanocomposite (Fig. 3-3b), which is probably induced by the shear flow together with the geometry extruder die.[84]

3.3.3 Effect of MWNT loading on the dielectric properties

Figure 3-5a shows the dielectric permittivity values for the MWNT/PVDF nanocomposites as a function of MWNT volume fraction (f_{MWNT}) at room temperature and different frequencies. According to Fig. 3-5a, it can be clearly seen that the logarithmic values of dielectric permittivity at high frequencies (10^4 and 10^6 Hz) increase approximately linearly with f_{MWNT}, implying the high-frequency dielectric permittivity of the composites is dominated by the polarization of MWNT itself.[101] However, the dielectric permittivity at low frequencies (1 and 10^2 Hz) enhances significantly only when f_{MWNT} approaches the percolation threshold, which is largely from the interaction between PVDF and MWNT because of the two facts below. i) The enhanced dielectric permittivity (3800 at 1 Hz) of composite is larger than PVDF matrix (about 10)[60, 64] and carbon nanotube (about 2000)[177] alone. It suggests that a synergetic effect occurs between macromolecules and carbon nanotube fillers, especially when the low MWNT content (12 vol %) is taken into account. ii) According to MWS effect,[167] when a current flows across the two-materials interfaces, charges can be accumulated at the interface between two dielectric materials with different relaxation time ($\tau=\varepsilon/\sigma$, where ε is the dielectric permittivity and σ is the conductivity). In our case, the relaxation time of PVDF is about several orders of magnitude larger than MWNT. Therefore, charge carriers are blocked significantly at internal interfaces due to the MWS effect, accordingly enhancing the dielectric permittivity significantly. Meanwhile, owing to the formation of donor-acceptor complexes at MWNT-PVDF interfaces, the MWS effect can be intensified greatly, i.e., the delocalized 'π-electron' clouds of MWNTs

provide large domains for nomadic electrons, and the electrophilic F groups strongly attract these electrons, thus significantly reinforce the MWS effect at the interfaces. Furthermore, a thin insulating layer of semicrystalline PVDF is combined with the MWNTs to form a nanoscale structure in the polymer nanocomposites. This structure can fully realize the advantages of MWNTs (i.e., large specific surface area) and result in a huge interfacial area between MWNT and PVDF in the nanocomposite, which in turn provides numerous sites for the reinforced MWS effect.

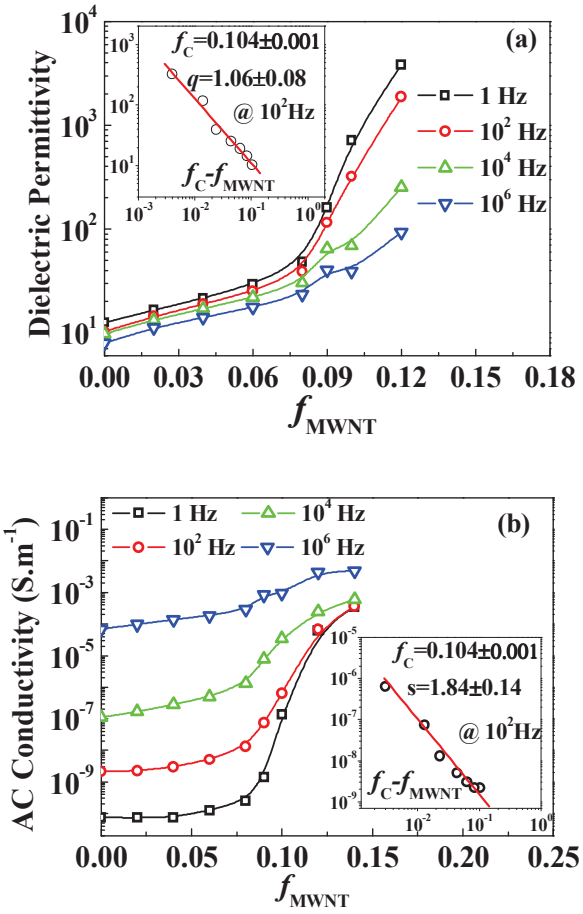

Fig. 3-5 *Dependence of (a) the dielectric permittivity and (b) the AC conductivity of the MWNT/PVDF nanocomposites on the MWNT volume fraction, f_{MWNT}, measured at room temperature and different frequencies. The insets in (a) and (b) show the best fits of the dielectric permittivity to Eq. 1-22 and the AC conductivity to Eq. 1-21b, respectively.*

In order to estimate f_c, we fit the experimental permittivity data at 10^2 Hz to the Eq. 1-22. The best linear fit of the data to the log–log plot of the power law gives f_c=0.104±0.001, q=1.06±0.08 (see the inset in Fig. 3-5a). The exponent q agrees well with the universal one (q≈1).[37, 60] However, the attained f_c (10.4 vol%) is higher than that reported for most other CNT/polymer nanocomposites.[60, 64, 95, 112] Generally for non functionalized multi-walled carbon nanotubes embedded into a non modified matrix, typical values for f_c are in the range 1-3 wt %.[178] In this case, the higher f_c may be as a consequence of three factors: i) the geometry of the extruder die may induce preferred alignment of MWNTs (as seen in Fig. 3-3b) and reduce the number of MWNT-MWNT contact points. ii) the presence of PVDF layer coated on nanotube surfaces further decreases the effectiveness (conduction) of inter nanotube contacts, and thus a higher concentration of MWNTs is required to reach the percolation threshold; iii) the breakage of MWNTs may occur during melt mixing and result in a slight decrease in aspect ratio. A lower aspect ratio usually gives rise to a higher percolation threshold.[59]

In fact, besides the high dielectric permittivity, the desired composites serving as dielectrics should also have low conductivity. Presented in Fig. 3-5b is the AC conductivity of the MWNT/PVDF nanocomposites as a function of f_{MWNT}, measured at room temperature and different frequencies. The conductivities at high frequencies (10^4 and 10^6 Hz) increase slightly with f_{MWNT} and exhibit relatively higher values than those at low frequencies (1 and 10^2 Hz) due to a remarkable dissipative effect.[101] However, the low-frequency conductivities increase significantly as f_{MWNT} approaches f_c. The variation can show a good agreement with Eq. 1-21b.[37, 60]

The best fit of the conductivity data at 10^2 Hz to the log–log plot of the power law gives f_c=0.104±0.001, s=1.84±0.14 (see the inset in Fig. 3-5b). The exponent s is larger than the universal one (s=0.8-1).[37, 60] This discordance has been also found in other percolative composites[60, 107] and could probably derive from the fact that the electrical connectivity in composites is achieved by tunneling, as there are no physical contacts between the conducting CNT. The wide inter-particle distance distribution can lead to non-universal high

s values, as proposed by Balberg.[179] The absence of physical contacts between the nanotubes can be ascribed to the formation of a much thin PVDF layer around the CNT walls, which prevents the formation of physical (direct) contacts between them. Because of this, although the conductivity is increased significantly when f_{MWNT} falls into the neighborhood of percolation threshold ($0.09<f_{MWNT}<0.12$), it is noted that the maximal conductivity of composites in this region is still below 6.3×10^{-5} $S.m^{-1}$ (at 1 Hz). Such semi-conductive composites can be still supposed to serve as dielectric materials, because the conduction in these composites is dominated by the tunneling effect, which only results in a minimal leakage current because of the existence of PVDF insulation layers, which serve as electrical barriers to impair the direct contacts between MWNT particles. Moreover, this feature brings about a relatively flat portion on the loading curve of composite conductivity so as to provide a much wide processing window (3 vol%) and thus makes it possible to adjust dielectric properties of composites near the percolation threshold, which is generally hard to realize in the normal percolative composites.

3.3.4 Frequency dependence of the dielectric properties

Figure 3-6 presents the dependence of dielectric properties of the MWNT/PVDF nanocomposites with different f_{MWNT} on frequency. The data indicates that the dielectric permittivity (Fig. 3-6a) and loss tangent (Fig. 3-6b) are almost independent of frequency in the measured frequency range when $f_{MWNT} < f_c$. Additionally, as f_{MWNT} is in the neighborhood of f_c, both the dielectric permittivity and the loss tangent decreased in the low frequency region ($<10^3$ Hz) and no remarkable dielectric relaxation was observed as that in other percolative systems.[60, 64, 101] This result suggests that the established percolation network, which consisted of MWNTs nearly touching each other but still remaining electrically insulated because of the existence of a thin insulating PVDF layer, was stable and not easily damaged by external frequency disturbances with the help of donor-acceptor complexes.

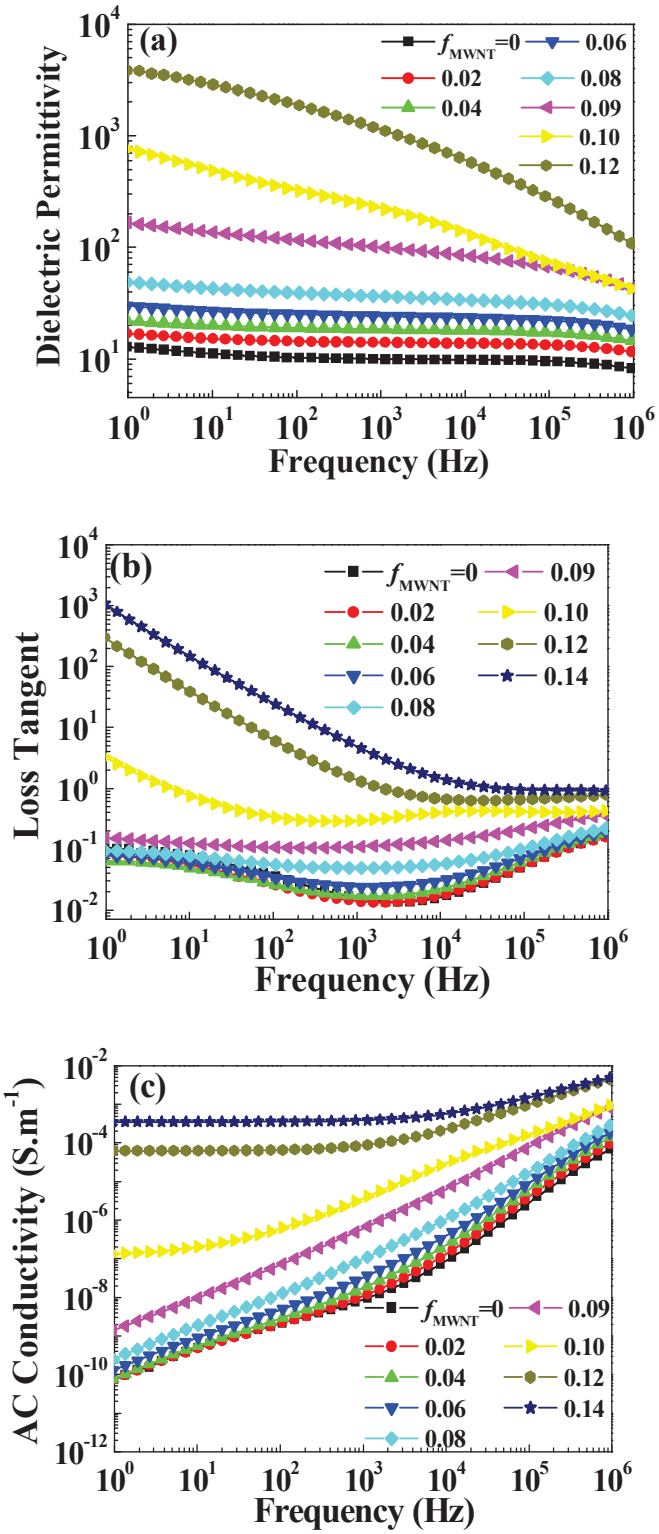

Fig. 3-6 *Dependence of (a) the dielectric permittivity (b) loss tangent and (c) AC conductivity of the MWNT/PVDF nanocomposites with different f_{MWNT} on frequency ranging from 1 Hz to 10^6 Hz, measured at room temperature.*

The conductivity of composites as a function of frequency in Fig. 3-6c presents the identical result that the conductivity increases gradually with f_{MWNT} and frequency when f_{MWNT} approaches f_c (0.104), which does not change several orders of magnitude like that in the normal percolative composites,[64] and also confirms the stability of the established percolation network mentioned above.

3.3.5 Temperature dependence of the dielectric properties

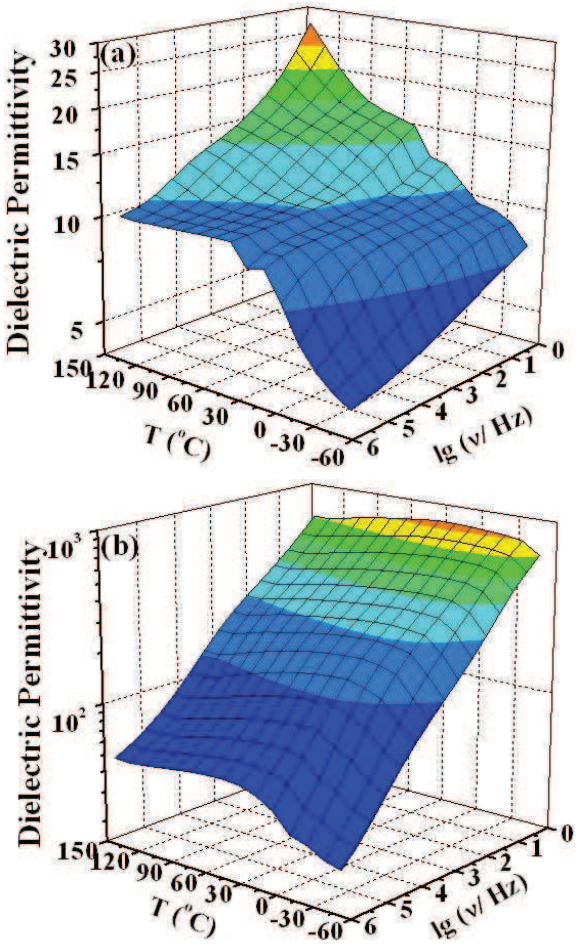

Fig. 3-7 *Dependence of the dielectric permittivity on frequency, v, and temperature, T, for (a) the PVDF matrix and (b) the MWNT/PVDF nanocomposite with* f_{MWNT}*=0.10.*

To illustrate the thermal stability of pure PVDF and MWNT/PVDF composite (f_{MWNT}=0.10), we plot in Fig. 3-7 the variation of the dielectric permittivity as a function of the temperature and frequency. From Fig. 3-7a, it can be seen that the dielectric permittivity

of pure PVDF becomes higher with the temperature increasing for the whole frequency range (1-10^6 Hz). Meanwhile, two obvious peaks ranging from -40 °C to 10 °C and from 100 °C to 150 °C occur and become more significant at upper and lower frequency, respectively. This means two compensation laws could be revealed in the diagram which are related to cooperative molecular motions involving both intra- and intermolecular interactions.[180] Indeed, dipoles are chemically connected to the backbone in polymer dielectrics, and their rotation involves cooperative conformational changes accompanied by not only rotation of one chain with respect to the backbone but also surrounding segments in a cooperative manner. The length of mobile units as well as the size of relaxing sequences could be reflected by the variation in activation energy,[180] which can be obtained by fitting conductivities with the well-known Arrhenius relation expressed as:[181]

$$\sigma \propto \frac{1}{T}\exp\left[-\frac{E_a}{K_b T}\right] \tag{3-1}$$

where E_a is the activation energy, T is the absolute temperature and K_b is Boltzmann constant. When we apply the PVDF conductivity ranging from -30 °C to 10 °C and from 80 °C to 140 °C into Eq. 3-1, the activation energies of 0.27 eV and 0.92 eV are obtained. The increase in activation energies corresponding to the two compensation laws, for increasing temperature, reflects the increase in the length of mobile units.[180] Therefore, it can be concluded that the high temperature peak at low frequency corresponding to α relaxation could ascribe to molecular motions that alter the dipole direction only along the applied electrical field, and the lower temperature permittivity peak at high frequency corresponding to β relaxation is probably associated with the glass transition and derives from rotational motions of dipolar groups in the amorphous regions of the PVDF polymer.[182] However, the dielectric permittivity of the MWNT/PVDF nanocomposite (as shown in Fig. 3-7b) only presents one peak region corresponding to the β relaxation of PVDF, suggesting the dominant contribution of the PVDF polarization at low temperature and high frequency.

As the α relaxation peak disappears after incorporated MWNTs (Fig. 3-7b), we apply

conductivity data ranging from 80 °C to 140 °C into Eq. 3-1 by least squares fit as shown in Fig. 3-8, and obtain the slope of Arrhenius plot with a linear correlation coefficient above 0.97. When $f_{MWNT} < f_C$, the activation energy are 0.92 eV, 0.47 eV and 0.15 eV for composites with f_{MWNT} = 0, 0.04 and 0.08 respectively, as presented in the inset of Fig. 3-8.

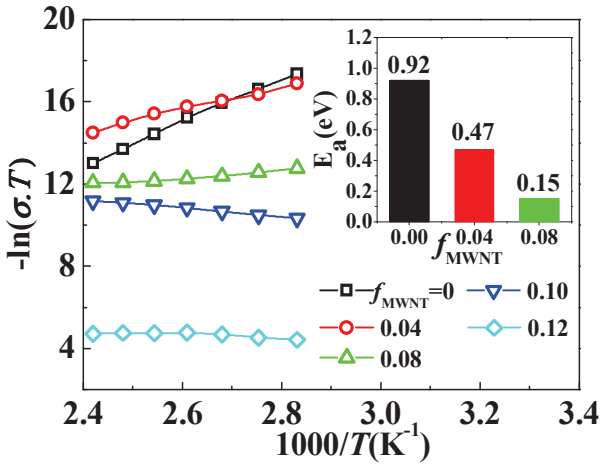

Fig. 3-8 *-ln(σ.T) versus 1000/T for the MWNT/PVDF nanocomposites with different* f_{MWNT}. *The inset shows the activation energies at different* f_{MWNT}.

The significant decrease of E_a with increasing f_{MWNT} indicates that after incorporated MWNTs the PVDF molecular motions become difficult due to the formation of numerous donor-acceptor complexes between PVDF and MWNTs. However, when $f_{MWNT} \geqslant f_c$, the slopes of Arrhenius plot are below 0. This indicates the conduction process is dominated by the percolation network and the temperature effects weaken.[183] Therefore, we can conclude that the dielectric permittivity of the MWNT/PVDF nanocomposite is dominated by the reinforced MWS effect as the existence of numerous interfaces between MWNT and PVDF, and this reinforcement possesses an excellent thermal stability. It is important to note that the dielectric permittivity of the nanocomposite near the percolation threshold maintained a stable value at ca. 800 (at 1Hz) with temperatures ranging from -50 °C to 150 °C. Such a high dielectric permittivity and temperature independence strongly suggest potential applications as advanced dielectric materials over a broad range of temperature.

3.4 Conclusions

We have fabricated an advanced nanocomposite by blending pristine MWNTs within PVDF in molten state and significantly enhanced the dielectric permittivity of PVDF by breaking through the common bottleneck of limited interfacial interactions displayed in other C-moieties-based composites.

The Raman spectra shows that a remarkable interaction at molecular level is achieved by establishing donor-acceptor complexes between the delocalized π-electron clouds of MWNTs and strongly electrophilic F groups of PVDF chains. The SEM and TEM images give evidence for the effective wrapping of PVDF chains and resultant much thin PVDF layer on nanotube surfaces, respectively.

The MWNT/PVDF nanocomposite exhibited a giant dielectric permittivity of 3800 over a critical content of MWNT, while retaining a low conductivity of 6.3×10^{-5} $S.m^{-1}$. We suggest that the giant dielectric permittivity originates from a reinforced Maxwell-Wagner-Sillars (MWS) effect based on the donor-acceptor complexes. The delocalized π-electron clouds of MWNTs provide large domains for nomadic electrons, and the electrophilic F groups strongly attract these electrons thus significantly reinforce the MWS effect at the interfaces.

This simple and robust method has been demonstrated to be effective to realize an advanced material with giant dielectric permittivity over a wide temperature range and can be easily scalable from laboratory to industrial scale. These polymer-based composites with giant dielectric permittivity values could find potential applications as high-performance embedded capacitors in the electronic industry

Chapter IV
Biphasic polymer blends containing carbon nanotubes

4.1 Introduction

The electrically percolative polymer-based composites are arousing considerable interest because their physical properties often display a significant change if an electrically conducting filler's concentration in the composites is near critical threshold, i.e., dramatic increases in conductivity and/or dielectric permittivity. Their potential applications can be electromagnetic interference shielding materials,[138, 184] electroactive materials,[95, 185] and dielectrics for charge-storage capacitors.[56, 57, 60, 66, 107, 114, 186]

In this field, continuous effort has been devoted to raise the electrical conductivity or dielectric permittivity of composites at low percolation threshold f_c in order to maintain the inherent polymer matrix flexibility and low cost. For this purpose, the fillers with large aspect ratio are of particular interest, such as one-dimensional nanotubes and fibers,[60, 66, 114, 187] and two-dimensional graphene nanosheets.[188, 189] Among these fillers, CNTs are the most promising candidate due to the good combination of mechanical, electrical and thermal properties as well as their availability at large scale.[3]

To prepare CNTs/polymer nanocomposites, several processing methods have been developed, such as solution casting,[60, 114] melt mixing,[65, 66, 190] and in situ polymerization.[191] Among them, melt mixing is particularly desirable as the process is fast, simple, free of solvents and contaminants, most importantly easily scalable from laboratory to industrial scale.[65, 84, 178] McNally et al.[84] incorporated MWNTs into PE matrix by melt mixing using a mini-twin screw extruder. The electrical conductivity of PE was increased significantly, by 16 orders of magnitude, from 10^{-18} to 10^{-2} $S.m^{-1}$. However the percolation threshold (f_c =7.5 wt %) was relatively high due to the decrease of MWNT aspect ratio as a consequence of inevitable breakage during melt-mixing. In Chapter III, We also

fabricated a nanocomposite by melt-blending the pristine MWNTs within PVDF.[65] A giant dielectric permittivity (3800) was observed over a critical content of MWNT. Unfortunately, the composites possessed a high value of f_c (10.4 vol %) mainly due to a significant polymer wrapping on the nanotubes. The large quantities of MWNTs added into the host polymer may cause the poor mechanical properties, difficulty of processing, and high costs. Therefore, new methods are needed to fabricate such composites by melt-mixing technique for reducing the percolation threshold.

The recent theoretical and experimental investigations indicate that the percolation threshold of CNTs/polymer composites depends strongly on not only the physical properties of CNTs[59] (e.g., conductivity and aspect ratio) but also their dispersion state[116] and distribution status[117] in polymer matrices. Therefore, tremendous research and development efforts are devoted to design an optimized state of aggregation and distribution of CNTs in host polymers to reduce the percolation threshold. An efficient strategy is to confine CNTs in any one of the phases of a co-continuous biphasic polymer blend or at the interface, by which the percolation threshold can be substantially reduced due to the double percolation. The concept of double percolation was initially described by Sumita et al.[118] in 1991 for carbon black (CB) filled immiscible blends. Since then, it has been implemented for several blend systems and can be applied to a variety of carbonaceous fillers, such as CB,[118-120] carbon fibers,[121] CNTs,[83, 117, 122-124] and graphite nanosheets.[125] In the case of CNT-filled polymer blends, preliminary studies have explicitly studied the heterogeneous morphologies (sea-island or co-continuous phase structure) of various blend systems characterized by the preferential location of CNTs in one of the phases. It has been substantially demonstrated that the electrical and/or mechanical properties of CNT-filled polymer blends can be significantly improved, once the double percolation occurs, i.e., the CNT-filled blend phase percolates (first percolation) and the CNTs forms a network within the percolated blend phase (second percolation). For instance, Pötschke et al.[117] have introduced MWNTs into thermoplastic matrices, PC and PA, by melt blending using PE based concentrates with high MWNT loading (24-44 wt%). The MWNTs migrated from PE concentrates to PC or PA phase and remained in their excellent dispersion state. Thus, electrical percolation is achieved at significantly lower MWNT contents as compared to

direct incorporation. Wu et al.[124] have prepared CNT-filled PET/PVDF blend composites. It was observed a 2500 % improvement in electrical conductivity, 36 % augment in tensile strength and 320 % increase in elongation over the CNT-filled PET with the same filler content. The author ascribed the improved properties to the formation of a double percolated structure resulting from the selective location of CNTs in the PET phase. Despite tremendous progress toward understanding the effect of the double percolated structure on the electrical and mechanical properties by intensively investigating the cocontinuity of polymer phases,[83, 122-124] to the best of our knowledge, double percolated structure based dielectric blends with CNTs have rarely been investigated in the literature. The effect of double percolation on the dielectric permittivity is still elusive and requires a thorough investigation, especially when the interactions between the two continuous polymer phases would be involved.

In this chapter, biphasic polymer blends (PVDF and low density polyethylene (LDPE) with different proportions) were selected as host matrices to prepare MWNT-filled polymer blends. Images of SEM together with TEM confirmed the remarkable selective localization of MWNTs in the LDPE phase, and provided morphological evidence for the double percolated structure in MWNT-LDPE/PVDF composites. As a result, the percolation threshold was reduced greatly. This allows for easy processing, preserving the mechanical properties of the matrix and reducing as much as possible the cost of the final composites. The effect of double percolation on the dielectric properties of MWNT-filled biphasic polymer composites was elucidated in detail. A model based on the Lichtenecker rule and percolation theory was used to predict the dielectric permittivity in biphasic polymer composites below percolation threshold.

4.2 Experimental Section

4.2.1 Materials

The MWNTs are synthesized by CVD method, provided by Shenzhen Nanotech Port Company (China). The purity and density of the MWNTs used are about 97 % and 1.97 g/cm^3, respectively. The tube diameters are in the range of 20-40 nm with lengths of 5-15 μm.

The PVDF (Kynar 721) with density of 1.78 g/cm^3 and melt flow index (MFI) of 7.0 g/10 min is used in the blends as received. The typical commercial LDPE has a density of 0.92 g/cm^3 and MFI of about 260 g/10min.

4.2.2 Fabrication of biphasic polymer composites

Blends of LDPE and PVDF with and without MWNTs have been prepared by mixing in a co-rotating twin-screw microcompounder (DSM Xplore Microcompounder, 5 cm^3) with two stainless steel screws and a bypass allowing continuous recycling of the material at the head of the mixing chamber. The volume ratios of PVDF/LDPE are fixed at 1:4, 1:2, 1:1, 2:1, and 4:1. An appropriate amount of MWNTs and the polymer blends with fixed volume ratio were mixed all together at 200 °C, for 30 min and at a mixing speed of 60 rpm. Such a long mixing duration aims to ensure the complete disentanglement of MWNTs clusters at relatively low screw rotation speed. The whole mixing process was under the protection of Ar atmosphere to prevent samples from oxidation. Final slabs with a thickness of 1.5 mm were prepared by injection molding of the melt blends using a press at 1.6 MPa for 1 min (DSM Xplore Microinjection Molder, 5 cm^3), while the temperature was kept at 50 °C, Then, the temperature would be decreased from 50 °C to room temperature.

4.2.3 Sample characterizations

For the dielectric characterization, specimens with a dimension of about 10 mm×10 mm×1.5 mm were cut from the as-prepared composite slabs. Silver paint was applied on the two surfaces of the specimens to ensure good contact. The dielectric properties were measured using a broadband dielectric spectrometer (Novocontrol BDS 20) in the wide frequency range of 10^{-1}–10^6 Hz at room temperature. Each sample was measured for four times and mean values were taken to plot curves. Morphologies of fractured surfaces of the MWNT-LDPE/PVDF composites were observed using a SEM (LEO Gemini 1530). The fractured surfaces were prepared in liquid nitrogen and were sputtered with gold in vacuum prior to observation. The microstructure of the specimens was also examined by TEM, (Hitachi H7650), and the ultrathin sections (120 nm) were sliced by ultramicrotome under liquid nitrogen cooling.

4.3 Results and discussion

4.3.1 Morphologies of the biphasic polymer composites

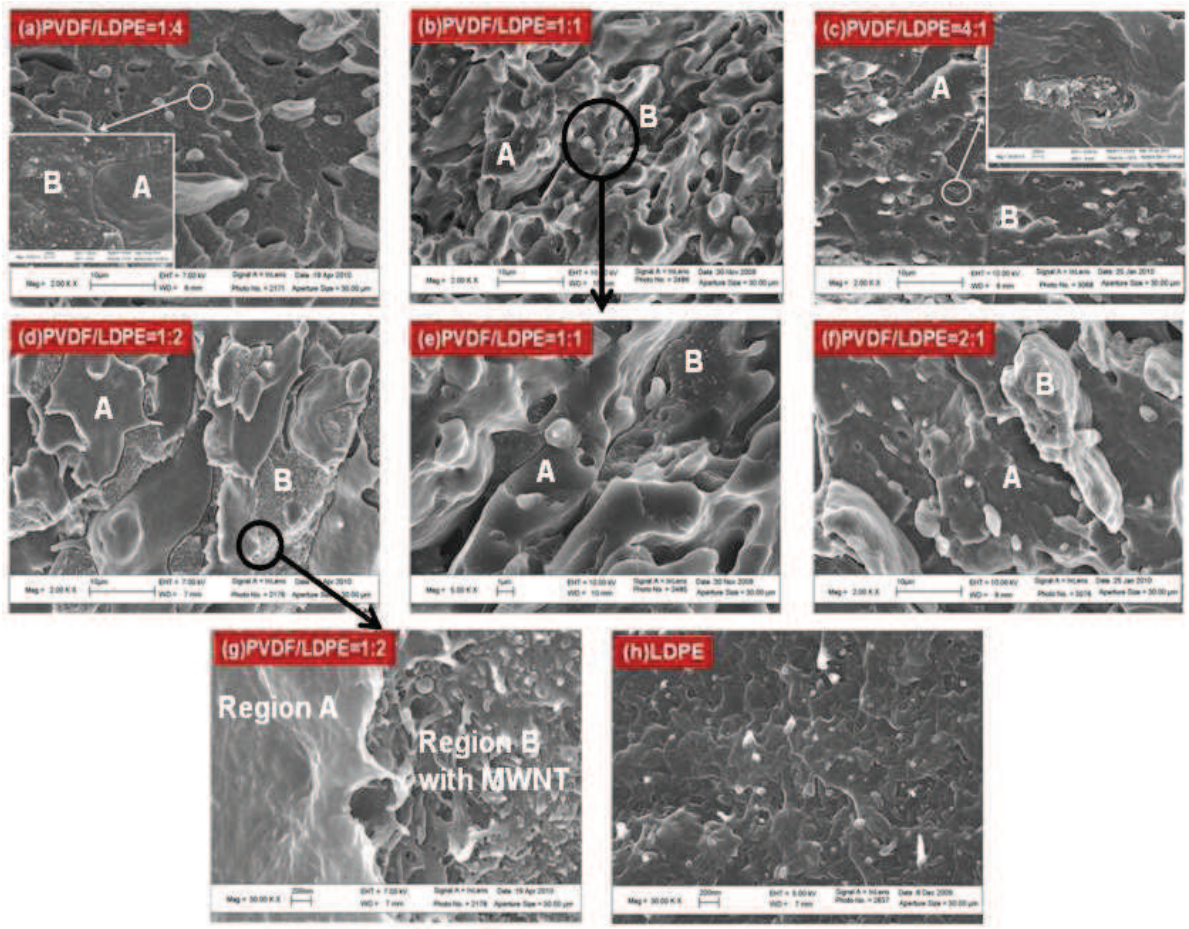

Fig. 4-1 *SEM images of fracture surfaces of the MWNT-LDPE/PVDF composites with a fixed overall volume concentration of MWNT (f_{MWNT}=8.0 vol%). (a-c) correspond to composites at volume ratios of PVDF/LDPE=1:4, 1:1, 4:1 respectively, the insets in (a) and (c) show the magnified images of the region B with MWNT. (d) and (f) correspond to composites at volume ratios of PVDF/LDPE=1:2, 2:1, respectively. (e) and (g) are the magnified images of the composites at volume ratios of PVDF/LDPE=1:1, 1:2. (h) shows the image of MWNT filled single LDPE composite at f_{MWNT}=8.0 vol%.*

Figure 4-1 shows the SEM micrographs of the MWNT-LDPE/PVDF composites with a fixed overall volume concentration of MWNT (f_{MWNT}=0.08) and variable volume ratio of

PVDF/LDPE. From the SEM images shown in Fig. 4-1a-f, two distinct regions are noted, one contains MWNTs (Region B, polymer exhibiting heterogeneity) and the other is free of MWNTs (Region A). The area ratio of Region A to B increases with increasing the volume ratio of PVDF/LDPE. Thus, it is reasonable to conclude that Region A is the PVDF phase, whereas Region B is the LDPE phase containing MWNTs. It is clear that the composites exhibit a heterogeneous MWNT distribution in matrix. In order to further confirm that MWNT is indeed localized in the LDPE phase, a composite with MWNT filled in single LDPE matrix (PVDF/LDPE=0:1) was also prepared under the same processing conditions. It can be clearly seen that the macroscopic Region B (see Fig. 4-1g) is very similar to the morphology of the MWNT/LDPE composite (see Fig. 4-1h), which further confirms that MWNT is preferentially located in the LDPE phase.

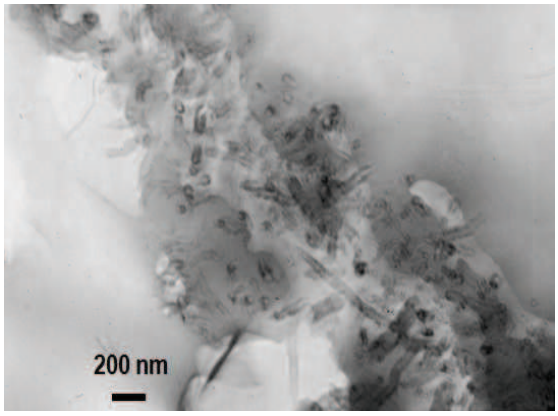

Fig. 4-2 *TEM image of the MWNT-LDPE/PVDF composite with a fixed overall MWNT content (f_{MWNT}=8.0 vol%). The corresponding volume ratio of PVDF/LDPE in the composite is 1:1.*

The remarkable heterogeneous distribution of MWNT in the polymer blend can be also clearly seen in the TEM images of the MWNT-LDPE/PVDF composites at volume ratio of PVDF/LDPE=1:1, as shown in the Fig. 4-2.

Table 4-1 Surface free energies of the polymers and MWNT

Material	γ at 20 ℃ (mJ/m^2)	-$d\gamma/dt$ (mJ/m^{2}K)	χ^p	γ at 200 ℃ (mJ/m^2)	γ^d at 200 ℃ (mJ/m^2)	γ^p at 200 ℃ (mJ/m^2)
LDPE[a]	35.7	0.057	0	25.4	25.4	0
PVDF[a]	30.3	–	0.23	30.3	23.3	7
MWNT[b]	27.8	–	0.37	27.8	17.6	10.2
MWNT[c]	45.3	–	0.59	45.3	18.4	26.9

$\gamma=\gamma^d+\gamma^p$, $\chi^p=\gamma^p/\gamma$, γ :total surface energy, γ^d: dispersive component, γ^p :polar component, χ^p :polarity. [a]according to ref.[192] [b]according to Barber.[193] [c]according to Nuriel.[194]

Table 4-2 Interfacial energies as calculated using harmonic and geometric mean equations at 200℃

Materials	γ_{12}^a (mJ/m^2)	γ_{12}^b (mJ/m^2)
LDPE/PVDF	7.09	7.05
LDPE/ MWNT[b]	11.61	10.91
LDPE/ MWNT[c]	28.02	27.46
PVDF/MWNT[b]	1.39	0.70
PVDF/MWNT[c]	12.26	6.74

γ_{12}^a : interfacial energy by harmonic mean equation. γ_{12}^b : interfacial energy by geometric mean equation.

Table 4-3 Wetting coefficients and predictions of MWNT location in the LDPE/PVDF blend

System	ω_a	ω_a	Predicted location	Observed location
	Harmonic	Geometric		
MWNT[b]-LDPE/PVDF	-1.44	-1.45	PVDF	LDPE
MWNT[c]-LDPE/PVDF	-2.22	-2.94	PVDF	LDPE

The location of carbon nanotubes in a polymer blend is generally dictated by the state of the minimum interfacial energy if the thermodynamic equilibrium is attained.[117, 124] According to Young's equation, ones can find the thermodynamic equilibrium filler position by evaluating the wetting coefficient ω_a.[195]

$$\omega_a = \frac{\gamma_{CA} - \gamma_{CB}}{\gamma_{AB}} \qquad (4\text{-}1)$$

here, γ_{CA}, γ_{CB} and γ_{AB} are the interfacial energy between MWNT and polymer A, MWNT and polymer B, and polymer A and B, respectively. The values $\omega_a > 1$, $-1 < \omega_a < 1$, and $\omega_a < -1$ imply MWMT preferentially locates within polymer B, at the interface between two polymers and polymer A, respectively. The interfacial energy γ_{12} derived from the surface free energies of phase 1 (γ_1) and phase 2 (γ_2). Two approaches can be used depending on the type of phase surfaces: the harmonic mean equation and the geometric mean equation. The former is suitable for evaluating the interfacial energy between low-energy materials:

$$\gamma_{12} = \gamma_1 + \gamma_2 - 4\left(\frac{\gamma_1^d \gamma_2^d}{\gamma_1^d + \gamma_2^d} + \frac{\gamma_1^p \gamma_2^p}{\gamma_1^p + \gamma_2^p}\right) \quad (4\text{-}2)$$

and the latter is valid between a low energy material and a high energy material:

$$\gamma_{12} = \gamma_1 + \gamma_2 - 2\left(\sqrt{\gamma_1^d \gamma_2^d} + \sqrt{\gamma_1^p \gamma_2^p}\right) \quad (4\text{-}3)$$

Surface free energies of LDPE, PVDF and MWNT as well as their dispersion and polar components are listed in Table 4-1. Based on these values, the calculated interfacial energies between the polymers and the MWNT are reported in Table 4-2. Submitting these interfacial energies into Eq. 4-1 results in wetting coefficients (see Table 4-3). The value is of below -1 according to either the harmonic or geometric mean equation, if PVDF is chosen as phase A and LDPE as phase B. Therefore, the consideration of the minimum interfacial energy predicts that MWNT should explicitly distribute into the PVDF phase (more polar phase) during melt-mixing. Unfortunately, this prediction is contradictory with the preferred arrangement of MWNT inside LDPE phase experimentally observed in this study. It must be emphasized that thermodynamics of wetting is not the only factor influencing the final equilibrium morphology (filler location, shape and size of the polymeric phase) of blend systems,[196] which can be also determined by the kinetic effects induced by the mixing procedure,[197] mixing time,[198] especially the rheology of each polymer phase.[199-201] Feng et al.[199] investigated the effect of viscosity ratio of PMMA/PP on the final equilibrium location position of CB particles. The calculation of the wetting parameter predicted that CBs should definitely locate in PMMA while they actually tend to preferentially incorporated into PP phase as PMMA showed a higher viscosity. Clarke et

al.[200] and Zhou et al.[201] even argued that the interfacial energy of particle-polymer can be considered as the dominant factor only when the viscosity ratio of both polymer phases is nearly one. In our study, in the very beginning of the melt-mixing, LDPE can first melt at a temperature (104℃) significantly lower than PVDF (171℃), the MWNT particles may be incorporated into LDPE preferentially although it does not have the better affinity as PVDF is in solid state then. This thermodynamically unstable status can be retained for a long mixing time even after PVDF becomes viscous fluid, probably because of the colossal difference in viscosity between PVDF (6000 Pa.s at 232 ℃) and LDPE phase (160 Pa.s at 190 ℃) even the latter one is loaded with 8.0 vol % MWNT. In this case, kinetic effect dominates the thermodynamic wetting to determine MWNTs locating in the much lower viscosity LDPE phase.

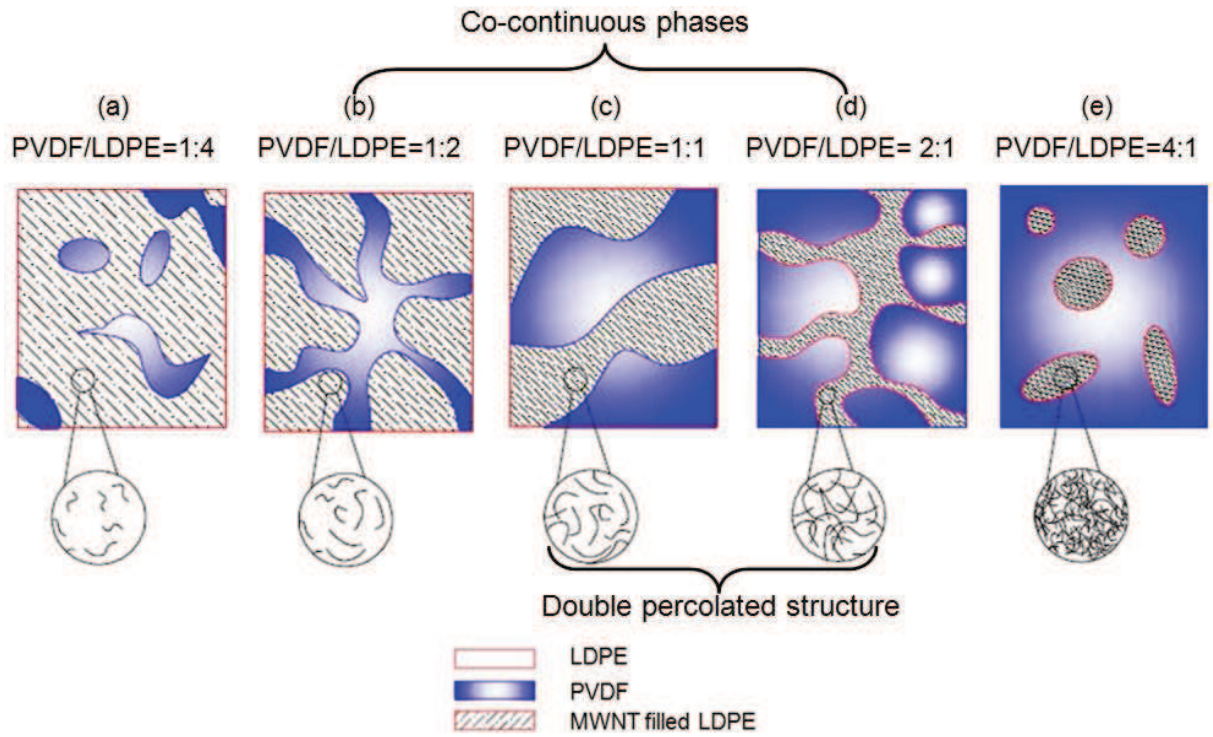

Fig. 4-3 *Schematic image for the microstructure evolution of the biphasic polymer composites with increasing volume ratio of PVDF/LDPE.*

Based on the remarkable selective location of MWNT in the LDPE phase, a 3D double percolated structure can definitely be formed in MWNT-LDPE/PVDF composites once two requirements are satisfied: i) The matrix is a co-continuous system, namely, both LDPE and PVDF phase are continuous in 3D space (see Fig. 4-3b-d), meaning the volume ratio of two polymers is not far from 1:1 (1:2, 1:1 and 2:1); ii) The conductive MWNT is preferentially localized in the LDPE phase and form a continuous 3D conductive network, meaning that its concentration is higher than the percolation threshold (Fig. 4-3c,d). Such a double percolated structure allows for enhancing the electrical conductivity of polymer composites at low MWNT concentration since the conductive pathway of MWNT is only formed in one polymer phase, not through the entire matrix. This further improves the processability and flexibility because of the low inorganic filler concentration required. However, when the volume ratio of binary polymers is far from 1:1, such as 1:4 and 4:1, the double percolated structure can not form, as the PVDF and LDPE phases are presented as isolated droplets in the cases of 1:4 (Fig. 4-1a and Fig. 4-3a) and 4:1 (Fig. 4-1c and Fig. 4-3e), respectively, even there are numerous conductive networks in LDPE phase for the latter case. Principally, there should exist a critical volume ratio of PVDF/LDPE, the lowest content of LDPE to form co-continuous phases in matrix, at which a lowest MWNT loading is needed to reach the percolation threshold. Pötschke et al.[83] have demonstrated that a double percolated structure could be still observed with the concentration of MWNT filled PC phase in blend with PE as low as 30 vol %.

4.3.2 Dependence of AC conductivity on the blend composition

It is interesting to evaluate the dependence of AC conductivity on the blend composition. The conductivity (at 1 Hz) of the composites at a given overall MWNT concentration (f_{MWNT}=8 vol%, based on the entire polymer blend) is strongly related to the PVDF phase content, as shown in Fig. 4-4. According to the morphology of MWNT-LDPE/PVDF composite, the evolution process of the conductivity can be divided into three stages (I, II, III). It should be first emphasized that MWNT-filled LDPE composite (at f_{PVDF}=0) shows a much low conductivity, indicating that most MWNTs are isolated to each other at such concentration (f_{MWNT}=0.08). When the PVDF content increases but below the co-continuous

range (Stage I, Fig. 4-4), the PVDF forms the microsized domains (～10 μm) and the MWNT-filled LDPE forms continuous phase (Fig. 4-1a and Fig. 4-3a). The conductivity increase can be attributed to the more effective tunneling conduction with continuously reducing the distance between neighboring MWNTs, as a result of the increase of the effective CNTs concentration in the LDPE phase.

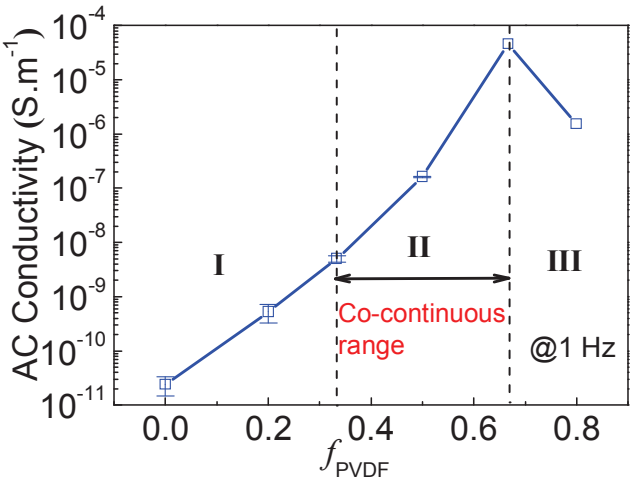

Fig. 4-4 *Dependence of the AC conductivity on the volume fraction of PVDF phase (f_{PVDF}) in the PVDF/LDPE polymer blends, measured at 1 Hz and room temperature. The total volume concentration of CNTs based on the entire polymer blends is fixed at 8.0 vol %.*

Table 4-4 Concentrations of carbon nanotubes in composites at different polymer blend compositions

Volume concentration of LDPE phase in the polymer blends	Total CNT concentration based on entire polymer blend (vol %)	Effective CNT concentration in the LDPE phase (vol %)
0.80	8.0	9.8
0.67	8.0	11.5
0.50	8.0	14.8
0.33	8.0	20.7
0.20	8.0	30.3

The detailed concentrations of CNTs in the composites are shown in Table 4-4. Furthermore, when PVDF content increases up to the co-continuous phase range (Stage II, Fig. 4-4), the

MWNT-filled LDPE phase shirks further but still exhibits 3D continuity. The distance between neighboring MWNTs decreases greatly so that MWNTs contact with each other and finally form a conductive network in the LDPE phase (Fig. 4-3c-d). Such trinary-continuous structure induces the double percolation effect, which refers to the percolation of MWNT in the LDPE phase and the continuity of the MWNT-filled LDPE phase in the polymer blend. Thus a notable increase of about 6 orders of magnitude in conductivity is observed in comparison with the MWNT-filled single LDPE composite. However, with further increasing the PVDF content (Stage III, Fig. 4-4), the conductivity starts to decrease. Though the MWNT-filled LDPE phase is highly electrically conductive, the MWNT-LDPE/PVDF composites are of lower conductivity because of the discontinuous MWNT-filled LDPE phase in the PVDF phase (Fig. 4-1c and Fig. 4-3e). The evolution of the conductivity with blend composition can be an indirect evidence for the preferential location of MWNTs in LDPE phase rather than PVDF phase.

4.3.3 Frequency dependence of the dielectric properties

Figure 4-5 presents the frequency dependence of dielectric properties of the MWNT-LDPE/PVDF composites with fixed overall f_{MWNT} (0.08) and different blend compositions. As indicated, for the MWNT-filled LDPE composite, the dielectric permittivity is of low value (14) and almost independent of frequency in the measured frequency range (Fig. 4-5a). The AC conductivity exhibits strong correlation to the frequency (Fig. 4-5b), implying that it is mainly determined by the polarization effect and the electron motion owing to the absence of the conductive path.[202] However, as the ratio of PVDF/LDPE increases up to 1:1, the permittivity values are dramatically increased, especially at low frequencies (e.g., 14 to 840 at 10^{-1} Hz, Fig. 4-5a) The microcapacitor principle can be invoked as being responsible for such increment. With the increase of effective CNT content in LDPE phase (Table 4-4), the isolation distances between neighboring MWNTs are continuously reduced. Finally, a network of microcapacitors with the MWNTs as electrodes and a very thin LDPE layer in between as dielectric can be formed in the composite near f_c (in the case of PVDF/LDPE=1:1). Each microcapacitor contributes an abnormally large capacitance, which can then be correlated with the significant increase in the dielectric

permittivity.

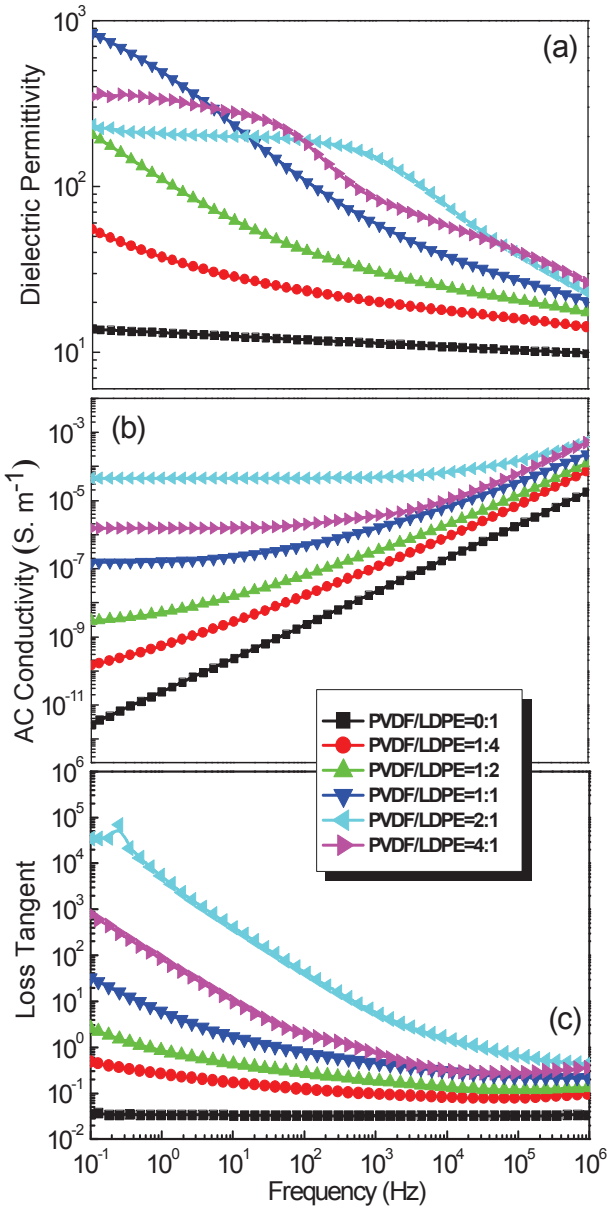

Fig. 4-5 *Frequency dependence of (a) the dielectric permittivity, (b) AC conductivity and (c) loss tangent of the biphasic composites with a fixed total* f_{MWNT}*=0.08 and various polymer blend compositions.*

At the same time, the direct conductive characteristic (flat plateau of the conductivity) occurs and becomes more visible in the 1:1 case. (Fig. 4-5b) This confirms 1:1 volume ratio composite is indeed near its percolation threshold, because at this point, conductive paths

(referring to the flat plateau at low frequencies) are limited and the contribution of microcapacitors to the conductivity is of large importance and becomes dominant after a critical frequency (referring to the linear increase at high frequencies).[203] Additionally, as the ratio of PVDF/LDPE increases further from 1:1 to 2:1, numerous CNT percolating paths are formed and the electrons can move freely in the entire frequency range, thus the frequency independence of the AC conductivity is observed in the 2:1 composites. While the dielectric permittivity starts to decrease due to the formation of the conductive network in the LDPE phase, which facilities charges to delocalize in a macroscopic scale and induces high current leakage. As shown in Fig. 4-5c, an increasing trend of loss tangent with increasing PVDF phase content is observed, the loss tangent remains at low values (0.034) with increasing frequency in MWNT-filled LDPE composite, however, in the biphasic polymer composites, the loss tangent is very high at low frequency.

4.3.4 Dependence of the dielectric properties on MWNT content

We prepared four groups of polymer composites (with volume ratio of PVDF/LDPE at 0:1, 1:1, 2:1, and 1:0). In each group, overall f_{MWNT} (based on the entire polymer blends) was varied to reach the percolation threshold. The influence of MWNT content on the AC conductivity and dielectric permittivity of the composites is illustrated in Fig. 4-6. It is clearly seen that the AC conductivities for four systems increase dramatically when f_{MWNT} approaches f_c (Fig. 4-6a). The variations can show a good agreement with the typical power law, Eq. 1-21a and b.[60]

The parameters for each system are obtained by fitting the conductivity data at 1 Hz to the log–log plots of the power laws and the results are listed in Table 4-5. The plots of best linear fits are shown in Fig. 4-7.

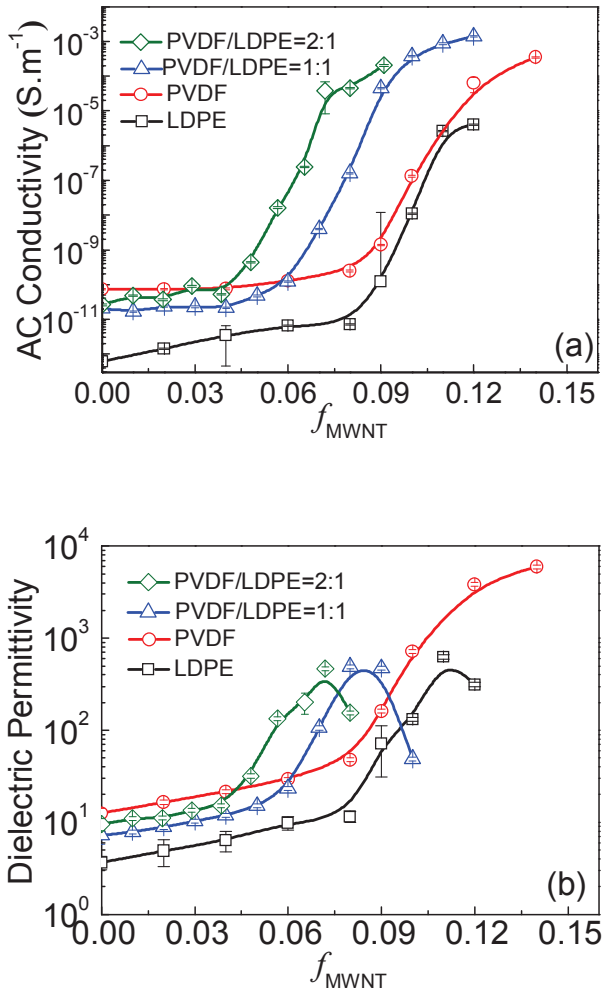

Fig. 4-6 *(a) The AC conductivity and (b) dielectric permittivity of biphasic polymer composites as a function of the MWNT content, measured at 1 Hz and room temperature. The data for MWNT-filled PVDF are cited from Chapter III.[65]*

Table 4-5 Parameters obtained by fitting AC conductivities to the power law and used to predict the effective dielectric permittivity of the biphasic composites

System	f_c (vol%)	t	q	α	ϕ
LDPE	9.6±0.1	3.49±0.42	1.655±0.08	–	–
PVDF	9.2±0.1	4.49±0.26	0.78±0.10	–	–
PVDF/LDPE(1:1)	7.1±0.1	5.42±0.58	1.23±0.23	0.25	0.50
PVDF/LDPE(2:1)	5.7±0.1	4.57±0.28	1.30±0.43	0.82	0.33

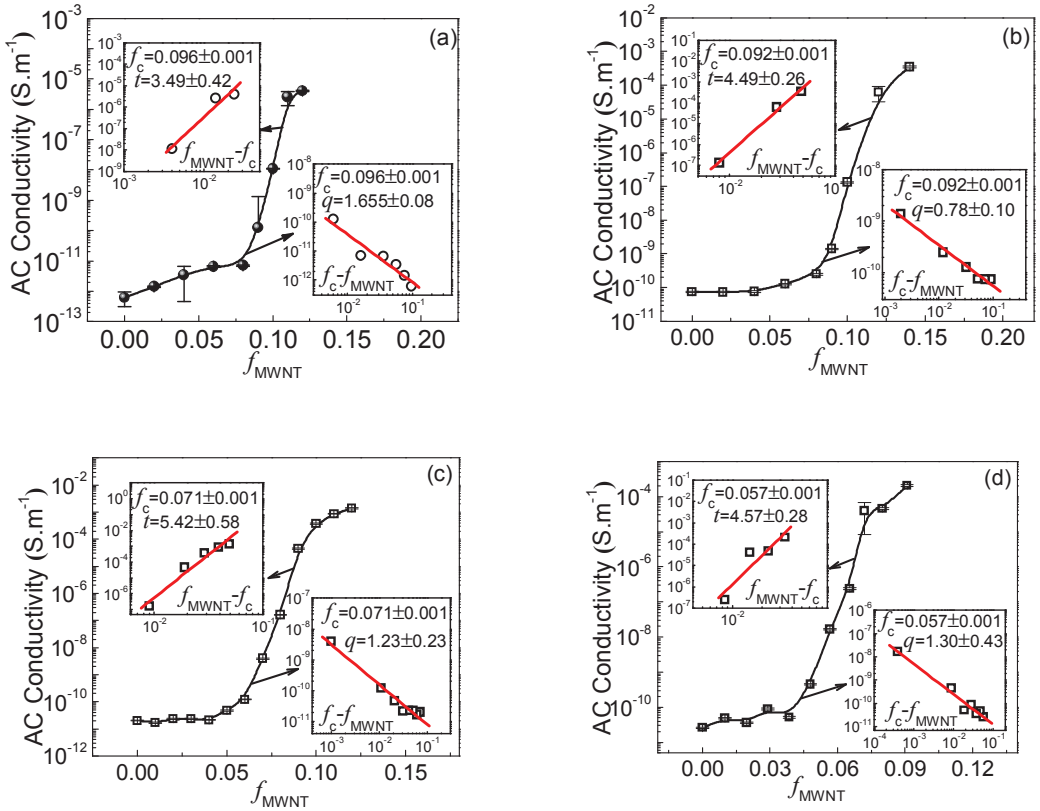

Fig. 4-7 *AC conductivity of the composites as a function of of f_{MWNT}, measured at room temperature and 1 Hz. The insets are variations of logσ versus log f for $f_{MWNT} > f_c$ (upper left side) and $f_{MWNT} < f_c$ (bottom right side) respectively. (a)-(d) correspond to the composites at volume ratios of PVDF/LDPE=0:1, 1:0, 1:1 and 2:1 respectively.*

It is noted that the MWNT-filled LDPE composites have a similar f_c (~0.09) with PVDF composites because of the completely identical processing conditions. A similar phenomenon was also recently reported by Panda et al.[204] in the hot-molded percolative Ni/polymer composites. The attained high f_c may be a consequence of the breakage of MWNTs and polymer wrapping on tube surfaces as abovementioned. However, once the double percolated structure forms in the 1:1 composites especially in the 2:1 one, the percolation value can be largely reduced without decreasing the maximum conductivity level to reach. The f_c value (5.7 vol%) is the lowest when the volume ratio of PVDF/LDPE is 2:1 in this study. The exponent q for each system studied nearly agrees well with the universal one (q_{un}≈0.8-1)[60] while the exponent t is larger than the universal values (t_{un}≈1.6-2)[60]. This discordance has been also found in other percolative composites[60, 106, 205] and can

be often suggested by the Swiss-Cheese model.[206]

Presented in Fig. 4-6b is the evolution process of the dielectric permittivity of biphasic polymer composites as a function of f_{MWNT}. It should be noted that the PVDF composite exhibits a higher dielectric permittivity than LDPE composites in the whole range of CNT content. Such difference in permittivity values may come from the polymer matrix since the processing condition is completely the same. More significant dipolar polarization present in PVDF matrix can usually give rise to a larger enhancement of dielectric permittivity of the composite.[204] Additionally, in comparison with 1:1 and LDPE composites, the 2:1 composite exhibits a lower f_c, but its maximum permittivity can be of the same level (~500 at 1Hz) with the other two systems. Of particular interest is that the dielectric permittivity of all systems enhances significantly with the f_{MWNT} approaching f_c. This behavior in single polymer composite can be well described by implementation of the classic percolation theory.[60, 65, 66, 107] However, for the biphasic percolative composite, no established model can directly apply on it to date. Because apart from the insulator-metal transition in CNT localized phase, the dielectric permittivity is also largely determined by the interaction between two polymer phases and the polarization in the phase free of CNTs, especially in polymers with large permittivity values, like PVDF (10 at 100 Hz)[107] and P(VDF-TrFE-CTFE) terpolymer (57 at 100 Hz)[111]. In this study, a simple model combining the Lichtenecker rule and percolation theory was established to analyze the permittivity data of biphasic percolative composites by considering all factors aforementioned.

Generally, for any two-phase composites, the dielectric permittivity, ε_c, must lie between the lower ($\varepsilon_{c,min}$) and upper limit ($\varepsilon_{c,max}$), no matter fillers form dispersed phases or a continuous structure in the matrix, and the two bounds are defined as:[207]

$$\varepsilon_{c,min}^{-1} = (1-\phi)\varepsilon_m^{-1} + \phi\varepsilon_{filler}^{-1} \quad (4\text{-}6)$$

$$\varepsilon_{c,max} = (1-\phi)\varepsilon_m + \phi\varepsilon_{filler} \quad (4\text{-}7)$$

here, ε_m, ε_{filler} is the dielectric permittivity of the matrix and filler, respectively. ϕ presents the filler volume fraction. Starting from the Eq. 4-6 and 4-7, Lichtenecker assumed that the

effective dielectric permittivity of two-phase composites follows a law:[76]

$$\varepsilon_c^\alpha = (1-\phi)\varepsilon_m^\alpha + \phi\varepsilon_{filler}^\alpha \quad (4\text{-}8)$$

The parameter α describes a specific microgeometrical topology of the composites and the value varies from -1 to 1. In our case, the CNTs are exclusively localized in the LDPE phase, the PVDF phase retains neat regardless of the variation of CNT content and the ratio of PVDF/LDPE. Therefore we regard the continuous MWNT-filled LDPE as filler and PVDF phase as matrix. Therefore, the law can be defined as:

$$\varepsilon_c^\alpha = (1-\phi)\varepsilon_P^\alpha + \phi\varepsilon_{ML}^\alpha \quad (4\text{-}9)$$

where, ε_P and ε_{ML} are the effective dielectric permittivity of pure PVDF and the MWNT-filled LDPE phase, respectively. ϕ is the volume fraction of LDPE in the polymer blend (the values are shown in Table 4-5). The parameter α here reflects the interactions between two polymers and is much related to the blend composition. In other words, the value should be constant for a given volume ratio of composites regardless of the variation of CNT loading content. Therefore, by using the permittivity data of LDPE/PVDF blends without MWNTs, pure PVDF and LDPE phase, α can be calculated for each polymer blend system. The results are shown in Table 4-5. The permittivity variation in MWNT filled LDPE is typically based on the percolation effect, and characterized by the power law:[65]

$$\varepsilon_{ML} = \varepsilon_L \left| \frac{f_c^{eff} - f_{MWNT}^{eff}}{f_c^{eff}} \right|^{-q} \quad (4\text{-}10)$$

where q is the critical exponent, f_{MWNT}^{eff} is the effective volume fraction of MWNT in LDPE phase, its relationship with the overall MWNT content based on the entire polymer blend (f_{MWNT}) is drawn as the following equation:

$$f_{MWNT}^{eff} = \frac{f_{MWNT}}{\phi + (1-\phi) f_{MWNT}} \quad (4\text{-}11)$$

Accordingly, f_c^{eff} corresponds to the percolation threshold based on only LDPE phase and can also be calculated.

$$f_c^{eff} = \frac{f_c}{\phi + (1-\phi) f_c} \tag{4-12}$$

By submitting Eqs. 4-10,11,12 into Eq. 4-9, the effective dielectric permittivity in biphasic percolative composites can be modeled as a function of the filler volume fraction.

$$\varepsilon_c^{\alpha} = (1-\phi)\varepsilon_P^{\alpha} + \phi\left(\varepsilon_L \left| 1 - \frac{f_{MWNT}\left[\phi + (1-\phi) f_c\right]}{f_c\left[\phi + (1-\phi) f_{MWNT}\right]}\right|^{-q}\right)^{\alpha} \tag{4-13}$$

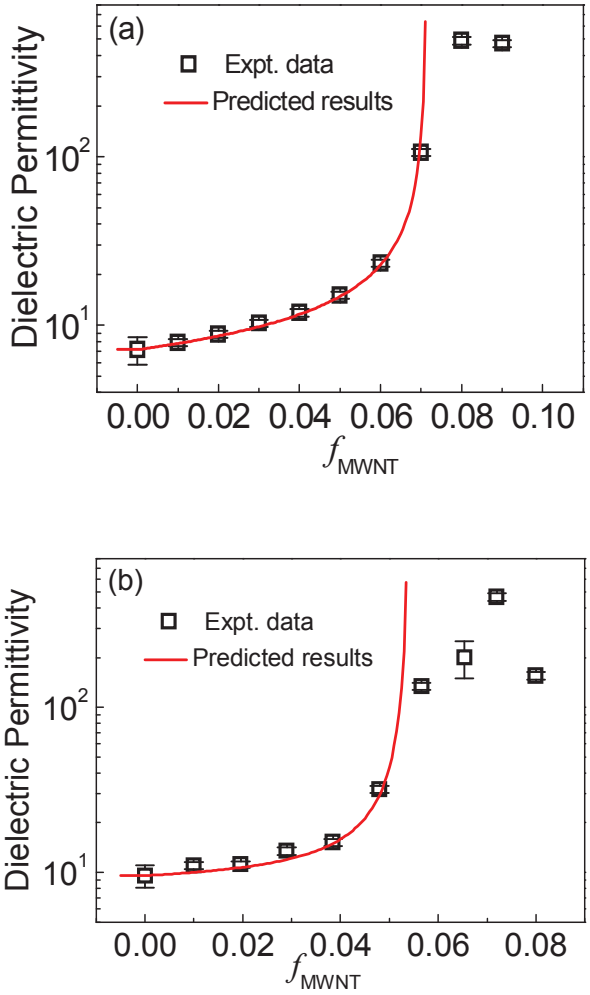

Fig. 4-8 *Comparison of the dielectric permittivity at 1 Hz predicted by Eq.4-13 and experimentally observed in biphasic composites with PVDF/LDPE volume ratio at (a) 1:1 and (b) 2:1.*

Using the parameters listed in Table 4-5, the plots of the dielectric permittivity predicted

by Eq. 4-13 are given in Fig. 4-8. All the permittivity values (ε_c , ε_p and ε_L) in the Eq. 4-13 are at 1 Hz. For a comparison, the experimental permittivity data at 1 Hz are also plotted. It is clearly seen that the prediction is in a good agreement with the experimental observation for both systems even for composites approaching f_c. The only divergence observed is in the composites (beyond f_c) with conductive but not dielectric nature. The experimental permittivity values are much lower than predicted ones owing to the unexpected decrease induced by the leakage current. Overall, our model has been still demonstrated effective to predict the effective dielectric permittivity of the double percolated structure based composites below the percolation threshold.

4.4 Conclusions

The double percolated structure has been realized in the MWNT-LDPE/PVDF composite systems, namely, the MWNTs are exclusively distributed and percolated within the LDPE phase that forms continuous electrically conductive channels in the matrix, and both polymer phases are co-continuous in 3D space. The uneven distribution of MWNTs was determined by the viscosity factor, which is proven possible to dominate the generally discussed thermodynamic effect to favor the final CNT location. Such a double percolated structure allows for achieving polymer composites with high permittivity at much lower filler concentrations. The biphasic composite with a PVDF/LDPE volume ratio at 2:1 exhibits a lowest percolation threshold (f_c=5.7 vol%) and a permittivity as high as 470 near f_c.

The effect of double percolation is well illustrated by modeling the permittivity of composites as a function of MWNT volumetric fraction. The model based on the well-known Lichtenecker rule and percolation theory has been evidenced to be much suitable to the biphasic polymer composites. Overall, we hope that our study would form a helpful reference to adapt the double percolation to largely enhance the dielectric permittivity of the biphasic polymer blend in practical applications.

Chapter V
Micro/nano hybrid structures and their application in the dielectric composites

5.1 Introduction

Electroactive polymers, such as PVDF and P(VDF-TrFE) copolymer, open opportunities for the application in high-charge storage capacitors.[49, 107, 208] In order to realize this application, it is highly desirable to substantially improve the dielectric permittivity of such electroactive polymers. One straightforward approach is to disperse high-ε_r ceramic powders into polymer to prepare 0-3 type composites.[53, 54] To realize a high enough value of dielectric permittivity, very high filler loading is in general necessary, usually over 50 vol% to reach. Such high loading of ceramic powders significantly deteriorates the mechanical performance of final composites. The porosity caused by high loading would dramatically decrease the dielectric properties of the composites.

An alternative strategy is to develop high-ε_r percolative composites filled with conductive or semiconductive fillers, such as metal particles,[55-57] carbon fibre,[58] CNTs,[59-61] and graphite nanoplates.[62] As described by the power law, the ε_r of PVDF can be dramatically increased by the introduction of conductive fillers near the f_c. In light of the microcapacitor model,[56-59, 62] fillers distributed in the insulated polymer matrix can form into a large number of microcapacitors so as to improve the ε_r of the polymer composites greatly. Among these fillers, CNTs have been most intensively studied, as their large aspect ratio can lead to percolation levels in nanocomposites at much low loading.[60] However, CNTs are always frizzy in the CNT/polymer composite, which is not beneficial in forming parallel pair electrodes of microcapacitors (Fig. 5-1a). Additionally, a general way to create microcapacitors is to increase the CNT content in the polymer matrix and thus to decrease the inter-nanotube distance. However, when this distance between neighboring

CNTs is reduced down to a certain value, there is a risk of tunneling that would relax the charges generated at CNT-polymer interfaces. To overcome the issues aforementioned, aligned CNT arrays can be used as filler to form local microcapacitors in series to store the charges, meanwhile good dispersion of CNT arrays ensures a large separation distance between each other, accordingly avoids the tunneling conduction between CNT arrays. Therefore, the synthesis of CNT array and their isolate distribution into polymer matrix is the key to realize this end.

We propose a microarchitecture of SiC-CNT hybrid as conductive filler, i.e., vertically aligned carbon nanotubes on SiC microplatelets. It should be emphasized that such hybrid microarchitecture is not the simple mechanically mixed SiC plus CNTs but obtained directly from CVD synthesis by growing CNTs on the platelike SiC substrates. When such hybrid fillers were homogenously dispersed into polymer, CNTs readily oriented on each platelet could give rise to more effective microcapacitors in composites (Fig. 5-1b) and thus result a high dielectric permittivity of composites.

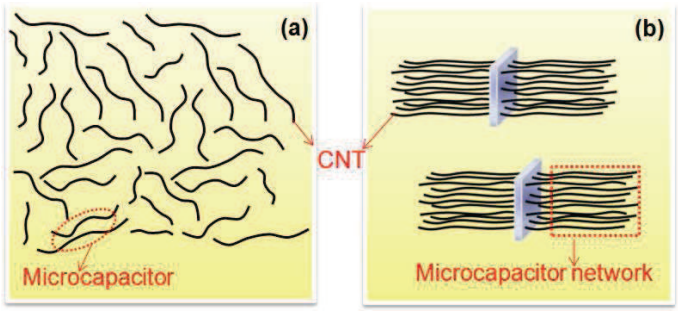

Fig. 5-1 *Schematics of microcapacitor structures formed in the composites based on (a) the randomly oriented CNTs and (b) CNT hybrids with platelet particles.*

In this chapter, we reported the controllable growth of CNTs on SiC micrometer plate-like particles by a floating catalytic CVD. The effects of experimental conditions (temperature, hydrogen ratio, etc.) as well as the nature of substrate particles on the morphology and organization mode of CNTs were evaluated. We also investigated hybrid SiC-CNT/PVDF composites with low volume fraction of CNTs to significantly enhance the dielectric permittivity of polymer matrix composites. Broadband dielectric spectroscopy has

been applied to study the electrical conductivity and dielectric permittivity of composites in a wide frequency range (10–10^6 Hz).

5.2 Experimental

5.2.1 SiC-CNT hybrid synthesis

SiC-CNT hybrids were produced by a floating catalytic CVD process. Acetylene C_2H_2 was used as carbon source and ferrocene $Fe(C_5H_5)_2$ as catalyst precursor. For a typical experiment, the preparation process of SiC-CNT hybrids was as below: firstly, the as-received SiC powders (Marion Technologies, France) were homogeneously dispersed on a quartz plate (4×30 cm^2) by using a sieve, the plate was placed in a quartz tube reactor (120 cm in length, 45 mm in inner diameter) heated to set temperature (ranging from 550 to 750 °C) by a horizontal tube furnace (75 cm long) under argon atmosphere. Then, ferrocene dissolved in xylene C_8H_{10} at a concentration of 0.05 g mL^{-1} was injected in the reactor by a syringe system and carried to the stable reaction zone in the form of spray by carrier gases (Ar and H_2). Accompanying with the injection of catalyst solution, acetylene was also fed into the reactor simultaneously. The gas flow rate was controlled by electronic mass flow meters (Bronkhorst). The CNT growth time was controlled at 10 min. After growth, the system was cooled to room temperature under argon atmosphere.

5.2.2 SiC-CNT/PVDF composites preparation

The SiC-CNT/PVDF composites were prepared by employing a solution cast and extrusion method. The former aimed at the total penetration of PVDF solution into the aligned CNTs, and the latter ensured a uniform dispersion of SiC-CNT through the composite. In detail, Firstly, the collected hybrid SiC-CNT particulates and PVDF powder were dispersed in the solvent DMF, and were then treated by magnetic stirring overnight to obtain the composite precursor solution. The mixed SiC-CNT/PVDF solution was coated on the glass substrate, and then thermally treated at 150 °C for 2 h. Afterwards, the as-prepared films were further mixed. The mixing was done in a co-rotating, conical, twin-screw microextruder/compounder (Micro 5 cm^3 Twin Screw Compounder, DSM) at 200 °C, for

over 10 min and at a mixing speed of 20 rpm in Ar atmosphere. It should be noted that too long mixing time would generate the detachment of CNTs from the surface of SiC particles leading to the nanotubes aggregating. Slabs with a thickness of 1.5 mm were prepared by injection molding of the mixed composites (Micro 5 cm^3 Injection Molder, DSM) using a press at 1.6 MPa for 1 min, while the temperature was kept at 60 °C. Then, the temperature would be decreased from 60 °C to room temperature at a sufficiently low rate.

5.2.3 Sample characterization

The as-prepared samples were characterized by the following techniques: SEM (LEO Gemini 530), TEM with electron diffraction analysis setup (JEOL JEM-3010 at 300 kV), Raman spectrometer (Jobin Yvon), X-ray diffraction (Siemens D5000, Cu K_α radiation (k = 1.54069 Angstrom)), thermogravimetric (TG) analysis (NETZSCH STA 449F3). The dielectric properties of the composites were characterized as a function of frequency using an impedance analyzer (Novocontrol BDS 20). Before measurement, silver paste has been applied on the sample surfaces for contacting.

5.3 SiC-CNT hybrid morphology

In the process of producing SiC-CNT hybrids by floating catalytic CVD, two main reactions were involved: the decomposition of carbon source (acetylene, C_2H_2) and the decomposition and agglomerate (into particles) of the catalyst precursor (ferrocene, $Fe(C_5H_5)_2$). Especially, the latter generally determines the CNT morphology and the hybrid organization. Both reactions are largely influenced by the experimental conditions as well as the substrate nature. In some cases, the experiment conditions would determine the morphology of the final hybrids through varying the substrate nature (e.g. surface composition, crystal type, etc.). In this study, we first investigated the effect of different experimental parameters (e.g., temperature, hydrogen ratio, etc.) on the orientation and organization of SiC-CNT hybrids. The effects of temperature and hydrogen ratio on the morphology of SiC-CNT hybrids were mainly presented. The effect of substrate nature on the organization mode of hybrids and the effect of experimental conditions on the substrate

nature were also discussed.

5.3.1 Effect of temperature

As shown in Fig. 5-2a, the SiC used was irregularly plate-like particle. The average thickness and width of the SiC microplate were about 1 μm and 5 μm respectively. Fig. 5-2b-e showed the CNT organization on the SiC particles at constant hydrogen content (H_2/Ar=0.1:0.9 L/min) and different temperatures from 550 to 750 °C. CNTs were grown uniformly along a single direction (denoted as "single-direction" hybrids) when the reaction temperature was below 700 °C. This phenomenon is definitely related to the nature of SiC substrate, i.e. some crystal orientation or crystal facet of the substrate was much active for CNT growth by interacting with catalyst and carbon source. More detailed explanation would be given in the following sections. However, at higher temperatures (>700 °C), CNT growth and organization appeared along multi-directions (Fig. 5-2f, denoted as "multi-directions" hybrids, most of them were along two opposite directions perpendicular to the flat surfaces of SiC particles). Such difference in the CNT growth and organization at different temperatures may result from the two main reactions aforementioned. In detail, at low temperatures (<700 °C), the decomposition of catalyst precursor was prone to occur on the SiC surface rather than in the gas atmosphere. As the activation energy of the decomposition reactions can be decreased dramatically due to the interaction between substrate and reactants, which thus greatly favors the CNT nucleation. Therefore, it can be concluded that the nature of SiC substrate influenced the organization more at low temperatures. However, at higher temperatures (>700 °C), the decomposition of catalyst precursor in gas atmosphere is possible and enable the formation of iron atoms or small particles that would fall down on the surface of substrate to favor the CNT growth along multi-directions. In this case, the influence of SiC substrate nature was largely weakened and the CNT growth and organization is mainly determined by the experimental conditions, such as temperature.

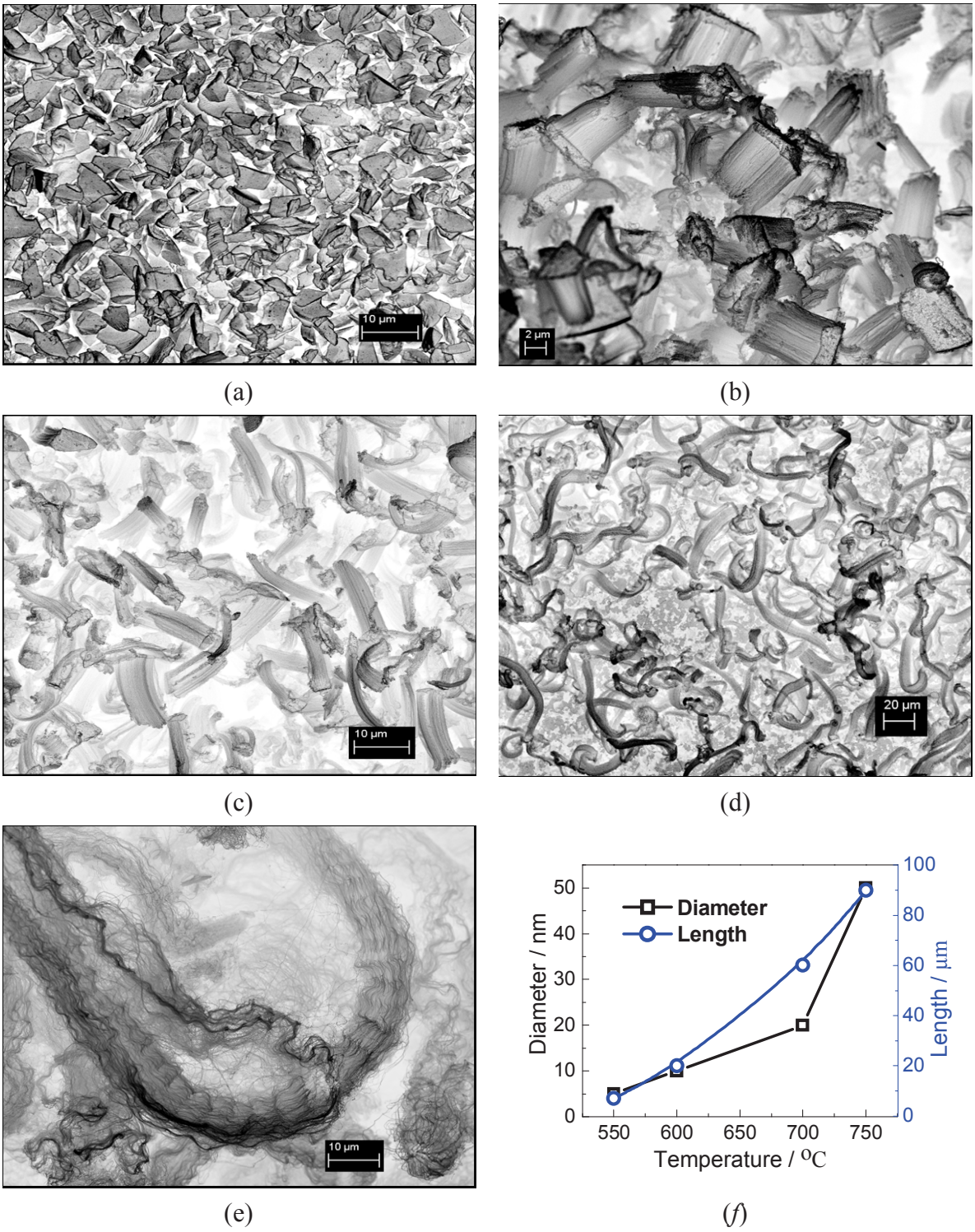

Fig. 5-2 *(a) SEM images of pristine SiC. CNT growth and organization on SiC particles at a constant H_2/Ar ratio of 0.1:0.9 L/min and varied temperatures: (b) 550 °C, (c) 600 °C, (d) 700 °C, (e) 750 °C, (f) evolution of diameter and length with temperature.*

As shown in Fig. 5-2f, the length of CNT arrays increased almost linearly with temperature, while the diameter of CNTs increased slowly with temperature below 700 °C and exhibited an abruptly increase (above 700 °C). The more easily agglomerated catalyst particles at high temperatures may be responsible for these large-diameter CNTs. In addition, the number density of CNTs decreased with temperature because of the diameter increase.

5.3.2 Effect of hydrogen ratio

Figure 5-3 showed the evolution of CNT growth and organization at constant temperature (600 °C) and different hydrogen ratios (over Ar, total flow rate is 1 L/min). With the increase of hydrogen ratio, the organization of CNTs on SiC particles changed from "single-direction" to "multi-directions" (most of them were along two directions). Especially, the organization of SiC-CNT hybrids presented a transitional phase (along "one and half direction") with the ratio H_2/Ar at 0.2:0.8. It should be emphasized that the "multi-directions" hybrids can also be obtained at low temperatures (e.g., 600 °C) by increasing the hydrogen ratio up to 0.3:0.7. This suggests that, apart from the temperature, the high hydrogen ratio can also dominate the substrate nature to determine the growth and organization of nanotubes in multi-directions. As compared to the "multi-directions" hybrids obtained at higher temperature (750 °C, Fig. 5-2e), the high hydrogen ratio induced ones exhibited higher number density yet much smaller length. As a result of such dense morphology, the nanotubes can be more aligned, as shown in the Fig. 5-3f. The dense and uniform "multi-directions" hybrid is much more favorable for the realization of proposed microcapacitor network and therefore will be employed to study the reinforcement effect in polymer composites.

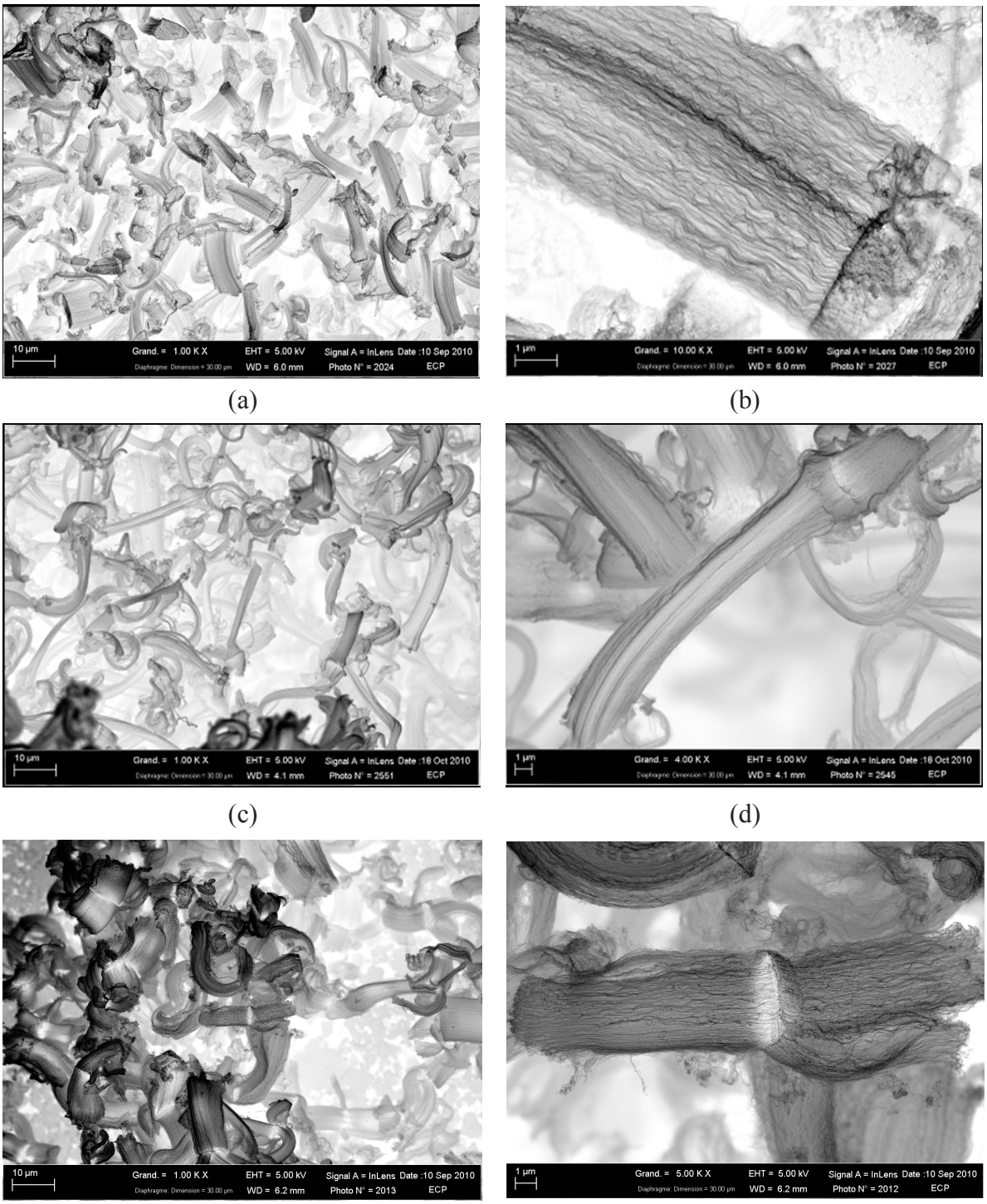

Fig. 5-3 *SEM images of CNT growth and organization on SiC particles at 600 ^{o}C with different H_2 ratios: (a),(b) H_2/Ar=0.1:0.9 L/min, (c),(d) H_2/Ar=0.2:0.8 L/min, (e),(f) H_2/Ar= 0.3:0.7 L/min.*

5.3.3 Effect of SiC substrate nature

5.3.3.1 "Single-direction" hybrid structure

The growth of CNTs on SiC was along single direction at low temperatures (<700 ^{o}C) and low hydrogen ratios (H_2/Ar= 0.1:0.9 L/min), which can be related to the nature of SiC substrate.

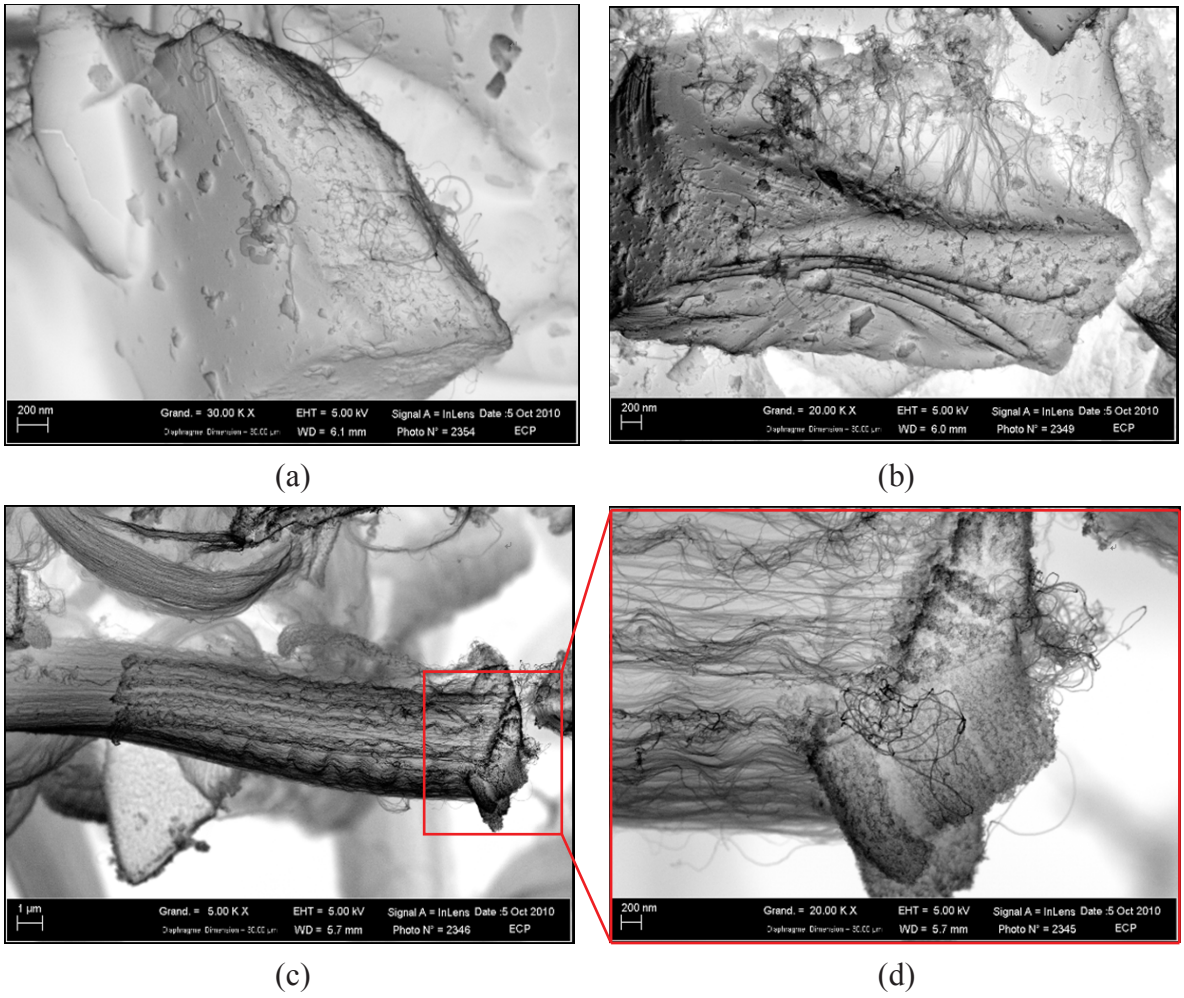

Fig. 5-4 *(a) and (b) SEM images of catalyst deposit and CNT growth on SiC by CVD of ferrocene and acetylene at 600 °C with the ratio H_2/Ar= 0.1:0.9 L/min and reaction duration=3min. (c) SEM picture about CNT growth on different crystal facets of one particle at 600 ^{o}C with the ratio: H_2/Ar= 0.1:0.9 L/min and reaction time=10 min. (d) is enlarged image of the rectangular area in (c).*

Fig. 5-4a and b showed the starting point for catalyst deposit on SiC surfaces as well as CNT growth by CVD of ferrocene and acetylene during 3 min. It can be seen that the catalyst particles were preferably deposited on certain facets of the substrate, and the growth of CNTs started solely on these deposition-desirable facets. Therefore, the deposition of catalyst particles and the growth of CNTs were facet-selective under certain CVD conditions. Fig. 5-4c and d showed the CNT growth at different crystal facets of one SiC particle. It can be observed three CNT bundles grew on different crystal facets of one particle and these CNT bundles were perpendicular to the corresponding facets. However, the lengths of three CNT bundles were different, although the three facets were exposed to the same CVD atmosphere at the same temperature, and had the same possibility to contact the carbon and iron feedstock. The results indicated that the interaction between catalyst particles and the diverse facets of SiC was distinguishable, which is plausibly resulted from the difference in activity of different crystal facets.

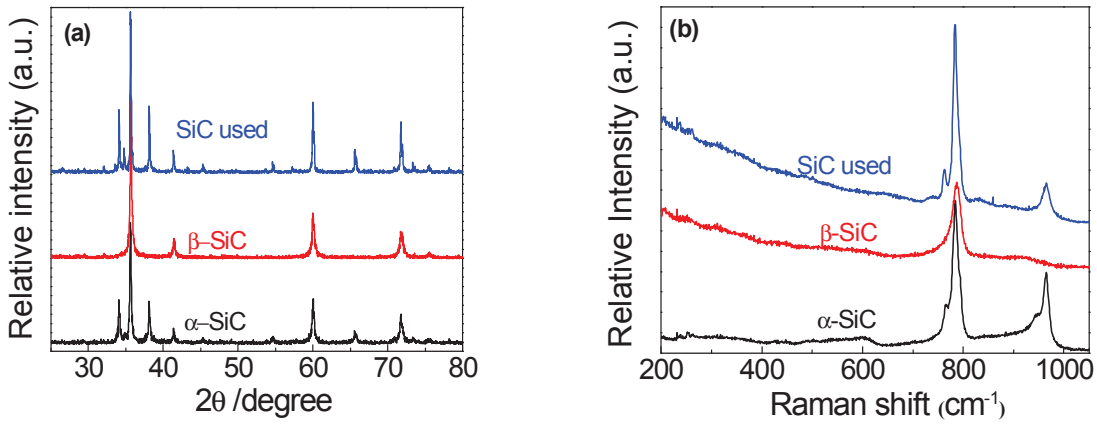

Fig. 5-5 *(a) XRD patterns and (b) Raman spectra of the SiC used, alpha-SiC and beta-SiC.*

In order to examine the nature of SiC substrate used, the XRD patterns and Raman spectra of SiC used and other two typical SiC (Alfa Aesar, crystal type known, 99.8%) were investigated, as shown in Fig. 5-5a and b. From XRD patterns, we found that the peaks of SiC matched well with those of α-SiC (6H-SiC), but it was not excluded that the existence of β-SiC (3C-SiC), because the diffraction peaks around $2\theta = 35.6^{o}$, 41.4^{o}, 60.0^{o}, 71.8^{o} and 75.5^{o} for the (111), (200), (220), (311) and (222) planes of β-SiC are overlapped with those for the

(102), (104), (110), (116) and (0012) planes of α-SiC.[209-211] The same conclusion can be drawn from Raman spectra, as shown in Fig. 5-5b. The Raman peaks of SiC used were in agreement with those of α-SiC (6H-SiC). Peaks centered at 783 and 965 cm^{-1} could be assigned to the TO and LO phonon peaks of α-SiC (6H-SiC), but the peak related to the TO phonon peak of β-SiC (3C-SiC) is also around 783 cm^{-1} and overlapped with that of α-SiC (6H-SiC).[212, 213] By combining this conclusion with the SEM results of uniform hybrid structure and organization morphology at the same conditions, we can conclude that the crystalline type of SiC used was single and mainly composed of α-SiC (6H-SiC).

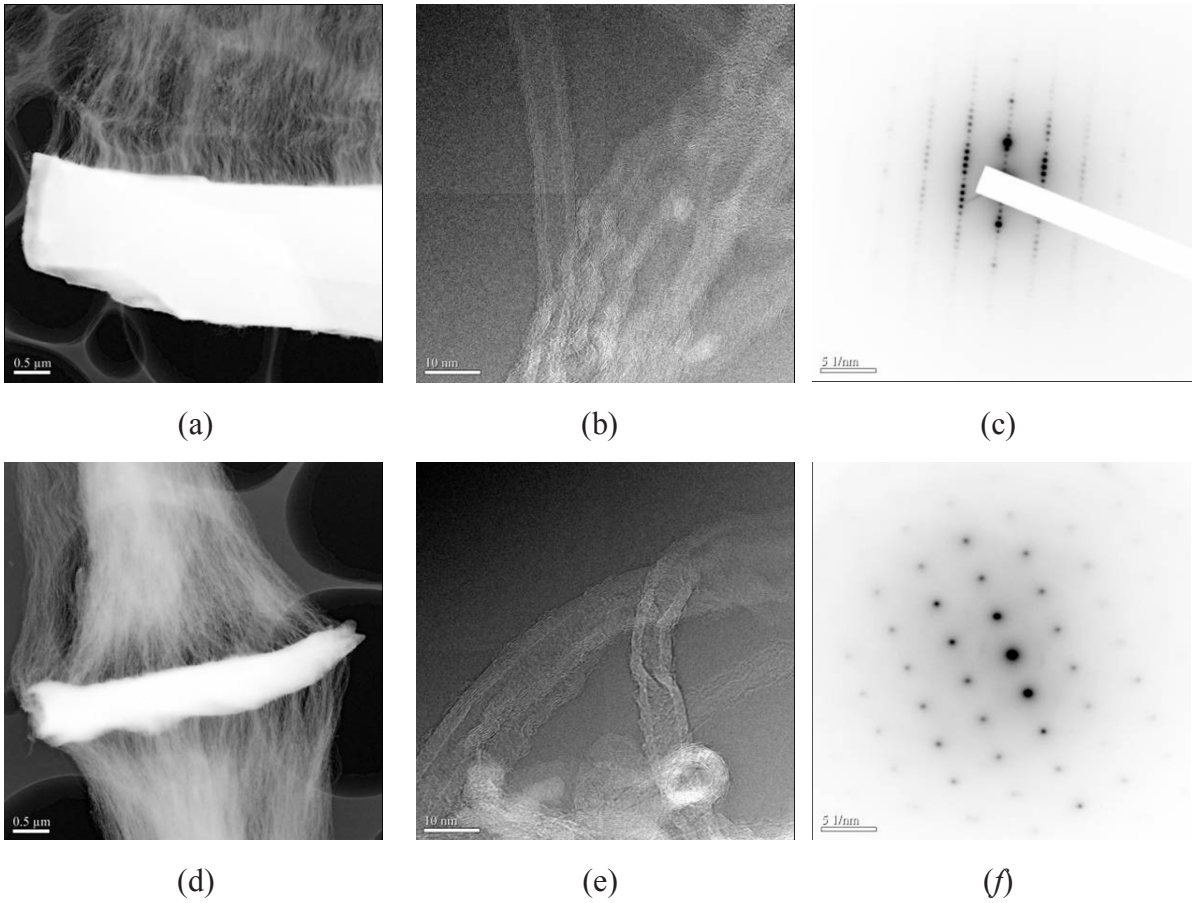

Fig. 5-6 *(a, b) TEM images of "single-direction" hybrid grown at 600 °C for 10 min with H_2/Ar=0.1:0.9 L/min. (c) is the selected area electron diffraction (SAED) patterns of the substrate (edge part) in (a). (d, e) TEM images of "multi-directions" hybrid prepared at 600 °C for 10 min with H_2/Ar=0.3:0.7 L/min. (f) is the SAED patterns of the substrate (edge part) in (d).*

The TEM images of "single-direction" SiC-CNT hybrids were shown in Fig. 5-6a and b. The aligned CNTs were grown on the surface of SiC substrate. High resolution images indicated that formed CNTs were multi-walled and composed of 4-6 walls, and the diameter was in the range of 8-10 nm. The SAED was performed at the edge of SiC particles (to make sure that the electron can transmit through the edge, the thickness must be less than 100nm). As shown in Fig. 5-6c, the SAED patterns indicated that the surface of SiC is typically hexagonal crystal structure, the same as that of 6H-SiC (α-SiC).[214] This result agreed well with those of XRD patterns and Raman spectra.

α-SiC (6H-SiC) is a hexagonal structure, carbon atom layer and silicon atom layer are stacked alternately along the axis of (001). The surfaces of SiC particles consist of different crystal facets, some facets are silicon atom layers (0001), and some are carbon atom layers (000-1). The surface energy of silicon facet is larger than that of carbon facet.[214] The silicon-rich facets are easier to react with the iron atoms produced from ferrocene decomposition during CVD process to form silicon-iron compounds (e.g. $FeSi_2$, Fe_2SiO_4), which are not desirable for the growth of CNTs. While on carbon-rich facets, the iron particles could keep their catalytic activity for the growth of nanotubes.[215, 216] Therefore, we presumed that the two flat surfaces of SiC microplates exhibited different crystalline orientation and structures. Namely, one is the silicon facet, and another is carbon facet. The CNT growth occurred preferentially on carbon-rich facets and formed "single-direction" hybrids.

5.3.3.2 "Multi-directions" hybrid structure

Organization mode of SiC-CNT hybrids can be changed by adjusting the reaction conditions, especially the hydrogen ratio and temperature. Fig. 5-6d and e showed the TEM images of "multi-directions" hybrids formed at high hydrogen ratio. CNT bundles grew vertically on the SiC substrate and mainly along two directions perpendicular to the flat surfaces of SiC platelet. The diameter and wall number of CNTs for "multi-directions" hybrids are almost the same as those of "single-direction" one. Fig. 5-6f was the SAED patterns for the substrate edge of "multi-directions" hybrids, which can be indexed to cubic

crystal structure and different from the diffraction patterns of "single-direction" hybrids. This result indicated that the crystal structure of the substrate (at least the surface layer of substrate) was changed from "hexagonal" to "cubic" at high Ar/H_2 ratio. This crystal structure transition may be responsible for the different organization modes of hybrid structure.

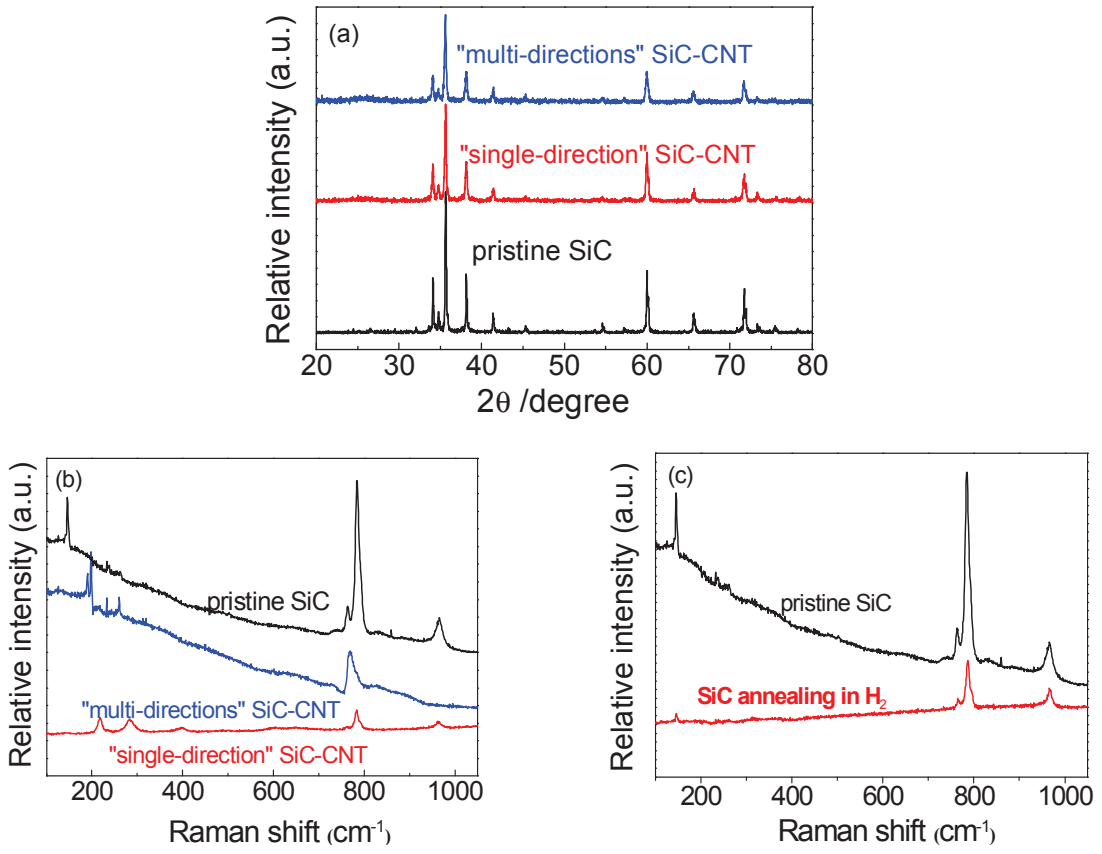

Fig. 5-7 *(a) XRD patterns and (b) Raman spectra of hybrids with different organization modes. (c) Raman spectra of pristine SiC and SiC annealed at 600 °C with H_2/Ar=0.3:0.7.*

To further verify the structure change of the substrate, the XRD patterns and Raman spectra of the hybrids with different organization modes were shown in Fig. 5-7. The XRD patterns of the two types of hybrids are almost the same, and showed no difference from the XRD patterns of pristine SiC (6H-SiC) except a small peak around $2\theta=26^{o}$, which is related to the carbon deposited on SiC substrate. It seems to be inconsistent with the results of the electron diffraction. The reason may be that X-ray can penetrate deeper into (through) the samples than the electron diffraction which was performed at the edge (thickness less than

100 nm) of particles. The XRD patterns were detected inside the bulk particles, while the electron diffraction is effective only for the surface structure of large particles. Therefore, at higher hydrogen ratios, the predominant bulk phase is still 6H-SiC (α-SiC), but the surface structure of SiC particles was already changed into cubic structure. This explanation can also be confirmed by Raman spectra of two types of hybrids. As shown in Fig. 5-7b, the spectra for two types of hybrid structures are totally different, the peak around 965 cm^{-1} corresponding to LO phonon peaks of α-SiC (6H-SiC) disappeared in the spectra of "multi-directions" hybrids. The disappeared peak is not due to CNT coverage on the surface of SiC substrate, because we can still detect the peak around 783 cm^{-1} which is related to the TO phonon peak of SiC. Therefore, the surface structure of SiC substrate was changed at higher hydrogen ratio.

How can higher hydrogen concentration in the system influence the structure and property of the substrate in CVD process? There are several possibilities. Firstly, higher hydrogen concentration may directly change the surface crystal type of SiC particles from 6H-SiC (α-SiC) to 3C-SiC (β-SiC) at the given temperature. β-SiC (3C-SiC) with cubic structure is symmetric in all directions. The interaction between the catalyst particles and the different crystal facets of SiC was almost the same, which led to the same activity of catalyst particles and the multi-directions growth of CNTs on different facets. To make a compare, pristine SiC was annealed at the same temperature and hydrogen ratio as the growth conditions of "multi-directions" hybrids. The Raman spectra of annealed SiC at higher hydrogen ratio (Fig. 5-7c) showed no obvious difference with that of pristine SiC. Annealing SiC in high H_2 atmosphere at reaction temperature can not change the crystal type of SiC particle (even its surface). Therefore, this possibility was excluded. Secondly, high H_2 ratio may lead to quickly deposit a layer of substance on the surface of SiC substrate. We know that it is difficult to decompose ferrocene below 800 ^oC without the presence of hydrogen.[217] At low H_2 ratio and reaction temperature (600 ^oC), the decomposition of ferrocene occurred mainly on the surface of substrate rather than in atmosphere. Therefore, the property of substrate and its interaction with the catalyst particles are important factors. However, at high H_2 ratio, H_2 can significantly accelerate the ferrocene decomposition and suppress the polymerization rate of C_2H_2 into carbon.[217, 218] As a result, large quantities

of iron atoms or particles were produced in atmosphere and deposited instantly on the surface of SiC substrate. No CNT growth happened at the beginning because low carbon feeding can not saturate the iron particles immediately. Therefore, a layer of iron (or iron carbide) was formed and covered the substrate surface. Based on the result of electron diffraction (Fig. 5-6f), we know that the structure of this layer is cubic, which was similar to the diffraction patterns of gamma iron or iron carbide (e.g. Fe_3C).[215, 219] This cubic-structure layer is symmetric and covered the surface of substrate to decrease its asymmetry, which resulted in the "multi-directions" growth of nanotubes on SiC substrate.

5.4 "Multi-directions" SiC-CNT/PVDF dielectric composites

The "multi-directions" SiC-CNT hybrids can be realized either at low H_2 hydrogen ratio (H_2/Ar=0.1:0.9) and high temperature (750 ^oC), or at low temperature (600 ^oC) and high hydrogen ratio (H_2/Ar=0.3:0.7). However, the latter condition properly gives rise to a more uniform and denser morphology of CNTs, and the resultant hybrids were consequently selected as filler to prepare the SiC-CNT/PVDF composites.

5.4.1 TG analysis of SiC-CNT hybrids

The TG analysis for "Multi-directions" hybrids was conducted in air atmosphere. The mass change has been recorded and presented in Fig. 5-8. The oxidation of carbon nanotube begins at about 450 °C as well as ends at about 550 °C. The abrupt mass drop in this range gives a CNT/SiC-CNT mass ratio of 27% for the "Multi-directions" hybrid architectures. By using this ratio, the detailed concentrations for each component in the as-prepared SiC-CNT/PVDF composites can be calculated and the results are shown in Table 5-1.

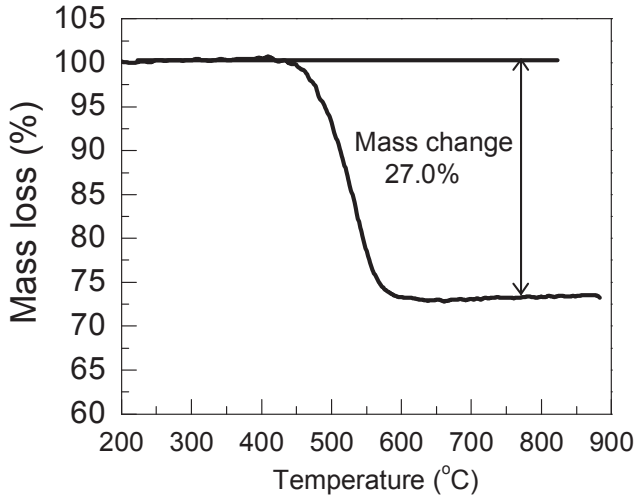

Fig. 5-8 *TG analysis for the "multi-directions" SiC-CNT hybrids in the air atmosphere.*

Table 5-1. The concentrations for each component in the "multi-directions" SiC-CNT/PVDF composites

Sample	SiC-CNT filler (wt%)	CNT (vol%)	SiC (vol%)
1	1.0	0.26	0.41
2	2.2	0.56	0.90
3	4.4	1.14	1.82
4	5.5	1.42	2.28
5	6.6	1.72	2.74
6	7.0	1.82	2.91
7	8.8	2.30	3.68

5.4.2 SEM morphology

SEM images of SiC-CNT hybrids and their composite with PVDF are presented in Fig. 5-9. A low-magnification SEM image shown in Fig. 5-9a aims to give the whole morphology of each SiC-CNT hybrid. The thickness of the SiC microplate is about 1 μm and the length of CNTs is about 10~15 μm. CNTs are aligned and perpendicular to the flat surfaces of SiC microplates, which can be clearly seen in the enlarged image of the circle area (inset of Fig. 5-9a). After blended with PVDF matrix, the original architecture can be remained, confirmed by the SEM micrograph at high magnification level (Fig. 5-9b). Namely, CNTs are oriented

along an axis and separated by a thin polymer matrix, giving rise to a network of microcapacitor with the CNTs as electrodes and a very thin PVDF layer in between, shown in the square area in Fig. 5-9b.

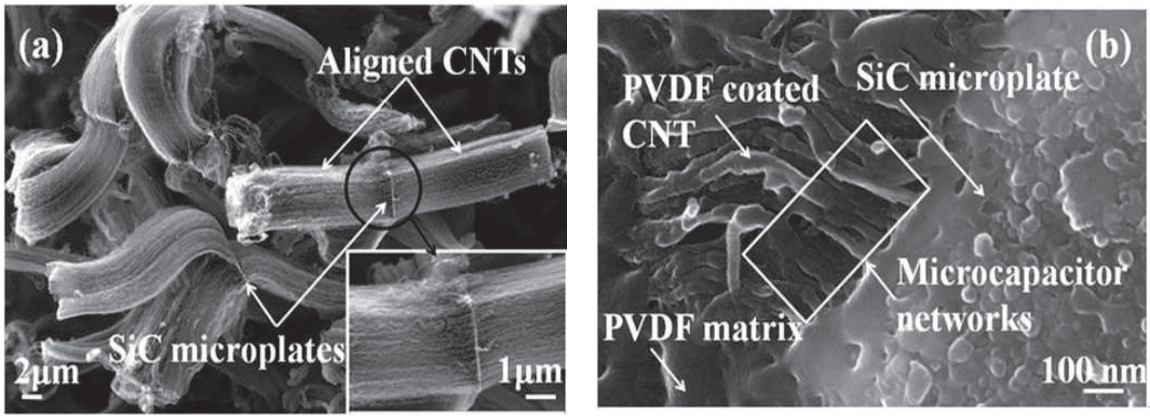

Fig. 5-9 *SEM micrographs of (a) "multi-directions" SiC-CNT hybrids obtained at 600 °C and H_2/Ar ratio of 0.3:0.7 L/min and (b) fractured cross-surface of the SiC-CNT/PVDF composite with 0.26 vol% of CNTs. The areas related to SiC, CNTs and PVDF matrix are indicated by arrows.*

5.4.3 Dependence of the dielectric properties on hybrid content

Figure 5-10 shows the evolution of the dielectric permittivity versus CNT content (f_{CNT}) at 100 Hz. In order to estimate f_c, we fit the experiment data to Eq. 1-22 derived from general percolation theories The linear fit of the data to the log–log plot of the power law with the highest correlation coefficient (0.99) gives f_c=0.0147±0.0001, q=0.93±0.06 (see the inset in Fig. 5-10). The exponent s agrees well with the universal one ($q \approx 1$) [37, 55] and the f_c (1.47 vol%) is much lower than that reported for most CNT/polymer nanocomposites.[60, 106, 220] Of particular interest is that the dielectric permittivity strongly increases with continuously adding the hybrid SiC-CNT filler. This can be well explained in light of the microcapacitor model. Namely, each two neighboring CNTs are treated as a local capacitor with the CNTs as two electrodes and a very thin PVDF layer in between as dielectric, and a network of these local capacitors expands between two virtual electrodes with increasing the CNT content. Each microcapacitor contributes an abnormally large capacitance. The large capacitance can then be correlated with a significant increase in the intensity of local electric field when the

CNTs are very close to each other near f_c. the significant increase in the intensity of the local electric field promotes the migration and accumulation of charges carriers at the interfaces between the CNTs and the matrix.

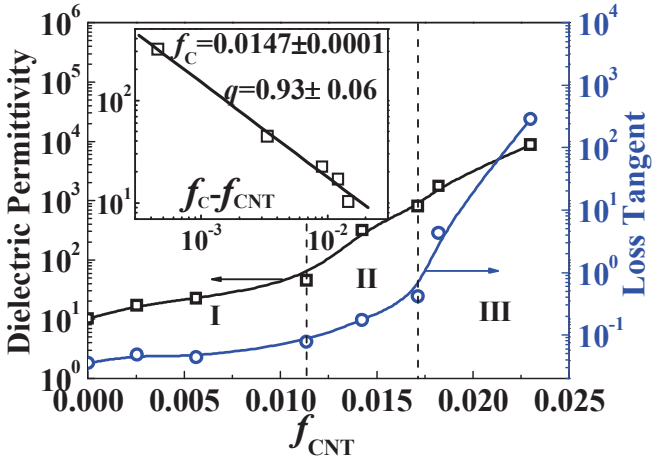

Fig. 5-10 *Dielectric permittivity and loss tangent of the SiC-CNT/PVDF composites as a function of f_{CNT}, measured at 100 Hz and at room temperature. The inset shows the best fit of the dielectric permittivity of the SiC-CNT/PVDF composites to Eq. 1-22.*

The evolution process of the dielectric permittivity in SiC-CNT/PVDF composites can be divided into three stages (I, II, III, see Fig. 5-10). Initially, when a small amount of SiC-CNT is incorporated into the PVDF matrix (f_{CNT}<0.011), SiC-CNT fillers are isolated to each other. Microcapacitor network on each SiC plate contributes to the dielectric permittivity individually, resulting in a slight increase of the dielectric permittivity relative to that of pure PVDF (10→45). Meanwhile the loss tangent can remain at a low level (below 0.08). It is worthy to mention that this permittivity level (45) was rarely seen in most CNT/polymer composites with such low f_{CNT},[59, 60, 106, 220] as parallel board microcapacitors are extremely hard to form in CNT/polymer composites due to the large distance between each two neighboring CNTs and the inherent waviness of CNTs themselves (Fig. 5-1a). However, in the SiC-CNT/PVDF composites, a microcapacitor network on individual SiC microplate can be rather easily formed with the SiC microplate assembling and fixing the aligned CNTs. As the SiC-CNT content is further increased, up to the vicinity

of f_c ($0.011<f_{CNT}\leqslant 0.017$), the dielectric permittivity of the SiC-CNT/PVDF composites undergoes a sharp increase from 45 to 806. This can be attributed to the fact that new microcapacitors are largely formed by CNTs from different SiC microplates due to the interaction of the SiC-CNT fillers near f_c, where the SiC-CNT hybrids are very close to each other. Additionally, thanks to the existence of very thin dielectric insulating-polymer layer between two neighboring CNTs, leakage current is blocked and the loss tangent remains below 0.41, which can be still acceptable for the application of high-charge storage capacitors.[62] When the f_{CNT} is beyond 0.017, the dielectric permittivity of the SiC-CNT/PVDF composites keeps increasing because of the additional formation of microcapacitors. Meanwhile, the loss tangent is increased dramatically due to the formation of a significant conductive network, and the resultant leakage current within the composites. The maximum dielectric permittivity of about 8700 is observed at f_{CNT}=0.023, though at this point the loss tangent is also high (286). This high-permittivity and high-loss composites have great potential for applications such as electromagnetic-wave absorption. Additionally, it should be emphasized that even at the highest CNT loading point (f_{CNT}=0.023), the corresponding SiC concentration in the SiC-CNT/PVDF composite is only 3.7 vol%, which allows to retain partially the flexibility of the PVDF matrix.

5.4.4 Frequency dependence of the dielectric properties

The dependence of dielectric properties of the SiC-CNT/PVDF composites with different CNT loading on frequency is presented in Fig. 5-11. The dielectric permittivity (Fig. 5-11a) is almost frequency-independent in the low frequency range (10-10^4 Hz) even when $f_{CNT} > f_c$. The absence of sharp decrease of dielectric permittivity at low frequency for composites near f_c suggests that the high dielectric permittivity of SiC-CNT/PVDF composites is largely from the network of microcapacitors.[107, 221]

According to Fig. 5-11b, When $f_{CNT} < f_c$, the conductivity increases almost linearly with the increase of frequency. When $f_{CNT} > f_c$, the conductivity values are much higher than those for $f_{CNT} < f_c$, and are almost independent of the change of frequency within the low-frequency range. When f_{CNT} approaches f_c, the percolation threshold power law can be described as following:[37, 62]

$$\sigma \propto \omega^{\mu}, \qquad \text{as } f_{CNT} \rightarrow f_c \tag{5-1}$$

where $\omega=2\pi\nu$, and ν and μ are the frequency and corresponding critical exponent, respectively. The experimental data for the composite with f_{CNT}=1.42 vol% (near f_c) give μ=0.92 (inset of Fig. 5-11b). The μ value of the composite system is higher than the normal value μ=0.7 obtained from percolation theory.[37] A similar result has been reported in the carbon black/PVDF composite.[221]

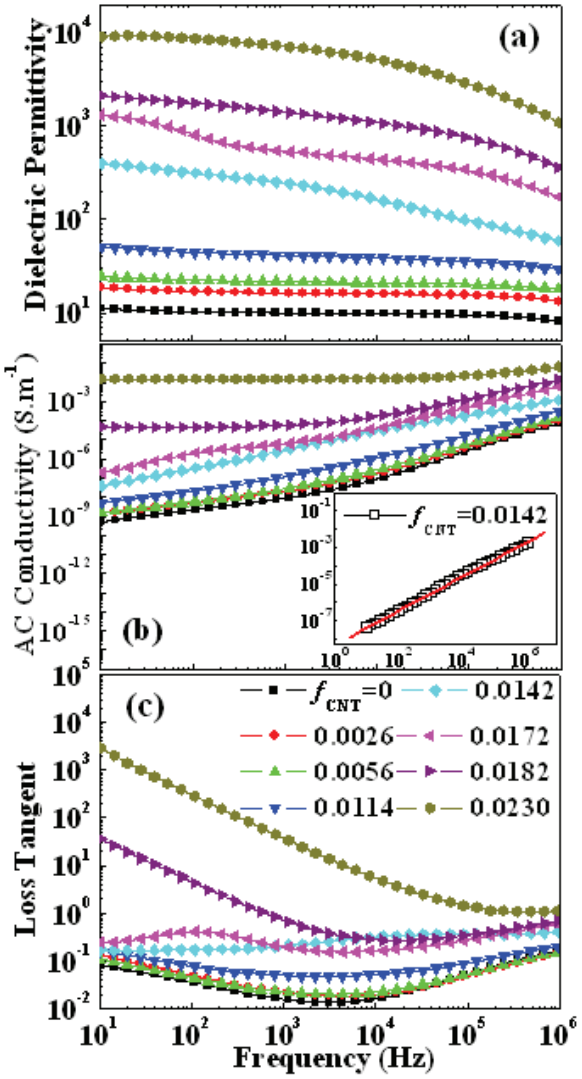

Fig. 5-11 *Dependence of (a) the dielectric permittivity, (b) AC conductivity and (c) loss tangent of the SiC-CNT/PVDF composites on frequency at room temperature. The inset shows the best fit of the AC conductivity of the SiC-CNT/PVDF composite with 1.42 vol% of CNTs to Eq. 5-1.*

As shown in Fig. 5-11c, the loss tangent remains at low values (0.4) with increasing frequency when $f_{CNT} \leqslant 0.017$ (above f_c) and displays a similar dielectric relaxation with PVDF matrix. But when $f_{CNT} > 0.017$, the loss tangent is very high at low frequency, indicating a high absorbing ability of electromagnetic waves by composites with 2.3 vol% CNTs.

5.4.5 Temperature dependence of the dielectric properties

Temperature dependence of the dielectric permittivity for the SiC-CNT/PVDF composite (f_{CNT}=0.017) is shown in Fig. 5-12. The composites demonstrate a good thermal stability at each frequency from -30 to 100 °C, showing a steady high value of 800 at 100 Hz, as shown in the grey grid area in Fig. 5-12. This indicates the established microcapacitors within composites are stable and not easily damaged by the thermal expansion of PVDF matrix.

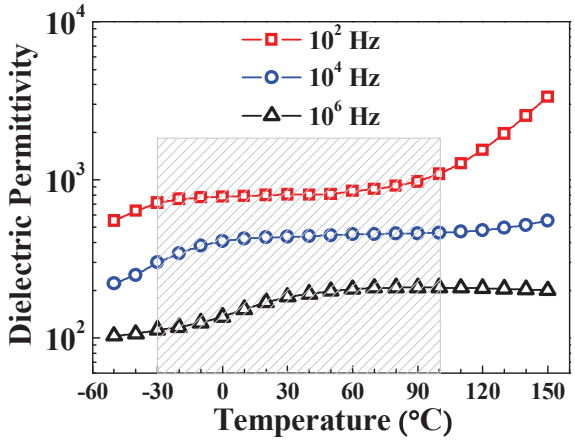

Fig. 5-12 *Temperature dependence of the dielectric permittivity of the SiC-CNT/PVDF composite (f_{CNT}=1.7 vol%) at different frequencies.*

It is important to note that with the temperature ranging from 100 to 150 °C, the dielectric permittivity at 100 Hz increases up to 3350 dramatically but the one at high frequency (10^4 and 10^6 Hz) maintains stable. The results can be explained as follows. Within high temperature range (100-150 °C), the composite turns into a flexible state and the

movement of PVDF molecules is improved. Therefore, at low frequency, the molecules have enough time for polarization. However, at high frequency, the polarization of molecules is still not fast enough to catch up with the change in electrical field frequency, resulting in the weak dependence of dielectric permittivity on temperature

5.5 "Single-direction" SiC-CNT/PVDF dielectric composites

"Single-direction" SiC-CNT hybrid can only be synthesized at low temperature and low hydrogen ratio. In this case, the SiC substrate would dominate the growth and organization of the carbon nanotubes on SiC particles. So, we prepared "single-direction" SiC-CNT/PVDF composites by using the SiC-CNT hybrids obtained at 600 °C and a H_2/Ar ratio of 0.1:0.9 L/min.

5.5.1 SEM morphology

Fig. 5-13a and b show the SEM images of "single-direction" SiC-CNT hybrids synthesized at 600 °C and H_2/Ar ratio of 0.1:0.9 L/min. Fig 5-13a is an enlarged image of single hybrid particle: carbon nanotubes are aligned and perpendicular to the flat surface of SiC particle. This feature is definitely the same with "multi-directions" hybrids. Therefore both types of hybrids can be geometrically considered as a rod. The low-magnification SEM image shown in Fig. 5-13b give the length of nanotubes in the range of 15-20 μm, which is nearly twice of the "multi-directions" hybrids (~10 μm). However, considering the difference in the organization model of CNTs (Fig. 5-9a), it is reasonable to conclude that both types of hybrids have the same geometry with respect to the aspect ratio of the rod.

After being blended with PVDF matrix, the integrality of the hybrids can be well retained, as confirmed by the SEM images of SiC-CNT/PVDF composites in Fig. 5-13c and d. The high-magnification SEM image clearly shows the CNTs strongly wrapped by the PVDF matrix are still aligned and perpendicularly connected to the surface of SiC microplate, which is of utmost importance to give rise to the microcapacitor network.

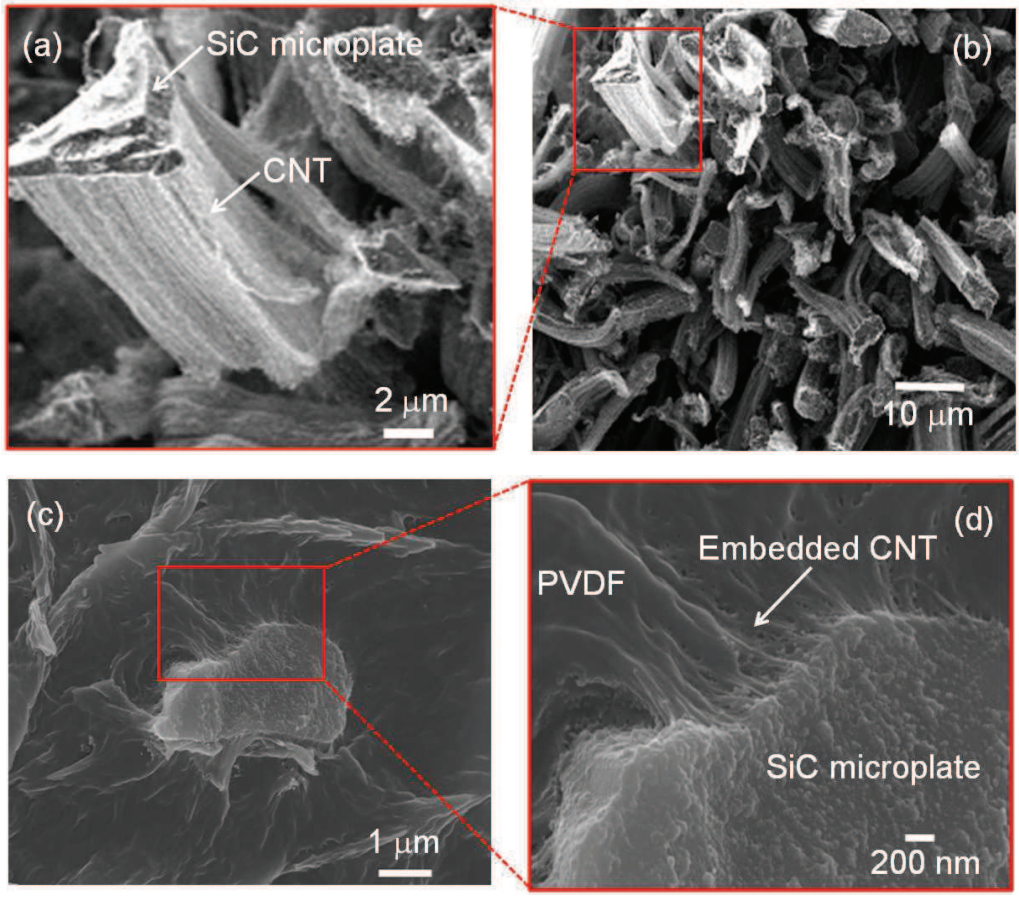

Fig. 5-13 *SEM micrographs of (a, b) "single-direction" SiC-CNT hybrids and (c, d) fractured cross-surface of the "single-direction" SiC-CNT/PVDF composite with 2.2 wt% SiC-CNT hybrids. The areas related to SiC, CNTs and PVDF matrix are indicated by arrows. (a) and (d) are the enlarged images of the square part marked in (b) and (c) respectively.*

5.5.2 TG analysis

Presented in Fig. 5-14 is the TG comparison between the "multi-directions" and "single-direction" SiC-CNT hybrids. It is intriguing to note that "single-direction" SiC-CNT hybrid exhibits a smaller mass change as well as a lower loss rate as compared to the "multi-directions" one. This may indicate a relatively lower number density in "single-direction" hybrids, as both types of rods have the same aspect ratio and their nanotubes have the same diameter. The lower number density in "single-direction" hybrids would result in a larger distance between neighboring nanotubes inside the CNTs arrays

perpendicular to the SiC surfaces.

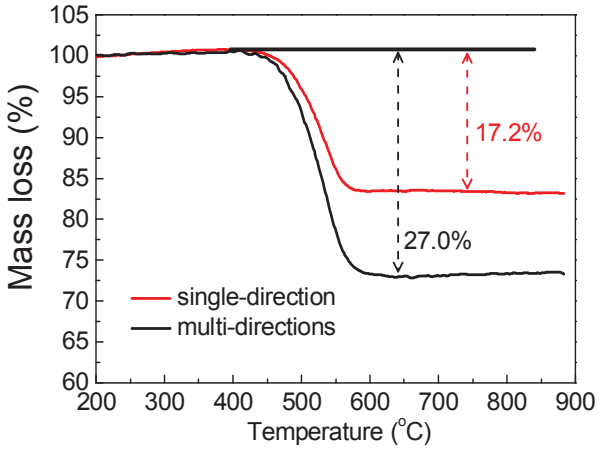

Fig. 5-14 *TG comparison between the "multi-directions" and "single-direction" SiC-CNT hybrids.*

By using the mass ratio CNT/SiC-CNT of 17.2%, the detailed concentrations for SiC and CNTs in the "single-direction" SiC-CNT/PVDF composites can be calculated and the results are shown in Table 5-2. It should be noted at the same mass content of hybrid fillers, the "single-direction" SiC-CNT/PVDF composite has less nanotubes and more SiC particles than its counterpart due to the lower CNT number density in the hybrid filler.

Table 5-2. The concentrations for each component in the "single-direction" SiC-CNT/PVDF composites

Sample	SiC-CNT filler (wt%)	CNT (vol%)	SiC (vol%)
1	1.0	0.16	0.46
2	2.2	0.36	1.02
3	4.4	0.73	2.06
4	5.5	0.92	2.58
5	6.6	1.11	3.11
6	7.0	1.18	3.30
7	8.8	1.48	4.17

5.5.3 Dielectric properties as a function of hybrid content

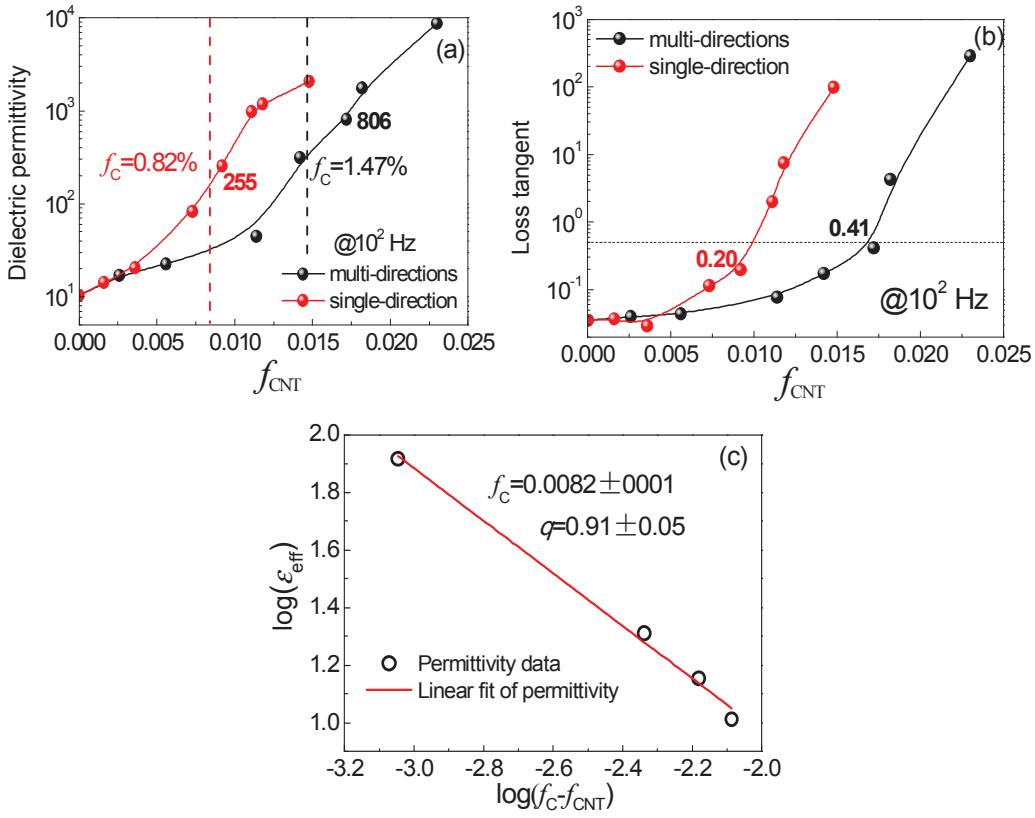

Fig. 5-15 *(a) Dielectric permittivity and (b) loss tangent of the SiC-CNT/PVDF composites as a function of f_{CNT}, measured at room temperature and 10^2 Hz. (c) shows the best fit of the dielectric permittivity of the "single-direction" SiC-CNT/PVDF composites to Eq.1-22.*

Figure 5-15 shows the evolution of the dielectric properties of SiC-CNT/PVDF composites with the concentration of CNTs. Intriguingly, at the same concentration of CNTs, the "single-direction" composite shows higher permittivity and larger loss tangent than its counterpart (Fig. 5-15a and b), especially when approaching the percolation threshold. To estimate f_c, we fit the experiment data to the power law in Eq. 1-22. The best linear fit of the permittivity to the log-log plot of the power law gives f_c=0.0082±0.0001, q=0.91±0.05 (Fig. 5-15c). It is obvious that the dielectric critical exponent observed in "single-direction" SiC-CNT/PVDF composites is in accordance with the universality of percolation theory (q≈1). [37, 78] However, the percolation threshold (0.82 vol%) is much lower than that for "multi-directions" composite (1.47 vol%). Recall that both types of hybrid fillers can be geometrically considered as a rod with the same aspect ratio, it is reasonable to conclude that

the lower percolation threshold mainly derive from the lower number density in "single-direction" SiC-CNT hybrids. In other words, the looser morphology of CNTs (Fig. 5-16a) tends to favor more uniform dispersion of nanotubes in the polymer matrix. The better dispersion of CNTs can generally lead to a much lower percolation level.[59] By showing the same increase trend as the case of "multi-directions" composites, the dielectric permittivity in "single-direction" composite augments from 82 to 255 near f_c=0.82 vol%, and also exhibits a continuous increase up to 2100 when f_{CNT}=1.48 vol%. The physical reason for such increment in permittivity is the evolution of microcapacitor networks, as is the case for "multi-directions" composites. The critical behavior of the dielectric permittivity near percolation threshold can be attributed to the steep rise of the number of microcapacitors as a result of interactions between hybrids near f_c. These interactions enable the abrupt increase in the permittivity, yet meanwhile induce the risk of tunneling between hybrids and thus the leakage current across two sample surface electrodes. That is why the loss tangent also increases dramatically near the percolation threshold (Fig. 5-15b).

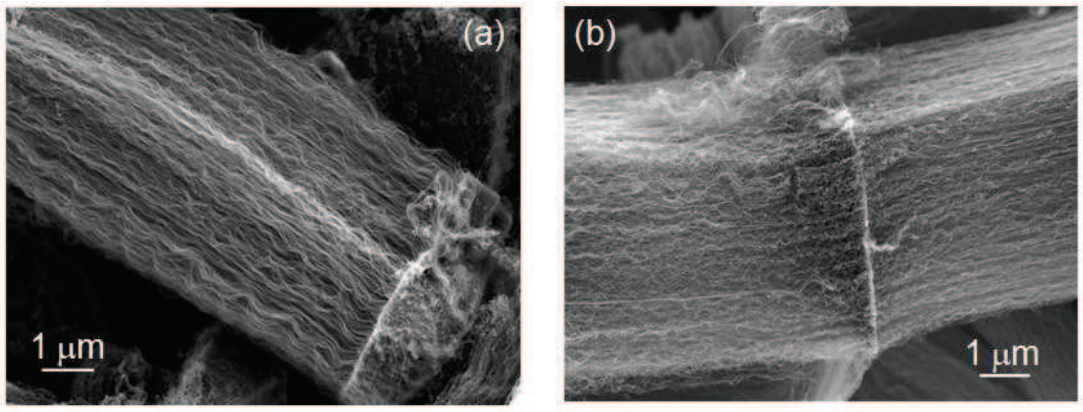

Fig. 5-16 *SEM images of SiC-CNT hybrids: (a) "single-direction" hybrid and (b) "multi-directions" hybrid. It is obvious to note that the "single-direction" hybrid shows a looser CNT morphology and a lower number density than its counterpart.*

In fact, Apart from the high permittivity, the desired composites serving as energy storage materials should also have low loss tangent. According to the literature,[62] the acceptable loss values should be below 0.5, where the dash line stands in Fig. 5-15b. With

meeting this requirement, the maximum dielectric permittivity realized is 255 and 806 in "single-direction" and "multi-directions" composite respectively, their corresponding loss tangent is 0.20 and 0.41. Although the lower number density of CNTs in "single-direction" hybrids can lead to percolation at a much low concentration of nanotubes, the larger distance between neighboring nanotubes as well as their waving morphology (Fig. 5-16a) is not desirable for the microcapacitors network. On the contrary, "multi-directions" hybrids have denser and more aligned CNT arrays (Fig. 5-16b). This means, at the starting point of hybrid interactions (near f_c), there would be more CNTs involved in the effective microcapacitor network. That is why the maximum permittivity (806) observed in "multi-directions" composites is larger than that (255) in "single-direction" ones.

5.5.4 Frequency dependence of dielectric properties

The dependence of dielectric properties of "single-direction" SiC-CNT/PVDF composites on frequency at room temperature is shown in Fig. 5-17. As shown in Fig. 5-17a, the dielectric permittivity of as-prepared composites at low CNT concentrations (<0.92 vol%) decreases slightly with frequency, which displays good frequency stability. This frequency independence arises from the microcapacitor structure nature that induces the increment in dielectric permittivity.[66, 221] On the other hand, the highly frequency-dependent dielectric permittivity is observed when the CNT concentration exceeds 1.11 vol%, compared with the frequency independence of pure PVDF. In this case, the conductive network formed in the composites largely favors the charge injection from the external electrodes so that a large number of charge carriers are accumulated at the CNT-polymer interfaces inside the microcapacitors. This interfacial polarization, also known as the MWS effect, is responsible for the enhancement of dielectric permittivity observed at low frequency. In other words, the introduction of large amount of CNTs would provide numerous dipoles that can re-orient with the change of the electric field. This can ascribe to the frequency dependence of the dielectric permittivity, because the dipoles are not able to follow the changing step of the electric field at high frequency,[222, 223] thus result in a reduced dielectric permittivity.

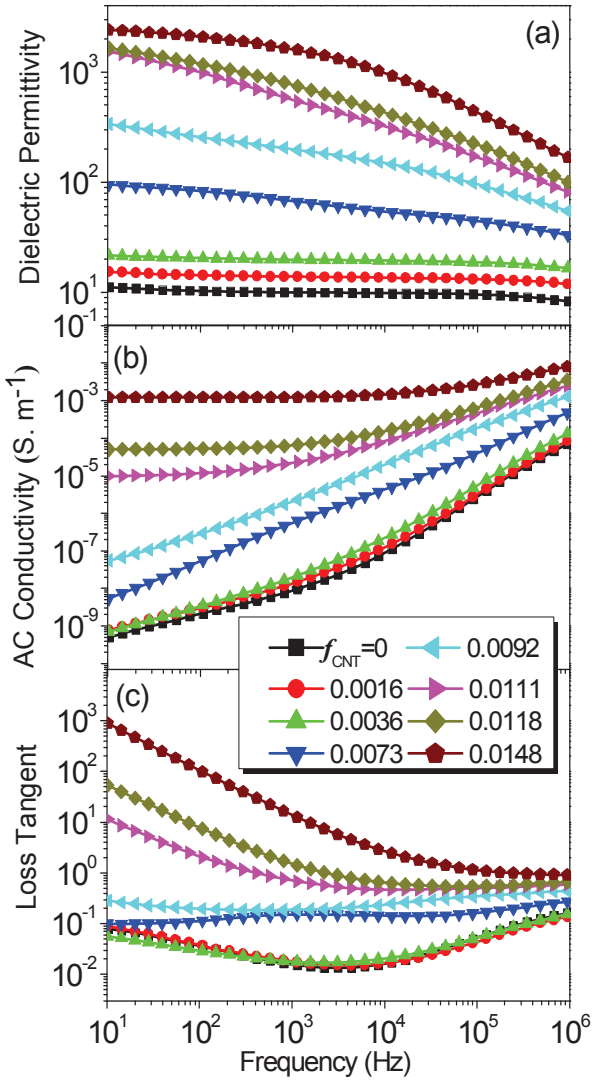

Fig. 5-17 *Dependence of (a) the dielectric permittivity, (b) AC conductivity and (c) loss tangent of the "single-direction" SiC-CNT/PVDF composites on frequency at room temperature.*

The variation of AC conductivity with frequency is depicted in Fig. 5-17b. It is noted that the AC conductivities of the composites with low CNT concentrations (<0.92 vol%) exhibit strong frequency dependence, showing a nearly linear increase with the frequency. However, when exceeding the percolation threshold region (>1.11 vol%), a characteristic of direct conductivity is observed that the unchanged AC conductivity is revealed in a particular low frequency range, and this range becomes larger and up limit shifts to higher frequency

with increasing CNT content further. At low CNT concentrations (<0.92 vol%), owing to the absence of the conductive path, the conductivity is dominated by the polarization effects and the electron motion, which highly depends on the frequency, consequently a frequency-dependent AC conductivity is exhibited. On the contrary, at high CNT contents (>1.11 vol%), CNT percolating paths are formed through the polymer matrix, which induces the direct conductive characteristic of the nanocomposites in the low frequency range. The microcapacitors also contribute to the conductivity and become dominant after a critical frequency. More current passing through the capacitors with the increasing frequency results in the conductivity improvement.

Figure 5-17c presents the loss tangent of the composites as a function of frequency. Generally, the dielectric loss consists of two parts: one is due to the Debye-type relaxation, and the other originates from the leakage current that happens near f_c.[78] When the CNT content is far below the percolation threshold ($f_{CNT} \leq 0.36$ vol%), the loss of composites does not show any increase and exhibits completely the same relaxations with PVDF matrix. The attained much low loss (0.03 at 100 Hz) is believed to come from the Debye-type relaxation in the polymer matrix. However, once the f_{CNT} enters into the neighborhood of percolation threshold (0.73 vol%$<f_{CNT}<$0.92 vol%), the frequency-independent dielectric loss indicates that apart from the Debye-type relaxation in the polymer matrix, there is an additional factor that contributes to the loss. Considering the fact that the interactions between neighboring hybrids would occur in this f_{CNT} range, the slight increase of loss from 0.11 to 0.20 possibly originates from the leakage current across the external electrodes as a result of the tunneling effect between CNT arrays of neighboring hybrids. Additionally, when f_{CNT} increases further ($f_{CNT}>$1.11vol%), the loss tangent increases significantly (2→98), especially for the one at low frequency range. This is attributed to the CNT percolating paths formed in the composites, which relaxes a lot the charges stored at the interfaces inside the microcapacitors.

5.6 Conclusions

Well-organized SiC-CNT hybrids were fabricated by floating catalytic CVD process. Aligned CNT arrays were grown on the plate-like SiC particles without any pretreatment. Multiform SiC-CNT hybrids can be obtained by varying experimental conditions. The effects of temperature and hydrogen ratio on the organization mode of CNTs on SiC particles were discussed in detail.

The organization mode of CNTs on SiC particles are controlled by both the experimental conditions and the substrate nature. At lower temperatures and hydrogen ratios, the decomposition of ferrocene is difficult in the atmosphere but mainly on the surface of substrate. Thus the surface property of substrate is the dominant factor to determine the CNT organization model. The silicon-rich facets of 6H-SiC can react with the iron atoms to form silicon-carbon compound which is inactive for CNT growth. The carbon-rich facets can keep iron particles active for CNT growth. As a result, “single-direction” hybrid structure was formed. At higher temperatures and hydrogen ratios, the decomposition of ferrocene happened instantly in the atmosphere and iron atoms were deposited on the SiC surface. Continuous feeding allowed the formation of a uniform layer of iron (iron carbide) and covered on the surface of substrate. This layer is cubic structure, symmetric and active for CNT growth in all directions. Therefore, “multi-directions” hybrid structure was formed.

Both types of hybrids were used as conductive filler to prepare the percolative SiC-CNT/PVDF composites. It was found that the SiC-CNT hybrid can significantly improve the dielectric permittivity of a SiC-CNT/PVDF composite with an extremely low CNT loading. CNTs on each SiC microplate are oriented along an axis and separated by a thin polymer matrix, giving rise to a network of microcapacitors. As a result, a large dielectric permittivity of more than 800 and 255 at 100 Hz could be obtained within the vicinity of percolation threshold of 1.47 vol% and 0.82 vol% in the “multi-directions” and “single-direction” composites respectively. These flexible SiC-CNT/PVDF composites with such high dielectric performance are potential materials for applications in high-charge storage capacitors.

General conclusions and perspectives

General conclusions

This thesis has focused on increasing the dielectric permittivity of CNT-based polymer composites by both carefully optimizing the dispersion of nanotubes as well as controlling the microstructure of the composites. The main results could be concluded as follows.

1. Solution casted MWNT/PVDF composites

The percolative MWNT/PVDF composite initially prepared via solution casting and hot-pressing technology could show a percolation threshold as low as 1.91 vol%. The increase in the dielectric permittivity was, however, limited ($\varepsilon_r/\varepsilon_m$=27 at 10^3 Hz) near the percolation threshold. The medium dielectric performance could largely derive from the limited number of microcapacitors as a result of the aggregated structure of MWNT as well as the weak interfacial interaction between the pristine MWNTs and PVDF matrix. The formed microcapacitors near the percolation threshold were found very sensitive to the external tensile strain applied on the composites. The MWNTs became aligned in response to the uniaxial mechanical stretching. The nanotube orientation state was quantitatively characterized by using TEM as well as the second order orientation tensor at a selected location. A high alignment degree happened when the necking began in composites. The change of nanotube distribution state highly affected the dielectric properties. A correlation of the tube orientation state with the evolution of dielectric properties was established. With increasing the alignment degree of nanotubes, the dielectric permittivity and ac conductivity exhibited complex but nearly opposite changing tendency. This could be attributed to the conductive pathways shift and microcapactor formation during the tensile deformation. This was further confirmed by using an equivalent circuit model of two parallel RC circuits in series to analyze the impedance data.

2. Melt-processed MWNT/PVDF composites

The advanced composite fabricated by blending pristine MWNTs within PVDF in molten state could realize a significantly enhanced dielectric permittivity by breaking through the common bottleneck of limited interfacial interactions displayed in other C-moieties-based composites. The Raman spectra shows that a remarkable interaction at molecular level is achieved by establishing donor-acceptor complexes between the delocalized π-electron clouds of MWNTs and strongly electrophilic F groups of PVDF chains. The SEM and TEM images give evidence for the effective wrapping of PVDF chains and resultant much thin PVDF layer on nanotube surfaces, respectively. The MWNT/PVDF nanocomposite exhibited a giant dielectric permittivity of 3800 over a critical content of MWNT, while retaining a low conductivity of 6.3×10^{-5} $S.m^{-1}$. We suggest that the giant dielectric permittivity originates from a reinforced Maxwell-Wagner-Sillars (MWS) effect based on the donor-acceptor complexes. The delocalized π-electron clouds of MWNTs provide large domains for nomadic electrons, and the electrophilic F groups strongly attract these electrons thus significantly reinforce the MWS effect at the interfaces. This simple and robust method has been demonstrated to be effective to realize an advanced material with giant dielectric permittivity over a wide temperature range and can be easily scalable from laboratory to industrial scale. These polymer-based composites with giant dielectric permittivity values could find potential applications as high-performance embedded capacitors in the electronic industry

3. Biphasic polymer blends containing carbon nanotubes

To reduce the percolation threshold in melt-processed CNT-based polymer composite, a double percolated structure has been realized in the MWNT-LDPE/PVDF composite systems, namely, the MWNTs are exclusively distributed and percolated within the LDPE phase that forms continuous electrically conductive channels in the matrix, and both polymer phases are co-continuous in 3-D space. The uneven distribution of MWNTs was determined by the viscosity factor, which is proven possible to dominate the generally discussed thermodynamic effect to favor the final CNT location. Such a double percolated structure allows for achieving polymer composites with high permittivity at much lower filler concentrations. The

biphasic composite with a PVDF/LDPE volume ratio at 2:1 exhibits a lowest percolation threshold (f_c=5.7 vol%) and a permittivity as high as 470 near f_c. The effect of double percolation is well illustrated by modeling the permittivity of composites as a function of MWNT volumetric fraction. The model based on the well-known Lichteneckerrule and percolation theory has been evidenced to be much suitable to the biphasic polymer composites.

4. SiC-CNT hybrids and their applications in the dielectric composites

Well-organized SiC-CNT hybrids were fabricated by floating catalytic CVD process. Aligned CNT arrays were grown on the plate-like SiC particles without any pretreatment. Multiform SiC-CNT hybrids can be obtained by varying experimental conditions. The effects of temperature and hydrogen ratio on the organization mode of CNTs on SiC particles were discussed in detail. The organization mode of CNTs on SiC particles are controlled by both the experimental conditions and the substrate nature. At lower temperatures and hydrogen ratios, the decomposition of ferrocene is difficult in the atmosphere but mainly on the surface of substrate. Thus the surface property of substrate is the dominant factor to determine the CNT organization model. The silicon-rich facets of 6H-SiC can react with the iron atoms to form silicon-carbon compound which is inactive for CNT growth. The carbon-rich facets can keep iron particles active for CNT growth. As a result, “single-direction” hybrid structure was formed. At higher temperatures and hydrogen ratios, the decomposition of ferrocene happened instantly in the atmosphere and iron atoms were deposited on the SiC surface. Continuous feeding allowed the formation of a uniform layer of iron (iron carbide) and covered on the surface of substrate. This layer is cubic structure, symmetric and active for CNT growth in all directions. Therefore, “multi-directions” hybrid structure was formed. Both types of hybrids were used as conductive filler to prepare the percolative SiC-CNT/PVDF composites. It was found that the SiC-CNT hybrid can significantly improve the dielectric permittivity of a SiC-CNT/PVDF composite with an extremely low CNT loading. CNTs on each SiC microplate are oriented along an axis and separated by a thin polymer matrix, giving rise to a network of microcapacitors. As a result, a large dielectric permittivity of more than 800 and 255 at 100 Hz could be obtained within the vicinity of

percolation threshold of 1.47 vol% and 0.82 vol% in the “multi-directions” and “single-direction” composites respectively. These flexible SiC-CNT/PVDF composites with such high dielectric performance are potential materials for applications in high-charge storage capacitors.

Perspectives

1. Although progress has been made, the most important issues that need to be addressed are the CNT/polymer interfaces and the interactions between the adjacent CNT particles. Quantum tunneling between adjacent CNTs is the main mechanism for electrical conductance, even when the content of CNTs is well above the percolation threshold. Remaining challenges include how to increase the contact resistivity associated with interfaces so as to suppress the leak-current and decrease dielectric loss of the percolative CNT/polymer composites.

2. Apart from the high dielectric permittivity, a desired composite serving as energy storage material should also have a capability of bearing high applied electric field, as the energy density of dielectric material is proportional to the product of permittivity and the square of applied electric field. However, up to date, most of the dielectric strength studies focused on the ceramic/polymer dielectric composites. The breakdown mechanism in percolative composite is still an open issue.

3. The percolation threshold f_c is the most important parameter in description of the dielectric properties of CNT/polymer composites near percolation. By controlling f_c, an optimal dielectric permittivity can be achieved at a desirable CNT loading. However, establishing the correlations between f_c and the microstrucuture features of composites is still challenging.

4. Though existing theoretical models for predicting the dielectric properties of polymer matrix composites have been presented in the first chapter. None of them explains, describes and/or predicts reasonably well the current results due to complexities in microstructure and composition of such composites. For a given composition, the dielectric properties can be significantly different, largely depending on the imperfections, intrinsic properties of fillers as well as the dispersion and distribution status of the filler. It is necessary to refine existing models or develop new ones for the dielectric composites.

References

[1] Iijima S. Helical microtubules of graphitic carbon. Nature. **1991** Nov;354(6348):56-8.

[2] Landi BJ, Ganter MJ, Cress CD, DiLeo RA, Raffaelle RP. Carbon nanotubes for lithium ion batteries. Energy & Environmental Science. **2009**;2(6):638-54.

[3] Baughman RH, Zakhidov AA, de Heer WA. Carbon nanotubes-the route toward applications. Science. **2002** Aug;297(5582):787-92.

[4] Elliott JA, Sandler JKW, Windle AH, Young RJ, Shaffer MSP. Collapse of single-wall carbon nanotubes is diameter dependent. Physical Review Letters. **2004** Mar 5;92(9):095501.

[5] Wildoer JWG, Venema LC, Rinzler AG, Smalley RE, Dekker C. Electronic structure of atomically resolved carbon nanotubes. Nature. **1998** Jan;391(6662):59-62.

[6] Liang WJ, Bockrath M, Bozovic D, Hafner JH, Tinkham M, Park H. Fabry-Perot interference in a nanotube electron waveguide. Nature. **2001** Jun;411(6838):665-9.

[7] Thess A, Lee R, Nikolaev P, Dai HJ, Petit P, Robert J, et al. Crystalline ropes of metallic carbon nanotubes. Science. **1996** Jul;273(5274):483-7.

[8] Hong S, Myung S. Nanotube electronics-A flexible approach to mobility. Nature Nanotechnology. **2007** Apr;2(4):207-8.

[9] Kociak M, Kasumov AY, Gueron S, Reulet B, Khodos, II, Gorbatov YB, et al. Superconductivity in ropes of single-walled carbon nanotubes. Physical Review Letters. **2001** Mar;86(11):2416-9.

[10] Tang ZK, Zhang LY, Wang N, Zhang XX, Wen GH, Li GD, et al. Superconductivity in 4 angstrom single-walled carbon nanotubes. Science. **2001** Jun;292(5526):2462-5.

[11] Berber S, Kwon YK, Tomanek D. Unusually high thermal conductivity of carbon nanotubes. Physical Review Letters. **2000** May;84(20):4613-6.

[12] Kim P, Shi L, Majumdar A, McEuen PL. Thermal transport measurements of individual multiwalled nanotubes. Physical Review Letters. **2001** Nov 19; 87 (21).215502

[13] Lu JP. Elastic properties of single and multilayered nanotubes. Journal of Physics and Chemistry of Solids. **1997** Nov;58(11):1649-52.

[14] Wong EW, Sheehan PE, Lieber CM. Nanobeam mechanics: Elasticity, strength, and toughness of nanorods and nanotubes. Science. **1997** Sep 26;277(5334):1971-5.

[15] Yu MF, Files BS, Arepalli S, Ruoff RS. Tensile loading of ropes of single wall carbon nanotubes and their mechanical properties. Physical Review Letters. **2000** Jun; 84 (24):5552-5.

[16] Yu MF, Lourie O, Dyer MJ, Moloni K, Kelly TF, Ruoff RS. Strength and breaking mechanism of multiwalled carbon nanotubes under tensile load. Science. **2000** Jan;287(5453):637-40.

[17] Dai HJ. Carbon nanotubes: opportunities and challenges. Surface Science. **2002** Mar;500(1-3):218-41.

[18] Chattopadhyay D, Galeska L, Papadimitrakopoulos F. A route for bulk separation of semiconducting from metallic single-wall carbon nanotubes. Journal of the American Chemical Society. **2003** Mar;125(11):3370-5.

[19] Iijima S, Ichihashi T. Single-shell carbon nanotubes of 1-nm diameter. Nature. **1993** Jun;363(6430):603-5.

[20] Puretzky AA, Geohegan DB, Fan X, Pennycook SJ. In situ imaging and spectroscopy of single-wall carbon nanotube synthesis by laser vaporization. Applied Physics Letters. **2000** Jan;76(2):182-4.

[21] Che G, Lakshmi BB, Martin CR, Fisher ER, Ruoff RS. Chemical vapor deposition based synthesis of carbon nanotubes and nanofibers using a template method. Chemistry of Materials. **1998** Jan;10(1):260-7.

[22] Thostenson ET, Li WZ, Wang DZ, Ren ZF, Chou TW. Carbon nanotube/carbon fiber hybrid multiscale composites. Journal of Applied Physics. **2002** May;91(9):6034-7.

[23] Veedu VP, Cao AY, Li XS, Ma KG, Soldano C, Kar S, et al. Multifunctional composites using reinforced laminae with carbon-nanotube forests. Nature Materials. **2006** Jun;5(6):457-62.

[24] Bozlar M, He D, Bai J, Chalopin Y, Mingo N, Volz S. Carbon nanotube microarchitectures for enhanced thermal conduction at ultra low mass fraction in polymer composites. Advanced Materials. **2010** Apr;22(14):1654-8.

[25] Simon P, Gogotsi Y. Materials for electrochemical capacitors. Nature Materials. **2008** Nov;7(11):845-54.

[26] Dang ZM, Yuan JK, Zha JW, Zhou T, Li ST, Hu GH. Fundamentals, processes and applications of high-permittivity polymer matrix composites. Progress in Materials Science. **2012** May;57(4):660-723.

[27] Rolison DR, Long RW, Lytle JC, Fischer AE, Rhodes CP, McEvoy TM, et al. Multifunctional 3D nanoarchitectures for energy storage and conversion. Chemical Society Reviews. **2009**;38(1):226-52.

[28] Pandolfo AG, Hollenkamp AF. Carbon properties and their role in supercapacitors. Journal of Power Sources. **2006** Jun;157(1):11-27.

[29] Toupin M, Brousse T, Belanger D. Charge storage mechanism of MnO2 electrode used in aqueous electrochemical capacitor. Chemistry of Materials. **2004** Aug;16 (16):3184-90.

[30] Zhai Y, Dou Y, Zhao D, Fulvio PF, Mayes RT, Dai S. Carbon Materials for Chemical Capacitive Energy Storage. Advanced Materials. **2011** Nov;23(42):4828-50.

[31] Liu C, Li F, Ma LP, Cheng HM. Advanced Materials for Energy Storage. Advanced Materials. **2010** Feb;22(8):E28-E62.

[32] Niu CM, Sichel EK, Hoch R, Moy D, Tennent H. High power electrochemical capacitors based on carbon nanotube electrodes. Applied Physics Letters. **1997** Mar;70(11):1480-2.

[33] An KH, Kim WS, Park YS, Moon JM, Bae DJ, Lim SC, et al. Electrochemical properties of high-power supercapacitors using single-walled carbon nanotube electrodes. Advanced Functional Materials. **2001** Oct;11(5):387-92.

[34] Frackowiak E, Beguin F. Electrochemical storage of energy in carbon nanotubes and nanostructured carbons. Carbon. **2002**;40(10):1775-87.

[35] Arico AS, Bruce P, Scrosati B, Tarascon JM, Van Schalkwijk W. Nanostructured materials for advanced energy conversion and storage devices. Nature Materials. **2005** May;4(5):366-77.

[36] DiLeo RA, Castiglia A, Ganter MJ, Rogers RE, Cress CD, Raffaelle RP, et al. Enhanced Capacity and Rate Capability of Carbon Nanotube Based Anodes with Titanium Contacts for Lithium Ion Batteries. Acs Nano. **2010** Oct;4(10):6121-31.

[37] Nan CW. Phsics of inhomogeneous inorganic materials. Progress in Materials Science. **1993**;37(1):1-116.

[38] SalverDisma F, Lenain C, Beaudoin B, Aymard L, Tarascon JM. Unique effect of mechanical milling on the lithium intercalation properties of different carbons. Solid State Ionics. **1997** Jun;98(3-4):145-58.

[39] Noerochim L, Wang JZ, Chou SL, Wexler D, Liu HK. Free-standing single-walled carbon nanotube/SnO_2 anode paper for flexible lithium-ion batteries. Carbon. **2012** Mar;50(3):1289-97.

[40] Li X, Cho JH, Li N, Zhang Y, Williams D, Dayeh SA, et al. Carbon nanotube-enhanced growth of silicon nanowires as an anode for high-performance lithium-ion batteries. Advanced Energy Materials. **2012** Jan;2(1):87-93.

[41] DiLeo RA, Frisco S, Ganter MJ, Rogers RE, Raffaelle RP, Landi BJ. Hybrid germanium nanoparticle-single-wall carbon nanotube free-standing anodes for lithium ion batteries. Journal of Physical Chemistry C. **2011** Nov;115 (45):22609-14.

[42] Zhang HK, Song HH, Chen XH, Zhou JS, Zhang HJ. Preparation and electrochemical performance of SnO_2@carbon nanotube core-shell structure composites as anode material for lithium-ion batteries. Electrochimica Acta. **2012** Jan;59:160-7.

[43] Ding Y, Li J, Zhao Y, Guan L. Direct growth of $LiMn_2O_4$ on carbon nanotubes as cathode materials for lithium ion batteries. Materials Letters. **2012** Feb;68:197-200.

[44] Reed CW, Cichanowski SW. The fundamentals of aging in HV polymer-film capacitors. Ieee Transactions on Dielectrics and Electrical Insulation. **1994** Oct;1 (5):904-22.

[45] Rabuffi M, Picci G. Status quo and future prospects for metallized polypropylene energy storage capacitors. Ieee Transactions on Plasma Science. **2002** Oct;30 (5):1939-42.

[46] Ihlefeld J, Laughlin B, Hunt-Lowery A, Borland W, Kingon A, Maria JP. Copper compatible barium titanate thin films for embedded passives. Journal of Electroceramics. **2005** Mar;14(2):95-102.

[47] Chu B, Zhou X, Ren K, Neese B, Lin M, Wang Q, et al. A dielectric polymer with high electric energy density and fast discharge speed. Science. **2006** Jul;313 (5785):334-6.

[48] Chu B, Zhou X, Neese B, Zhang QM, Bauer F. Relaxor ferroelectric poly(vinylidene fluoride-trifluoroethylene-chlorofluoroethylene) terpolymer for high energy density storage capacitors. Ieee Transactions on Dielectrics and Electrical Insulation. **2006** Oct;13(5):1162-9.

[49] Li WJ, Meng QJ, Zheng YS, Zhang ZC, Xia WM, Xu Z. Electric energy storage properties of poly(vinylidene fluoride). Applied Physics Letters. **2010** May;96(19):3.

[50] Li B, Liu T, Tang ZCW, Ji J, Zhong WH. Novel hydration induced flexible sulfonated poly(etherketoneketone) foam with super dielectric characteristics. Journal of Materials Chemistry. **2011**;21(35):13546-53.

[51] Thakur VK, Lin MF, Tan EJ, Lee PS. Green aqueous modification of fluoropolymers for energy storage applications. Journal of Materials Chemistry. **2012** 2012;22 (13):5951-9.

[52] Rahimabady M, Chen S, Yao K, Tay FEH, Lu L. High electric breakdown strength and energy density in vinylidene fluoride oligomer/poly(vinylidene fluoride) blend thin films. Applied Physics Letters. **2011** Oct;99(14):142901.

[53] Dang ZM, Xu HP, Wang HY. Significantly enhanced low-frequency dielectric permittivity in the $BaTiO_3$/poly(vinylidene fluoride) nanocomposite. Applied Physics Letters. **2007** Jan;90(1):012901.

[54] Arbatti M, Shan XB, Cheng ZY. Ceramic-polymer composites with high dielectric constant. Advanced Materials. **2007** May;19(10):1369-72.

[55] Dang ZM, Lin YH, Nan CW. Novel ferroelectric polymer composites with high dielectric constants. Advanced Materials. **2003** Oct;15(19):1625-29.

[56] Panda M, Srinivas V, Thakur AK. On the question of percolation threshold in polyvinylidene fluoride/nanocrystalline nickel composites. Applied Physics Letters. **2008** Mar;92(13):132905.

[57] Huang XY, Jiang PK, Xie LY. Ferroelectric polymer/silver nanocomposites with high dielectric constant and high thermal conductivity. Applied Physics Letters. **2009** Dec; 95(24):242901.

[58] Dang ZM, Wu JP, Xu HP, Yao SH, Jiang MJ, Bai J. Dielectric properties of upright carbon fiber filled poly(vinylidene fluoride) composite with low percolation threshold and weak temperature dependence. Applied Physics Letters. **2007** Aug;91(7):072912.

[59] Yao SH, Dang ZM, Jiang MJ, Xu HP, Bai JB. Influence of aspect ratio of carbon nanotube on percolation threshold in ferroelectric polymer nanocomposite. Applied Physics Letters. **2007** Nov;91(21):212901.

[60] Dang ZM, Wang L, Yin Y, Zhang Q, Lei QQ. Giant dielectric permittivities in functionalized carbon-nanotube/electroactive-polymer nanocomposites. Advanced Materials. **2007** Mar;19(6):852-7.

[61] Simoes R, Silva J, Vaia R, Sencadas V, Costa P, Gomes J, et al. Low percolation transitions in carbon nanotube networks dispersed in a polymer matrix: dielectric properties, simulations and experiments. Nanotechnology. **2009** Jan;20(3):035703.

[62] He F, Lau S, Chan HL, Fan JT. High Dielectric Permittivity and Low Percolation Threshold in Nanocomposites Based on Poly(vinylidene fluoride) and Exfoliated Graphite Nanoplates. Advanced Materials. **2009** Feb;21(6):710-5.

[63] Yao SH, Dang ZM, Xu HP, Jiang MJ, Bai J. Exploration of dielectric constant dependence on evolution of microstructure in nanotube/ferroelectric polymer nanocomposites. Applied Physics Letters. **2008** Feb;92(8):082902.

[64] Wang L, Dang ZM. Carbon nanotube composites with high dielectric constant at low percolation threshold. Applied Physics Letters. **2005** Jul;87(4):042903.

[65] Yuan JK, Yao SH, Dang ZM, Sylvestre A, Genestoux M, Bai J. Giant Dielectric Permittivity Nanocomposites: Realizing True Potential of Pristine Carbon Nanotubes in Polyvinylidene Fluoride Matrix through an Enhanced Interfacial Interaction. Journal of Physical Chemistry C. **2011** Apr;115(13):5515-21.

[66] Yuan JK, Li WL, Yao SH, Lin YQ, Sylvestre A, Bai J. High dielectric permittivity and low percolation threshold in polymer composites based on SiC-carbon nanotubes micro/nano hybrid. Applied Physics Letters. **2011** Jan;98(3):032901.

[67] Sillars R. The properties of a dielectric containing semi-conducting particles of various

shapes. J Inst Elect Eng. **1937**:378–94.
[68] Landauer R. The electrical resistance of binary metallic mixtures. J Appl Phys. **1952**:779–84.
[69] Maxwell-Garnett J. Colours in metal glasses and in metallic films. Philos Trans Roy Soc Lond. **1904**:385–9.
[70] Smith GB. Dielectric-constants for mixed media. Journal of Physics D-Applied Physics. **1977**;10(4):L39-L42.
[71] Tuncer E, Gubanski SM, Nettelblad B. Dielectric relaxation in dielectric mixtures: Application of the finite element method and its comparison with dielectric mixture formulas. Journal of Applied Physics. **2001** Jun;89(12):8092-100.
[72] Wagner K. The after effect in dielectrics. Arch Electrotech **1914**:378–80.
[73] Nelson SO, You TS. Relationships berween microwave permittivities of solid and pulverized plastics. Journal of Physics D-Applied Physics. **1990** Mar;23(3):346-53.
[74] Jayasundere N, Smith BV. Dielectric-constant for binary piezoelectric 0-3 composites. Journal of Applied Physics. **1993** Mar;73(5):2462-6.
[75] LKH VB. Dielectric behaviour of heterogeneous systems. Prog Dielect. **1967**:69–114.
[76] Zakri T, Laurent JP, Vauclin M. Theoretical evidence for 'Lichtenecker's mixture formulae' based on the effective medium theory. Journal of Physics D-Applied Physics. **1998** Jul;31(13):1589-94.
[77] Rubin Z, Sunshine SA, Heaney MB, Bloom I, Balberg I. Critical behavior of the electrical transport properties in a tunneling-percolation system. Physical Review B. **1999** May;59(19):12196-9.
[78] Nan CW, Shen Y, Ma J. Physical Properties of Composites Near Percolation. Annual Review of Materials Research, **2010**;40:131-51.
[79] Yuan JK, Yao SH, Sylvestre A, Bai J. Biphasic polymer blends containing carbon nanotubes: heterogeneous nanotube distribution and its influence on the dielectric properties. Journal of Physical Chemistry C. **2012** Jan;116(2):2051-8.
[80] Thostenson ET, Chou TW. Carbon nanotube networks: Sensing of distributed strain and damage for life prediction and self healing. Advanced Materials. 2006 **Nov**;18(21):2837-41.
[81] Haggenmueller R, Gommans HH, Rinzler AG, Fischer JE, Winey KI. Aligned single-wall carbon nanotubes in composites by melt processing methods. Chemical Physics Letters. **2000** Nov;330(3-4):219-25.
[82] Dang ZM, Fan LZ, Shen Y, Nan CW. Dielectric behavior of novel three-phase MWNTs/$BaTiO_3$/PVDF composites. Materials Science and Engineering B-Solid State Materials for Advanced Technology. **2003** Oct;103(2):140-4.
[83] Potschke P, Bhattacharyya AR, Janke A. Morphology and electrical resistivity of melt mixed blends of polyethylene and carbon nanotube filled polycarbonate. Polymer. **2003** Dec;44(26):8061-9.
[84] McNally T, Potschke P, Halley P, Murphy M, Martin D, Bell SEJ, et al. Polyethylene multiwalled carbon nanotube composites. Polymer. **2005** Sep;46(19):8222-32.
[85] Moniruzzaman M, Du FM, Romero N, Winey KI. Increased flexural modulus and strength in SWNT/epoxy composites by a new fabrication method. Polymer. **2006** Jan; 47(1):293-8.

[86] Sandler J, Shaffer MSP, Prasse T, Bauhofer W, Schulte K, Windle AH. Development of a dispersion process for carbon nanotubes in an epoxy matrix and the resulting electrical properties. Polymer. **1999** Oct;40(21):5967-71.

[87] Safadi B, Andrews R, Grulke EA. Multiwalled carbon nanotube polymer composites: Synthesis and characterization of thin films. Journal of Applied Polymer Science. **2002** Jun;84(14):2660-9.

[88] Qian D, Dickey EC, Andrews R, Rantell T. Load transfer and deformation mechanisms in carbon nanotube-polystyrene composites. Applied Physics Letters. **2000** May;76(20):2868-70.

[89] Watts PCP, Hsu WK, Chen GZ, Fray DJ, Kroto HW, Walton DRM. A low resistance boron-doped carbon nanotube-polystyrene composite. Journal of Materials Chemistry. **2001**;11(10):2482-8.

[90] Bower C, Rosen R, Jin L, Han J, Zhou O. Deformation of carbon nanotubes in nanotube-polymer composites. Applied Physics Letters. **1999** May;74(22):3317-9.

[91] Cadek M, Coleman JN, Barron V, Hedicke K, Blau WJ. Morphological and mechanical properties of carbon-nanotube-reinforced semicrystalline and amorphous polymer composites. Applied Physics Letters. **2002** Dec;81(27):5123-5.

[92] Ruan SL, Gao P, Yang XG, Yu TX. Toughening high performance ultrahigh molecular weight polyethylene using multiwalled carbon nanotubes. Polymer. **2003** Sep;44 (19):5643-54.

[93] Grady BP, Pompeo F, Shambaugh RL, Resasco DE. Nucleation of polypropylene crystallization by single-walled carbon nanotubes. Journal of Physical Chemistry B. **2002** Jun;106(23):5852-8.

[94] Paiva MC, Zhou B, Fernando KAS, Lin Y, Kennedy JM, Sun YP. Mechanical and morphological characterization of polymer-carbon nanocomposites from functionalized carbon nanotubes. Carbon. **2004**;42(14):2849-54.

[95] Zhang SH, Zhang NY, Huang C, Ren KL, Zhang QM. Microstructure and electromechanical properties of carbon nanotube/poly(vinylidene fluoride-trifluoroethylene-chlorofluoroethylene) composites. Advanced Materials. **2005** Aug; 17(15):1897-901.

[96] Lu KL, Lago RM, Chen YK, Green MLH, Harris PJF, Tsang SC. Mechanical damage of carbon nanotubes by ultrasound. Carbon. **1996**;34(6):814-6.

[97] Koshio A, Yudasaka M, Zhang M, Iijima S. A simple way to chemically react single-wall carbon nanotubes with organic materials using ultrasonication. Nano Letters. **2001** Jul;1(7):361-3.

[98] Zhang XF, Liu T, Sreekumar TV, Kumar S, Moore VC, Hauge RH, et al. Poly(vinyl alcohol)/SWNT composite film. Nano Letters. **2003** Sep;3(9):1285-8.

[99] Mitchell CA, Bahr JL, Arepalli S, Tour JM, Krishnamoorti R. Dispersion of functionalized carbon nanotubes in polystyrene. Macromolecules. **2002** Nov;35 (23):8825-30.

[100] Jiang MJ, Dang ZM, Xu HP, Yao SH, Bai J. Effect of aspect ratio of multiwall carbon nanotubes on resistance-pressure sensitivity of rubber nanocomposites. Applied Physics Letters. **2007** Aug;91(7)072907.

[101] Jiang MJ, Dang ZM, Bozlar M, Miomandre F, Bai JB. Broad-frequency dielectric

behaviors in multiwalled carbon nanotube/rubber nanocomposites. Journal of Applied Physics. **2009** Oct;106(8):084902.

[102] Barraza HJ, Pompeo F, O'Rear EA, Resasco DE. SWNT-filled thermoplastic and elastomeric composites prepared by miniemulsion polymerization. Nano Letters. **2002** Aug;2(8):797-802.

[103] Cochet M, Maser WK, Benito AM, Callejas MA, Martinez MT, Benoit JM, et al. Synthesis of a new polyaniline/nanotube composite: "in-situ" polymerisation and charge transfer through site-selective interaction. Chemical Communications. **2001** Aug; 21(16):1450-1.

[104] Clayton LM, Sikder AK, Kumar A, Cinke M, Meyyappan M, Gerasimov TG, et al. Transparent poly(methyl methacrylate)/single-walled carbon nanotube (PMMA/SWNT) composite films with increased dielectric constants. Advanced Functional Materials. **2005** Jan;15(1):101-6.

[105] Xie Z, Zhuang Q, Wang Q, Liu X, Chen Y, Han Z. In situ synthesis and characterization of poly(2,5-benzoxazole)/multiwalled carbon nanotubes composites. Polymer. **2011** Oct;52(23):5271-6.

[106] Li Q, Xue QZ, Hao LZ, Gao XL, Zheng QB. Large dielectric constant of the chemically functionalized carbon nanotube/polymer composites. Composites Science and Technology. **2008** Aug;68(10-11):2290-6.

[107] Yuan JK, Dang ZM, Yao SH, Zha JW, Zhou T, Li ST, et al. Fabrication and dielectric properties of advanced high permittivity polyaniline/poly(vinylidene fluoride) nanohybrid films with high energy storage density. Journal of Materials Chemistry. 2010;20(12):2441-7.

[108] Yao SH, Yuan JK, Dang ZM, Bai J. High dielectric performance of three-component nanocomposites induced by a synergetic effect. Materials Letters. **2010** Dec;64 (24):2682-4.

[109] Yao SH, Yuan JK, Dang ZM, Bai J, IEEE. Preparation of $BaTiO_3$-MWNT /polyvinylidene fluoride three-phase composites with novel dielectric behavior. Icpadm 2009: Proceedings of the 9th International Conference on Properties and Applications of Dielectric Materials, **2009**,1-3.765-8.

[110] Huang C, Klein R, Xia F, Li HF, Zhang QM, Bauer F, et al. Poly(vinylidene fluoride -trifluoroethylene) based high performance electroactive polymers. Ieee Transactions on Dielectrics and Electrical Insulation. **2004** Apr;11(2):299-311.

[111] Huang C, Zhang QM, Su J. High-dielectric-constant all-polymer percolative composites. Applied Physics Letters. **2003** May;82(20):3502-4.

[112] Wong M, Paramsothy M, Xu XJ, Ren Y, Li S, Liao K. Physical interactions at carbon nanotube-polymer interface. Polymer. **2003** Dec;44(25):7757-64.

[113] Dang ZM, Yao SH, Yuan JK, Bai J. Tailored dielectric properties based on microstructure change in $BaTiO_3$-carbon nanotube/polyvinylidene fluoride three-phase nanocomposites. Journal of Physical Chemistry C. **2010** Aug;114 (31):13204-9.

[114] Yang C, Lin YH, Nan CW. Modified carbon nanotube composites with high dielectric constant, low dielectric loss and large energy density. Carbon. **2009** Apr;47 (4):1096-101.

[115] Liu H, Shen Y, Song Y, Nan CW, Lin Y, Yang X. Carbon nanotube array/polymer

core/shell structured composites with high dielectric permittivity, low dielectric loss, and large energy density. Advanced Materials. **2011** Nov;23(43):5104-8.

[116] Li J, Ma PC, Chow WS, To CK, Tang BZ, Kim JK. Correlations between percolation threshold, dispersion state, and aspect ratio of carbon nanotubes. Advanced Functional Materials. **2007** Nov;17(16):3207-15.

[117] Poetschke P, Pegel S, Claes M, Bonduel D. A novel strategy to incorporate carbon nanotubes into thermoplastic matrices. Macromolecular Rapid Communications. **2008** Feb;29(3):244-51.

[118] Sumita M, Sakata K, Asai S, Miyasaka K, Nakagawa H. Dispersion of fillers and the electrical-conductivity of polymer blends filled with carbon black. Polymer Bulletin. **1991** Feb;25(2):265-71.

[119] Zhang MQ, Yu G, Zeng HM, Zhang HB, Hen YH. Two-step percolation in polymer blends filled with carbon black. Macromolecules. **1998** Sep;31(19):6724-6.

[120] Xu HP, Dang ZM, Jiang MJ, Yao SH, Bai J. Enhanced dielectric properties and positive temperature coefficient effect in the binary polymer composites with surface modified carbon black. Journal of Materials Chemistry. **2008**;18(2):229-34.

[121] Jin SH, Lee DS. Electrical and rheological properties of double percolated poly(methyl methacrylate)/Multiwalled carbon nanotube nanocomposites. Journal of Nanoscience and Nanotechnology. **2007** Nov;7(11):3847-51.

[122] Li Y, Shimizu H. Conductive PVDF/PA6/CNTs nanocomposites fabricated by dual formation of cocontinuous and nanodispersion structures. Macromolecules. **2008** Jul;41(14):5339-44.

[123] Gao X, Zhang S, Mai F, Lin L, Deng Y, Deng H, et al. Preparation of high performance conductive polymer fibres from double percolated structure. Journal of Materials Chemistry. **2011**;21(17):6401-8.

[124] Wu M, Shaw LL. On the improved properties of injection-molded, carbon nanotube-filled PET/PVDF blends. Journal of Power Sources. **2004** Sep;136 (1):37-44.

[125] Chen G, Lu J, Wu D. The electrical properties of graphite nanosheet filled immiscible polymer blends. Materials Chemistry and Physics. **2007** Aug;104(2-3):240-3.

[126] Jin L, Bower C, Zhou O. Alignment of carbon nanotubes in a polymer matrix by mechanical stretching. Applied Physics Letters. **1998** Aug;73(9):1197-9.

[127] Choi ES, Brooks JS, Eaton DL, Al-Haik MS, Hussaini MY, Garmestani H, et al. Enhancement of thermal and electrical properties of carbon nanotube polymer composites by magnetic field processing. Journal of Applied Physics. **2003** Nov; 94(9):6034-9.

[128] Abdalla M, Dean D, Theodore M, Fielding J, Nyairo E, Price G. Magnetically processed carbon nanotube/epoxy nanocomposites: Morphology, thermal, and mechanical properties. Polymer. **2010** Mar;51(7):1614-20.

[129] Park C, Wilkinson J, Banda S, Ounaies Z, Wise KE, Sauti G, et al. Aligned single-wall carbon nanotube polymer composites using an electric field. Journal of Polymer Science Part B-Polymer Physics. **2006** Jun;44(12):1751-62.

[130] Zhang C, Zhu J, Ouyang M, Ma CA. Electric field controlled formation and dissociation of multiwalled carbon nanotube conductive pathways in a polymer melt. Applied Physics Letters. **2009** Mar;94(11):3.

[131] Dang ZM, Yao SH, Xu HP. Effect of tensile strain on morphology and dielectric property in nanotube/polymer nanocomposites. Applied Physics Letters. **2007** Jan;90 (1):012907.
[132] Ajayan PM, Stephan O, Colliex C, Trauth D. Aligned carbon nanotube arrays formed by cutting a polymer resin-nanotube composite.Science. **1994** Aug;265(5176):1212-4.
[133] Tans SJ, Verschueren ARM, Dekker C. Room-temperature transistor based on a single carbon nanotube. Nature. **1998** May;393(6680):49-52.
[134] Pop E, Mann D, Wang Q, Goodson K, Dai HJ. Thermal conductance of an individual single-wall carbon nanotube above room temperature. Nano Letters. **200**6 Jan;6 (1):96-100.
[135] Coleman JN, Khan U, Gun'ko YK. Mechanical reinforcement of polymers using carbon nanotubes. Advanced Materials. **2006** Mar;18(6):689-706.
[136] Sreekumar TV, Liu T, Min BG, Guo H, Kumar S, Hauge RH, et al. Polyacrylonitrile single-walled carbon nanotube composite fibers. Advanced Materials. **2004** Jan;16 (1):58-61.
[137] Huang H, Liu CH, Wu Y, Fan SS. Aligned carbon nanotube composite films for thermal management. Advanced Materials. **2005** Jul;17(13):1652-6.
[138] Yang YL, Gupta MC. Novel carbon nanotube-polystyrene foam composites for electromagnetic interference shielding. Nano Letters. **2005** Nov;5(11):2131-4.
[139] Huang YY, Terentjev EM. Tailoring the electrical properties of carbon nanotube-polymer composites. Advanced Functional Materials. **2010** Dec;20 (23):4062-8.
[140] Wu JH, Kong LB. High microwave permittivity of multiwalled carbon nanotube composites. Applied Physics Letters. **2004** Jun;84(24):4956-8.
[141] Gefen Y, Aharony A, Alexander S. Anomalous diffusion on percolating clusters. Physical Review Letters. **1983**;50(1):77-80.
[142] Advani SG, Tucker CL. Closure approximation for 3-dimensional structure tensors. **1990** Apr;34(3):367-86.
[143] Tucker CL, Advani SG. Processing of short-fiber systems.Flow and Rheology in Polymer Composites Manufacturing. Elsevier:Amsterdam, **1994**.
[144] Fan ZH, Advani SG. Characterization of orientation state of carbon nanotubes in shear flow. Polymer. **2005** Jun;46(14):5232-40.
[145] Bhattacharyya AR, Sreekumar TV, Liu T, Kumar S, Ericson LM, Hauge RH, et al. Crystallization and orientation studies in polypropylene/single wall carbon nanotube composite. Polymer. **2003** Apr;44(8):2373-7.
[146] Hobbie EK, Wang H, Kim H, Han CC, Grulke EA, Obrzut J. Optical measurements of structure and orientation in sheared carbon-nanotube suspensions. Review of Scientific Instruments. **2003** Mar;74(3):1244-50.
[147] Sun LL, Li B, Zhang ZG, Zhong WH. Achieving very high fraction of beta-crystal PVDF and PVDF/CNF composites and their effect on AC conductivity and microstructure through a stretching process. European Polymer Journal. **2010** Nov;46 (11):2112-9.
[148] Broadhurst MG, Davis GT, McKinney JE, Collins RE. Piezoelectricity and pyroelectricity in polyvinylidene fluoride-model. Journal of Applied Physics.

1978;49(10):4992-7.
[149] El Mohajir BE, Heymans N. Changes in structural and mechanical behaviour of PVDF with processing and thermomechanical treatments. Polymer. **2001** Jun;42 (13):5661-7.
[150] Sajkiewicz P, Wasiak A, Goclowski Z. Phase transitions during stretching of poly(vinylidene fluoride). European Polymer Journal. **1999** Mar;35(3):423-9.
[151] Jonscher AK. Universal Relaxation Law. London: Chelsea Dielectric **1992**.
[152] Thomas P, Varughese KT, Dwarakanath K, Varma KBR. Dielectric properties of poly(vinylidene fluoride)/$CaCu_3Ti_4O_{12}$ composites. Composites Science and Technology. **2010** Mar;70(3):539-45.
[153] Snogren R. Embedded Passives: The Next Revolution. Printed Circuit Fabr. **2002**: 26-9.
[154] Ulrich R. Embedded resistors and capacitors for organic based SOP. Ieee Transactions on Advanced Packaging. **2004** May;27(2):326-31.
[155] Jillek W, Yung WKC. Embedded components in printed circuit boards: a processing technology review. International Journal of Advanced Manufacturing Technology. **2005** Feb;25(3-4):350-60.
[156] Shen Y, Lin YH, Li M, Nan CW. High dielectric performance of polymer composite films induced by a percolating interparticle barrier layer. Advanced Materials. **2007** May;19(10):1418-22.
[157] Zengin H, Zhou WS, Jin JY, Czerw R, Smith DW, Echegoyen L, et al. Carbon nanotube doped polyaniline. Advanced Materials. **2002** Oct;14(20):1480-3.
[158] Czerw R, Guo ZX, Ajayan PM, Sun YP, Carroll DL. Organization of polymers onto carbon nanotubes: A route to nanoscale assembly. Nano Letters. **2001** Aug;1 (8):423-7.
[159] Hong CY, You YZ, Wu DC, Liu Y, Pan CY. Multiwalled carbon nanotubes grafted with hyperbranched polymer shell via SCVP. Macromolecules. **2005** Apr;38 (7):2606-11.
[160] Holzinger M, Abraha J, Whelan P, Graupner R, Ley L, Hennrich F, et al. Functionalization of single-walled carbon nanotubes with (R-)oxycarbonyl nitrenes. Journal of the American Chemical Society. **2003** Jul;125(28):8566-80.
[161] Bahr JL, Tour JM. Covalent chemistry of single-wall carbon nanotubes. Journal of Materials Chemistry. **2002**;12(7):1952-8.
[162] Higginbotham AL, Stephenson JJ, Smith RJ, Killips DS, Kempel LC, Tour JM. Tunable permittivity of polymer composites through incremental blending of raw and functionalized single-wall carbon nanotubes. Journal of Physical Chemistry C. **2007** Dec;111(48):17751-4.
[163] Zhang ZN, Zhang J, Chen P, Zhang BQ, He JS, Hu GH. Enhanced interactions between multi-walled carbon nanotubes and polystyrene induced by melt mixing. Carbon. **2006** Apr;44(4):692-8.
[164] Ding W, Eitan A, Fisher FT, Chen X, Dikin DA, Andrews R, et al. Direct observation of polymer sheathing in carbon nanotube-polycarbonate composites. Nano Letters. **2003** Nov;3(11):1593-7.
[165] Potschke P, Fornes TD, Paul DR. Rheological behavior of multiwalled carbon nanotube/polycarbonate composites. Polymer. **2002** May;43(11):3247-55.
[166] Logakis E, Pollatos E, Pandis C, Peoglos V, Zuburtikudis I, Delides CG, et al. Structure-property relationships in isotactic polypropylene/multi-walled carbon nanotubes nanocomposites. Composites Science and Technology. **2010** Feb;70

(2):328-35.
[167] Tamura R, Lim E, Manaka T, Iwamoto M. Analysis of pentacene field effect transistor as a Maxwell-Wagner effect element. Journal of Applied Physics. **2006** Dec;100(11):114515.
[168] Baskaran D, Mays JW, Bratcher MS. Noncovalent and nonspecific molecular interactions of polymers with multiwalled carbon nanotubes. Chemistry of Materials. **2005** Jun;17(13):3389-97.
[169] Zhang J, Lee JK, Wu Y, Murray RW. Photoluminescence and electronic interaction of anthracene derivatives adsorbed on sidewalls of single-walled carbon nanotubes. Nano Letters. **2003** Mar;3(3):403-7.
[170] Li HP, Zhou B, Lin Y, Gu LR, Wang W, Fernando KAS, et al. Selective interactions of porphyrins with semiconducting single-walled carbon nanotubes. Journal of the American Chemical Society. **2004** Feb;126(4):1014-5.
[171] Gogotsi Y. Carbon Nanomaterials. Taylor and Francis: NewYork, **2006**.
[172] Owens FJ, Jayakody JRP, Greenbaum SG. Characterization of single walled carbon nanotube: Polyvinylene difluoride composites. Composites Science and Technology. **2006** Aug;66(10):1280-4.
[173] Chen GX, Li YJ, Shimizu H. Ultrahigh-shear processing for the preparation of polymer/carbon nanotube composites. Carbon. **2007** Oct;45(12):2334-40.
[174] Zhao Q, Wagner HD. Raman spectroscopy of carbon-nanotube-based composites. Philosophical Transactions of the Royal Society of London Series a-Mathematical Physical and Engineering Sciences. **2004** Nov;362(1824):2407-24.
[175] Rao AM, Eklund PC, Bandow S, Thess A, Smalley RE. Evidence for charge transfer in doped carbon nanotube bundles from Raman scattering. Nature. **1997** Jul;388 (6639):257-9.
[176] Venkateswaran UD, Rao AM, Richter E, Menon M, Rinzler A, Smalley RE, et al. Probing the single-wall carbon nanotube bundle: Raman scattering under high pressure. Physical Review B. **1999** Apr;59(16):10928-34.
[177] Perez R. Prediction of the Effective Dielectric constant in SWNT polyimide nanocomposites using the Bruggemann model. Journal of Applied Polymer Science. **2009** Aug;113(4):2264-70.
[178] Breuer O, Sundararaj U. Big returns from small fibers: A review of polymer/carbon nanotube composites. Polymer Composites. **2004** Dec;25(6):630-45.
[179] Balberg I. A comprehensive picture of the electrical phenomena in carbon black -polymer composites. Carbon. **2002**;40(2):139-43.
[180] Runt JP, Fitzgerald JJ. Dielectric spectroscopy of polymeric materials. American Chemical Society: Washington, D.C. **1997**.
[181] El Hasnaoui M, Graca MPF, Achour ME, Costa LC, Outzourhit A, Oueriagli A, et al. Effect of temperature on the electrical properties of copolymer/carbon black mixtures. Journal of Non-Crystalline Solids. **2010** Jul;356(31-32):1536-41.
[182] Xu HP, Dang ZM, Bing NC, Wu YH, Yang DD. Temperature dependence of electric and dielectric behaviors of Ni/polyvinylidene fluoride composites. Journal of Applied Physics. **2010** Feb;107(3):034105.
[183] Lebovka N, Dadakova T, Lysetskiy L, Melezhyk O, Puchkovska G, Gavrilko T, et al.

Phase transitions, intermolecular interactions and electrical conductivity behavior in carbon multiwalled nanotubes/nematic liquid crystal composites. Journal of Molecular Structure. **2008** Sep;887(1-3):135-43.

[184] Li N, Huang Y, Du F, He XB, Lin X, Gao HJ, et al. Electromagnetic interference (EMI) shielding of single-walled carbon nanotube epoxy composites. Nano Letters. **2006** Jun;6(6):1141-5.

[185] Zhang QM, Li HF, Poh M, Xia F, Cheng ZY, Xu HS, et al. An all-organic composite actuator material with a high dielectric constant. Nature. **2002** Sep;419(6904):284-7.

[186] Yuan JK, Dang ZM, Bai J. Unique dielectric properties in polyaniline/poly(vinylidene fluoride) composites induced by temperature variation. Physica Status Solidi-Rapid Research Letters. **2008** Oct;2(5):233-5.

[187] Kotaki M, Wang K, Toh ML, Chen L, Wong SY, He CB. Electrically conductive epoxy/clay/vapor grown carbon fiber hybrids. Macromolecules. **2006** Feb;39 (3):908-11.

[188] Stankovich S, Dikin DA, Dommett GHB, Kohlhaas KM, Zimney EJ, Stach EA, et al. Graphene-based composite materials. Nature. **2006** Jul;442(7100):282-6.

[189] Zhang HB, Zheng WG, Yan Q, Yang Y, Wang JW, Lu ZH, et al. Electrically conductive polyethylene terephthalate/graphene nanocomposites prepared by melt compounding. Polymer. **2010** Mar;51(5):1191-6.

[190] Song HT, Dang ZM, Lv J, Yao SH, Zha JW, Yin Y. Enhanced electrical properties in percolative low-density polyethylene/carbon nanotubes nanocomposites. Ieee Transactions on Dielectrics and Electrical Insulation. **2010** Jun;17(3):645-52.

[191] Grossiord N, Loos J, Regev O, Koning CE. Toolbox for dispersing carbon nanotubes into polymers to get conductive nanocomposites. Chemistry of Materials. **2006** Mar; 18(5):1089-99.

[192] http://www.surface-tension.de/solid-surface-energy.htm, accessed September 26, **2011**.

[193] Barber AH, Cohen SR, Wagner HD. Static and dynamic wetting measurements of single carbon nanotubes. Physical Review Letters. **2004** May;92(18):186103.

[194] Nuriel S, Liu L, Barber AH, Wagner HD. Direct measurement of multiwall nanotube surface tension. Chemical Physics Letters. **2005** Mar;404(4-6):263-6.

[195] Wu S. Polymer interface and adhension. Marcel Dekker Inc.:New York, **1982**.

[196] Fenouillot F, Cassagnau P, Majeste JC. Uneven distribution of nanoparticles in immiscible fluids: morphology development in polymer blends. Polymer. **2009** Mar;50(6):1333-50.

[197] Zaikin AE, Zharinova EA, Bikmullin RS. Specifics of localization of carbon black at the interface between polymeric phases. Polymer Science Series A. **2007** Mar; 49(3):328-36.

[198] Gubbels F, Jerome R, Teyssie P, Vanlathem E, Deltour R, Calderone A, et al. Selective localization of carbon black in immiscible of polymer blends-a useful tool to design electrical conductive composites. Macromolecules. **1994** Mar;27(7):1972-4.

[199] Feng JY, Chan CM, Li JX. A method to control the dispersion of carbon black in an immiscible polymer blend. Polymer Engineering and Science. **2003** May; 43(5):1058-63.

[200] Clarke J, Clarke B, Freakley PK, Sutherland I. Compatibilising effect of carbon black

on morphology of NR-NBR blends. Plastics Rubber and Composites. **2001**;30(1):39-44.

[201] Zhou P, Yu W, Zhou C, Liu F, Hou L, Wang J. Morphology and electrical properties of carbon black filled LLDPE/EMA composites. Journal of Applied Polymer Science. **2007** Jan;103(1):487-92.

[202] Wilkinson D, Langer JS, Sen PN. Enhancement of the dielectric constant near a percolation threshold. Physical Review B. **1983**;28(2):1081-7.

[203] Song Y, Noh TW, Lee SI, Gaines JR. Experimental study of the 3-dimensional AC conductivity and dielectric constant of a conductor-insulator composite near the percolation threshold. Physical Review B. **1986** Jan 15;33(2):904-8.

[204] Panda M, Srinivas V, Thakur AK. Role of polymer matrix in large enhancement of dielectric constant in polymer-metal composites. Applied Physics Letters. **2011** Jul; 99(4):042905.

[205] Jiang MJ, Dang ZM, Xu HP. Giant dielectric constant and resistance-pressure sensitivity in carbon nanotubes/rubber nanocomposites with low percolation threshold. Applied Physics Letters. **2007** Jan;90(4):042914.

[206] Halperin BI, Feng S, Sen PN. Differences between lattice and continuum percolation transport exponents. Physical Review Letters. **1985**;54(22):2391-4.

[207] Barrow DA, Noteboom R, Sayer M. Design and fabrication of macroscopic piezoelectric actuators based on thick PZT films. Integrated Ferroelectrics. **1995**; 8(1-2):1-11.

[208] Zhang QM, Bharti V, Zhao X. Giant electrostriction and relaxor ferroelectric behavior in electron-irradiated poly(vinylidene fluoride-trifluoroethylene) copolymer. Science. **1998** Jun;280(5372):2101-4.

[209] Iwanowski RJ, Fronc K, Paszkowicz W, Heinonen M. XPS and XRD study of crystalline 3C-SiC grown by sublimation method. Journal of Alloys and Compounds. **1999** May;286(1-2):143-7.

[210] Ortiz AL, Sanchez-Bajo F, Cumbrera FL, Guiberteau F. X-ray powder diffraction analysis of a silicon carbide-based ceramic. Materials Letters. **2001** Jun;49(2):137-45.

[211] Liu ZC, Shen WH, Bu WB, Chen HR, Hua ZL, Zhang LX, et al. Low-temperature formation of nanocrystalline beta-SiC with high surface area and mesoporosity via reaction of mesoporous carbon and silicon powder. Microporous and Mesoporous Materials. **2005** Jul;82(1-2):137-45.

[212] Li Z, Gao W, Meng A, Geng Z, Gao L. Large-scale synthesis and Raman and photoluminescence properties of pingle crystalline beta-SiC nanowires periodically wrapped by amorphous SiO_2 nanospheres. Journal of Physical Chemistry C. **2009** Jan;113(1):91-6.

[213] Soueidan M, Ferro G, Nsouli B, Roumie M, Polychroniadis E, Kazan M, et al. Characterization of a 3C-SiC single domain grown on 6H-SiC(0001) by a vapor-liquid-solid mechanism. Crystal Growth & Design. **2006** Nov;6(11):2598-602.

[214] Kusunoki M, Suzuki T, Hirayama T, Shibata N, Kaneko K. A formation mechanism of carbon nanotube films on SiC(0001). Applied Physics Letters. **2000** Jul; 77(4):531-3.

[215] Jung YJ, Wei BQ, Vajtai R, Ajayan PM. Mechanism of selective growth of carbon nanotubes on SiO_2/Si patterns. Nano Letters. **2003** Apr;3(4):561-4.

[216] Cao AY, Ajayan PM, Ramanath G, Baskaran R, Turner K. Silicon oxide thickness-dependent growth of carbon nanotubes. Applied Physics Letters. **2004** Jan; 84(1):109-11.

[217] Kuwana K, Saito K. Modeling ferrocene reactions and iron nanoparticle formation: Application to CVD synthesis of carbon nanotubes. Proceedings of the Combustion Institute. **2007**;31:1857-64.

[218] Norinaga K, Deutschmann O. Detailed kinetic modeling of gas-phase reactions in the chemical vapor deposition of carbon from light hydrocarbons. Industrial & Engineering Chemistry Research. **2007** May;46(11):3547-57.

[219] Kim H, Sigmund W. Iron particles in carbon nanotubes. Carbon. **2005** Jul; 43(8):1743-8.

[220] Logakis E, Pandis C, Peoglos V, Pissis P, Pionteck J, Potschke P, et al. Electrical/dielectric properties and conduction mechanism in melt processed polyamide/multi-walled carbon nanotubes composites. Polymer. **2009** Oct;50 (21):5103-11.

[221] Chen Q, Du PY, Jin L, Weng WJ, Han GR. Percolative conductor/polymer composite films with significant dielectric properties. Applied Physics Letters. **2007** Jul; 91 (2):022912.

[222] Raja V, Sharma AK, Rao V. Impedance spectroscopic and dielectric analysis of PMMA-CO-P4VPNO polymer films. Materials Letters. **2004** Oct;58(26):3242-7.

[223] Sun LL, Zhao Y, Zhong WH. Dependence of dielectric properties and percolative behavior on phase separation structure induced by heterogeneous carbon nanofiber distribution in polymer blend nanocomposites. Macromolecular Materials and Engineering. **2011** Nov ;296(11):992-1001.